Universidade de Aveiro Departamento de Física
2013

ANA OLIVEIRA PRATAS E SOUSA

TÉCNICAS DE MONITORIZAÇÃO EM REDES ÓPTICAS DE PRÓXIMA GERAÇÃO

Universidade de Aveiro Departamento de Física
2013

ANA OLIVEIRA PRATAS E SOUSA

TÉCNICAS DE MONITORIZAÇÃO EM REDES ÓPTICAS DE PRÓXIMA GERAÇÃO

Tese apresentada à Universidade de Aveiro para cumprimento dos requisitos necessários à obtenção do grau de Doutor em Engenharia Física, realizada sob a orientação científica do Doutor Paulo André, Professor auxiliar convidado a tempo parcial e investigador auxiliar do Instituto de Telecomunicações e co-orientação do Doutor Rogério Nogueira, investigador auxiliar do Instituto de Telecomunicações.

Apoio financeiro da Fundação para a Ciência e a Tecnologia – FCT através da bolsa SFRH / BD / 61650 / 2009.

o júri

presidente

Prof. Doutor Fernando Manuel dos Santos Ramos
Professor Catedrático da Universidade de Aveiro

Prof. Doutor João de Lemos Pinto
Professor Catedrático da Universidade de Aveiro

Prof. Doutora Maria do Carmo Raposo de Medeiros
Professora Associada da Faculdade de Ciências e Tecnologia da Universidade de Coimbra

Prof. Doutor Henrique Manuel de Castro Faria Salgado
Professor Associado da Faculdade de Engenharia da Universidade do Porto

Prof. Doutor Paulo Sérgio de Brito André
Professor Associado do Instituto Superior Técnico da Universidade Técnica de Lisboa

Prof. Doutor Rogério Nunes Nogueira
Investigador Auxiliar do IT – Instituto de Telecomunicações de Aveiro

agradecimentos

Durante estes quatro anos contei com o apoio e colaboração de várias pessoas que foram fundamentais para a realização deste trabalho.
Começo por expressar um agradecimento especial aos meus orientadores, Professor Paulo André e Professor Rogério Nogueira, pela disponibilidade e experiência, que me ajudaram muito durante a realização deste trabalho e sem as quais este não seria possível.
Agradeço também ao Carlos Marques, pela paciência e colaboração nas diversas gravações de redes de Bragg; e ao Ali, pela ajuda preciosa na realização do trabalho em transmissão coerente.
Quero também deixar aqui uma palavra especial a todos os meus colegas e amigos do Instituto de Telecomunicações de Aveiro pelo bom ambiente vivido durante estes anos: Álvaro, Gil, Fernando, Vítor, Carlos Vicente, Carlos Marques, Fátima, Nélia, Paulo, Lúcia, Nuno, Ana, Ali, Prata, Bruno, Nélson, Vanessa, Sofia, Rogério Dionísio… obrigada!

Finalmente quero agradecer à minha família e amigos por tudo, pelo apoio incondicional e compreensão, especialmente agora que o futuro se adivinha desafiante e arriscado, mas promissor.

Um muito obrigada a todos!

palavras-chave

Comunicações ópticas; monitorização de redes ópticas; redes de comunicação de próxima geração; relação sinal-ruído óptico; dispersão cromática; integridade física da rede

resumo

Neste trabalho foram desenvolvidas diversas técnicas que permitem a monitorização de desempenho das redes de comunicações ópticas. Estas técnicas dedicam-se quer à determinação de parâmetros do próprio sinal de dados (como a relação sinal ruído óptico e a dispersão), quer à detecção de eventuais falhas físicas na infra-estrutura da rede.

Relativamente à monitorização da relação sinal-ruído óptico foram desenvolvidos métodos baseados na aplicação de redes de Bragg gravadas em fibras birrefringentes que permitiram distinguir o sinal do ruído através das suas propriedades de polarização.

A monitorização da dispersão cromática sofrida pelo sinal durante a sua propagação também foi possível. Neste caso foi testada uma técnica baseada na análise do espectro eléctrico do sinal. Demonstrou-se que esta técnica pode ser aplicada quer em sinais modulados na amplitude quer em sinais modulados na fase.

Foi também desenvolvida uma técnica para a monitorização da infra-estrutura física de uma rede de acesso. Mais uma vez, aqui foi utilizado um método baseado na presença de redes de Bragg, desta vez gravadas em fibras monomodo que são utilizadas como pontos de monitorização em locais estratégicos da rede.

keywords

Optical communications; next generation communication networks; optical performance monitoring; optical signal to noise ratio; group-velocity dispersion; physical integrity of he network.

abstract

In this work several techniques to monitor the performance of optical networks were developed. These techniques are dedicated either to the measurement of the data signal parameters (optical signal to noise ratio and dispersion) or to the detection of physical failures on the network infrastructure.
The optical signal to noise ratio of the transmitted signal was successfully monitored using methods based on the presence of Bragg gratings imprinted on high birefringent fibres that allowed the distinction of the signal from the noise due to its polarization properties.
The monitoring of the signal group-velocity dispersion was also possible. In this case, a method based on the analysis of the electric spectrum of the signal was applied. It was experimentally demonstrated that this technique is applicable on both amplitude and phase modulated signals.
It was also developed a technique to monitor the physical infrastructure of an optical access network. Once again, the application of Bragg gratings (this time imprinted on standard single mode fibres) was the basis of the developed method.

Contents

List of Acronyms

10G EPON	10 Gigabit Ethernet Passive Optical Network
3DTV	Three Dimension Television
ANN	Artificial Neural Networks
ASE	Amplified Spontaneous Emission
AWG	Array Waveguide
B2B	Back to Back
BER	Bit Error Rate
BLS	Broadband Light Source
BPF	Bandpass filter
CNR	Carrier to Noise Ratio
CO	Central Office
CW	Continuous Wave
DCF	Dispersion Compensation Fibre
DFB	Distributed Feedback
DP	Dual Polarization
DPSK	Differential Phase Shift Keying
DSF	Dispersion Shifted Fibre
DUT	Device Under Test
EDFA	Erbium Doped Fibre Amplifier
EPON	Ethernet Passive Optical Network
ER	Extinction Ratio
FBG	Fibre Bragg Grating
FFT	Fast Fourier Transform
FP-LD	Fabry Perot Laser Diode
FTTH	Fibre to the Home
FTTx	Fibre to the x
FWM	Four Wave Mixing
GPON	Gigabit Passive Optical Network
GVD	Group Velocity Dispersion

HiBi	High Birefringent
HNLF	Highly Nonlinear Fibre
IEEE	Institute of Electrical and Electronics Engineers
IPTV	Internet Protocol Television
IQM	IQ Modulator
IT	Instituto de Telecomunicações
ITU	International Telecommunication Union
MZM	Mach-Zehnder Modulator
NEB	Noise Equivalent Bandwidth
NG-PON	Next Generation Passive Optical Network
NRZ	Non-Return-to-Zero
NTT	Nippon Telegraph and Telephone Corporation
NZ-DSF	Non-zero Dispersion Shifted Fibre
OADM	Optical Add Drop Multiplexer
O-E-O	Optical-Electrical-Optical
OFDR	Optical Frequency Domain Reflectometry
OLT	Optical Line Terminal
ONA	Optical Network Analyser
ONU	Optical Network Unit
OOK	On-Off Keying
OPM	Optical Performance Monitoring
OSA	Optical Spectrum Analyser
OSNR	Optical Signal to Noise Ratio
OTDR	Optical Time Domain Reflectometry
OXC	Optical Cross Connect
P2P	Point-to-Point
PBS	Polarization Beam Splitter
PC	Polarization Controller
PIN-PD	PIN Photodiode
PM	Power Meter
PMD	Polarization Mode Dispersion

PON	Passive Optical Network
PRBS	Pseudo Random Bit Sequence
QoS	Quality of Service
QPSK	Quadrature Phase Shift Keying
RF	Radio Frequency
RN	Remote Node
ROADM	Reconfigurable Optical Add Drop Multiplexer
RZ	Return-to-Zero
SBS	Stimulated Brillouin Scattering
SMF	Single Mode Fibre
SOA	Semiconductor Optical Amplifier
SPM	Self Phase Modulation
TDM	Time Division Multiplexing
TLS	Tuneable Light Source
TWDM	Time-Wavelength Division Multiplexing
UV	Ultra-Violet
VOA	Variable Optical Attenuator
WDM	Wavelength Division Multiplexing
XPM	Cross Phase Modulation

Chapter 1: Introduction

1.1 Motivation

In the past years, the demand for telecommunication high connection speeds due to technologies such as video streaming, IPTV, 3DTV, online gaming, etc., has been a constant, and will continue to be in the future, as other technologies emerge. In order to respond to this demand, optical networks are evolving into more complex and higher capacity architectures, with the introduction of dynamic networks, multi-channel systems and higher bitrates, among other factors.

As a consequence, the importance of implementing systems to monitor the quality of the network is crucial. This thesis focuses on this topic and the main goal was to study and develop techniques to monitor the data signal parameters and the physical integrity of optical networks.

1.2 Optical networks: historical background

In the 1960's, the first experiments to guide light in a glass fibre waveguide were successfully demonstrated. However, these glass fibres presented high attenuation (around 1000 dB/km) and the application in signal transmissions for long distances was impracticable. It was only in the seventies decade (of the 20th century) that the silica fibres, proposed by *Charles Kao*, were produced and made it possible for optical signals to propagate through this medium for long distances. This work earned *Kao* the Physics *Nobel* Prize in 2009. Nowadays, optical fibres present attenuations of 0.2 dB/km in some spectral regions, namely around 1550 nm. This breakthrough occurred simultaneously with the development of the first semiconductor lasers and both originated the initial boost for optical communications to become a reality [1].

When optical fibres were first introduced in telecommunications networks, these were used as simple static connections: a transmitter generated the optical signal that was sent along the optical fibre to the receiver, through only one possible path. Therefore there was no optical processing, switching or routing, and those tasks were performed in the electronic domain [2].

In the late 70's, early 80's (of the 20th century) the first telecommunication systems were implemented with multimode fibres, which have a large core diameter, when compared to the signal wavelength. In this type of fibres the signal propagates through different modes, each one travelling different distances and consequently imposing a temporal dispersion of the signal. This intermodal dispersion was the main limitation of these systems and the signal had to be regenerated about every

ten kilometres. In the regeneration, the degraded optical signal is converted into the electric domain, from which it is once again converted into a rehabilitated optical signal after processed - this is called optical-electrical-optical (O-E-O) conversion [2].

The advent of the single mode fibre (SMF), with a single propagation mode, was a major breakthrough, eliminating the intermodal dispersion, and allowing the increase of the distance between electronic regenerators. However, other degrading issues were still present, such as the attenuation, the chromatic dispersion and polarization mode dispersion (PMD) [2].

With the introduction of optical amplifiers, such as the Erbium Doped Fibre Amplifier (EDFA), in the nineties (of the 20th century), the signal is amplified optically and the O-E-O conversion has become less frequent. The signals can now be transmitted through longer distances, without the need of such a frequent electronic regeneration [2]. Nonetheless these amplifiers introduce a significant amount of noise that needs to be considered and monitored.

Also, the advent of wavelength division multiplexing (WDM) appears as a response to the strong demand for high transmission rates imposed by the globalization of the internet. The WDM technology enables the simultaneous transmission of different signals in the same optical fibre. Each of these signals is transmitted using a different wavelength, which constitutes an optical channel. The transmission of several channels in the same optical fibre increases drastically the aggregate bitrate, which can reach several Tb/s. This technology, along with EDFA's, reduced dramatically the cost of the network, where one EDFA was able to replace several regenerators (one per optical channel). Nowadays, WDM with EDFA's or Raman amplification is the predominant technology in long-haul networks, where each channel can reach a bitrate of 10 Gb/s, being the total fibre capacity at a few Tb/s and the data transmitted over several thousands of kilometres [1, 3].

Recently, a tendency to turn these networks into totally optical networks has been verified. Actually, totally transparent optical networks are the ultimate goal of optical communications, where no electronic processing takes place and all those tasks are performed in the optical domain, providing a faster and more reliable signal transmission. Some optical devices, such as optical cross connects (OXC) and reconfigurable optical add-drop multiplexers (ROADM), have already been introduced turning static links into dynamic networks. ROADMs enable the addition and/or removal of channels in strategic places in the network and OXCs let the different channels be forwarded to different paths.

In Figure 1.1 is presented a diagram that displays the evolution of the optical networks as previously described.

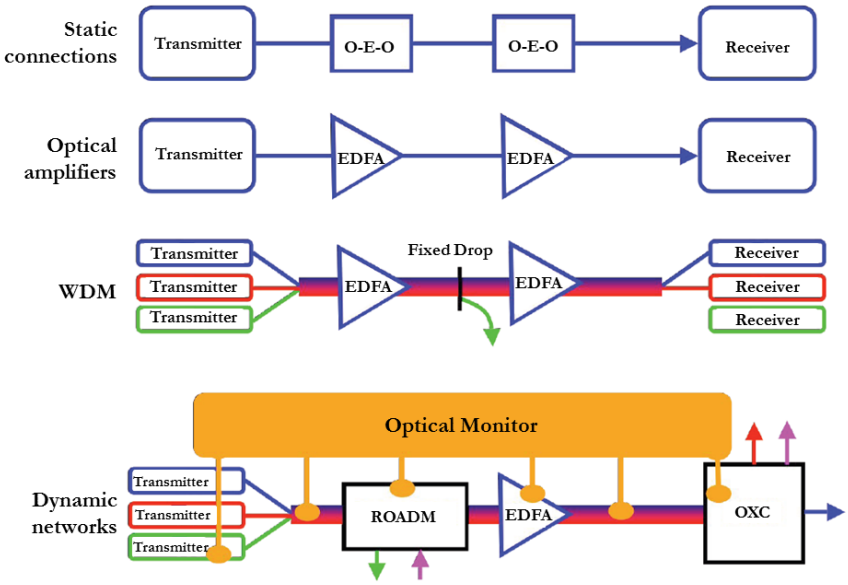

Figure 1.1 - Optical networks evolution, from top to bottom: static connections with O-E-O regenerators every 10 km; the advent of amplifiers eliminated part of those regenerators; WDM enabled the propagation of several optical channels along the same optical fibre; ROADM and OXC turned the static networks into dynamic ones giving rise to the necessity of an optical monitor plane [4]

Optical network architectures can be divided into three hierarchal categories, where each covers different ranges of span. Long-haul (or core) networks constitute the basis of the communications world as they span over hundreds or thousands of kilometres connecting different countries and continents via terrestrial and submarine optical fibres. Metro networks span for tens or a few hundreds of kilometres and can link different cities. Access networks constitute the connection between the end user and the carrier network and have more complex architectures, being also the most cost sensitive part of the optical communication network hierarchy.

1.2.1 Core and metro networks: current status and the future

Core networks are the most technologically challenging ones, as they support the worldwide traffic of information and require the largest spectral bandwidths and highest transmission rates. Nowadays, the predominant transmission systems deployed all over the world are based on multi-channel WDM with EDFA amplification, where each channel is usually amplitude modulated - On-Off Keying (OOK) - at bitrates of 10 Gb/s [3]. Regarding metro networks, these are often composed by rings that connect several access nodes through ROADMs and the transmission of the data is also based on WDM [5].

The continuous increase in traffic and the demand for even higher transmission rates is leading research to find other solutions to increase spectral efficiency, i.e., to increase the bitrate per

bandwidth. One way to do that is using other parameters of the optical signal, besides its amplitude, to modulate the optical signal with the data, such as phase and polarization. Actually, the most advanced system commercially available up to date consists of 100 Gb/s dual-polarization quadrature phase-shift-keying (DP-QPSK) channels. In these transmission systems, the signal phase is modulated usually in one of the four possible states (for instance: 45º; 135º; 225º; 315º) and to each phase is assigned a set of two bits ("11"; "10"; "00"; "01"). Furthermore, in a single wavelength, two separate channels with orthogonal polarizations (dual-polarization - DP) can carry information, which are then detected using a coherent receiver [6].

As this evolution occurs in the core network field, access networks are also evolving but at a different technological level.

1.2.2 Next generation access networks

Access networks are also known as the "last mile" of a communications network as they provide the connection to the end user. Their architecture will define the bandwidth available to each subscriber and some architectures allow the optical fibre itself to reach the home of the service subscriber, denominated fibre to the home (FTTH) networks.

Several architectures for access networks have been proposed throughout the years. However, point-to-multipoint passive optical networks (PON) have gained popularity and are now predominant in most countries, as they provide a flexible and cost-effective solution for fibre to the x (FTTx) deployment (where x stands for home, building, curb, etc.). FTTx were first deployed in 2004 with Ethernet passive optical networks (EPON) in Asia, and later on with Gigabit Passive Optical Network (GPON) with a predominant presence in Europe and North America [7]. Both of these architectures are point-to-multipoint based on Time Division Multiplexing (TDM), where one fibre carries one channel and the information from each client is associated to a time slot, as illustrated in Figure 1.2.

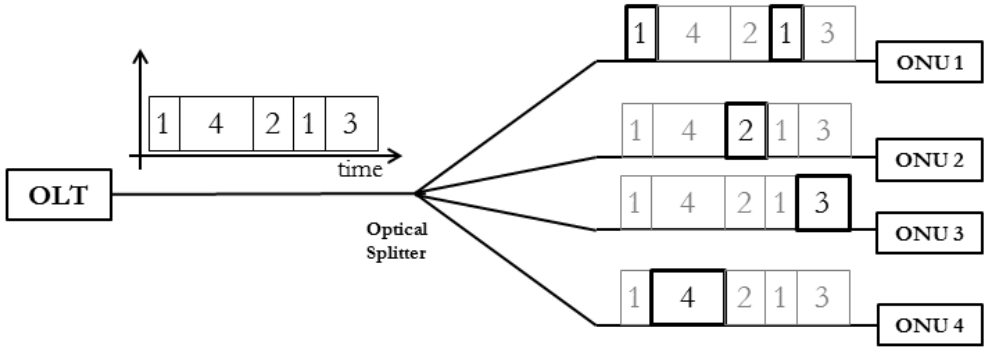

Figure 1.2 - Time Division Multiplexing (OLT – Optical Line Terminal; ONU – Optical Network Unit)

The main differences between these two technologies (GPON and EPON) is in the protocol used to send and encapsulate the data in the time slots and also in the bitrate supported: while EPON supports a 1 Gb/s for both upstream and downstream links, GPON offers a 2.5 Gb/s bitrate for downstream and 1.25 Gb/s for the upstream [8]. With the growth in traffic information, the need for higher bitrates is increasing and new standards for PON's have already been defined.

In 2009, Institute of Electrical and Electronics Engineers (IEEE) defined a new standard to update the EPON architecture, the 10 Gigabit EPON (10G EPON), providing two different variations: one asymmetric (10 Gb/s for the downstream link and 1 Gb/s for the upstream); and one symmetric that supports a bitrate of 10 Gb/s for both downstream and upstream links. This architecture is now being tested and in preparation for initial deployments [9].

The International Telecommunication Union (ITU) has also already defined the standard for the GPON successor. Actually, a plan with solutions until 2015 is in the preparation. The first phase, Next Generation PON (NG-PON) 1, identifies an architecture that is compatible with the existing infrastructures and may coexist with GPON. This standard was defined in 2010 and supports a bitrate of 10 Gb/s for downstream and 2.5 Gb/s for upstream. Another standard, providing a symmetric solution (10 Gb/s for both upstream and downstream) was also approved. However due to the high costs that it implied, the asymmetric solution was selected as NG-PON1 by ITU. The higher upstream bandwidth of NG-PON1 over the asymmetric solution of 10G-EPON, places NG-PON as the most likely architecture to become predominant in the future, as it provides a solution in a longer term [8].

The second phase planned by ITU, which is predicted for 2015, is the NG-PON2 and isn't yet defined (at the time of writing). This solution will likely disrupt with the installed infrastructures and will definitely provide a much higher bandwidth and a longer reach than GPON and NG-PON1 [8, 10]. Several technologies can be adopted for NG-PON2 to respond to the demand for higher bitrates. However, the most likely one to be adopted in the future is a hybrid time-wavelength division

multiplexing (TWDM) architecture where four 10 Gb/s multiplexed channels in the time domain propagate in the same optical fibre at different wavelengths [10].

Whatever the future regarding optical access networks, it is certain that these will provide higher bitrates, extended fibre spans (from 20 km to 50 km or more, from the optical line terminal until reaching the subscriber's home), higher splitter ratios (from 1/32 up to 1/128 or higher) among other factors. Within this evolution, it will become increasingly important to monitor the network infrastructure and the quality of the signals in order to guarantee a good quality of service. With the implementation of optical performance monitoring (OPM) techniques in the network it will be possible to analyse the signals impairments such as power, noise, and dispersion and help identify eventual faults in the network.

1.3 Signal Impairments

As an optical signal propagates in a fibre, it undergoes several impairments that degrade its quality and limit the transmission performance, such as attenuation, dispersion among others.

The optical signal attenuation, during the propagation in a fibre, can result from several factors: scattering; absorption by the material or even the bending of the fibre. The scattering of photons can be originated by the presence of impurities and homogeneity imperfections in the optical fibre core, creating a spatial variation in the core refractive index that consequently scatters some photons. Absorption is probably the major source of attenuation due to the presence of OH^- ions, which absorb radiation in the following spectral regions: 1.39 μm, 1.24 μm and 0.95 μm. In the past years, single mode fibres manufacturing has evolved and there are SMFs that present reduced OH^- absorption peaks thus increasing the low-loss transmission window [11, 12]. The silica molecules also absorb radiation, mostly at wavelengths lower than 0.4 μm (ultra-violet spectral region) and at wavelengths over 2 μm (infrared spectral region)[13]. In Figure 1.3 is shown the absorption spectrum of different SMFs that were introduced along the years, where the evolution on reducing those absorption peaks is visible.

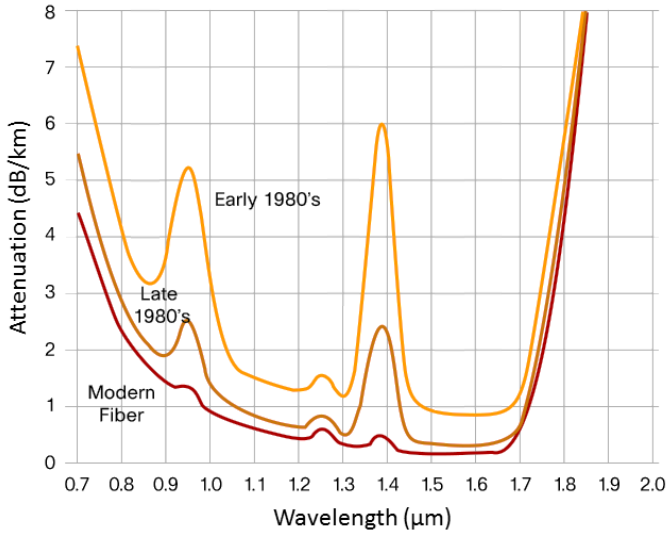

Figure 1.3 - Absorption spectrum of standard single mode fibres [14]

Along with attenuation, the signal is subjected to other impairments such as chromatic dispersion and polarization mode dispersion (PMD). These two phenomena result in the broadening of the signal temporal pulses generated along the propagation.

Chromatic dispersion occurs due to the fact that fibre core refractive index value is dependent on the signal frequency. As a consequence, the different spectral components that compose the signal will propagate at different velocities and induce the pulse broadening. Also, some components propagate in the cladding region (which has different refractive index than the core) which also results in dispersion [2]. In Figure 1.4 is displayed the dispersion of different types of fibres (according to the respective ITU standards) as function of the signal wavelength.

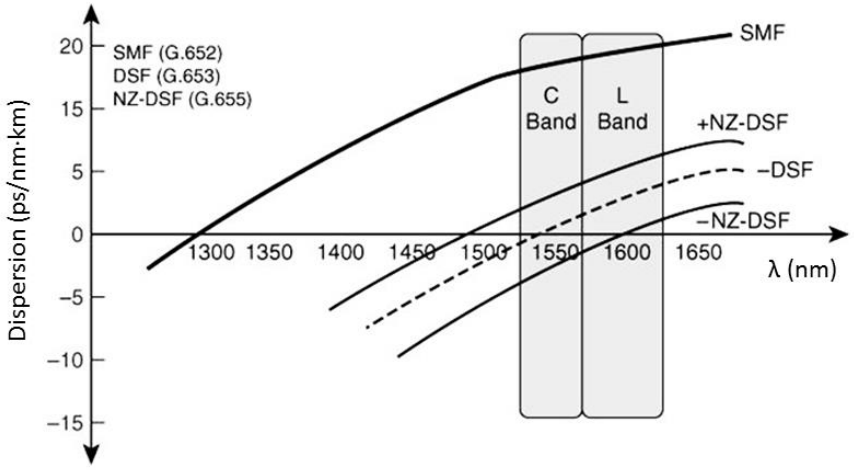

Figure 1.4 - Dispersion of different types of fibres [15]

Standard SMFs have the zero dispersion value at approximately 1310 nm and, at 1550 nm, its value is approximately 18 ps/nm·km. Dispersion shifted fibres (DSF) were developed in order to decrease the amount of dispersion in the 1550 nm region, which is useful due to the low attenuation in this spectral region. However, the absence of dispersion may induce the occurrence of undesired nonlinear effects such as self-phase modulation (SPM), cross-phase modulation (XPM) or four wave mixing (FWM). So, it is important to have a controllable dispersion management mechanism. Non-zero dispersion fibres (NZ-DSF) appear as a response to that need as they present a residual value of dispersion in the 1550 nm window, which can either be positive (+NZ-DSF) or negative (-NZ-DSF).

Besides chromatic dispersion, there is also another phenomenon that can induce pulse broadening. The presence of defects as well as forces applied to the fibre can generate perturbations to its cylindrical geometry. Actually, the fibre core refractive index profile and geometry are not perfectly isotropic being different for each of the orthogonal polarization modes. If the incident signal is composed by polarization components along the two orthogonal directions, they will experience different refractive indexes and, consequently, contribute to the pulse broadening – polarization mode dispersion (PMD) [1]. However, this effect, due to PMD, is usually negligible (mainly on signals modulated up to 10 Gb/s).

Attenuation and dispersion represent the main degrading factors to the quality of the signal transmission. So, besides monitoring the physical integrity of the network it is also important to develop methods that measure these impairment parameters.

1.4 Goals and thesis outline

The main purpose of this work was to study, theoretical and experimentally, optical performance analysers and their application in the next generation optical networks. It was intended to develop methods that enable the monitoring of the quality for a set of optical channels, namely optical signal to noise ratio (OSNR) and dispersion, as well as monitoring the physical integrity of the network.

The overall goal was to develop techniques that met a few fundamental requirements, which were:

- Based on optical processes in order to increase the speed of monitoring;
- Cost-effective solutions;
- Not to interrupt the normal data traffic;
- Suitable for current and next-generation optical networks.

The state of the art regarding this topic is very wide. Methods that measure the data signal parameters or monitor the network are abundant. It is a topic that has been discussed over the past years, but an optimal solution that satisfies all fundamental requirements is unlikely and some compromises must always be made.

In this Ph.D. it was proposed alternative techniques that either provide a simpler solution to the ones presented so far, or a more cost-effective and/or more robust. Three main techniques were developed, each dedicated to the monitoring of a different parameter: OSNR, dispersion and fibre fault. Some of these methods (OSNR and fibre fault monitor) were focused on the use of fibre Bragg gratings (FBG), which presents two main advantages: it is a relatively low-cost component and is a flagship technology implemented in *Instituto de Telecomunicações – Aveiro* (IT-Aveiro).

Each of these methods is covered on an individual chapter of this thesis. So, it is organized and divided into five chapters:

• The first and present chapter includes a brief introduction into the field of optical communications networks and describes the main impairments suffered by the signal; it also mentions the motivation and main goals of this Ph.D. work; a list of the main contributions is presented as well;

• The second chapter is dedicated to the measurement of the signal OSNR: the most relevant methods introduced so far are firstly described in the state of the art section; then the developed approach and respective results (both simulation and experimental) are presented;

• Chapter three covers the group velocity dispersion (GVD) monitoring topic: the state of the art techniques are described in the first section and our alternative technique is presented in the following sections;

• The fourth chapter is focused on the monitoring of the network structure, where, similarly to the previous chapters, the state of the art methods are firstly described and then the proposed method is presented;

• The fifth and last chapter of this document gathers the final conclusions and includes as well a few suggestions for future work.

1.5 Main achievements

The importance of optical performance monitoring in today and next generation networks is unquestionable. So, several techniques have been presented over the past years and the major challenge faced throughout the realization of this work was the development of novel and better ones.

Nevertheless, the investigation of several methods and the respective experimental implementation was achieved. Each of these techniques focuses on the measurement of a different parameter and provides an alternative way to perform monitoring.

To monitor the optical signal to noise ratio (OSNR) of a signal we propose a novel technique based on the implementation of a Bragg grating imprinted on high birefringent fibre. Due to its polarization characteristic, this grating enables the distinction of the signal from the noise making it relatively easy to estimate the OSNR. The dispersion measurement is also studied and a method that is applicable on different modulation formats is presented. It is a simple approach of a known technique and, to the best of our knowledge, it's the first time it is experimentally tested on a phase modulated signal. Finally, a proof-of-concept experiment on the monitoring of an optical access network infrastructure is also presented in this work which is based on the presence of fibre Bragg gratings as monitoring units distributed along the network.

1.6 Contributions

The methods developed during this Ph.D. work have resulted in several publications in both journals and conferences.

Publications in journals:

- **Ana O. P. Sousa**, Carlos A. F. Marques, Rogério Nogueira, Paulo S. André, "OSNR Monitoring Using Fiber Bragg Grating in High Birefringent Optical Fibers", Microwave and Optical Technology Letters, Vol. 55, No. 1, January 2013
- **Ana Sousa**, Paulo André, "Online Group-Velocity Dispersion Monitor Based on Clock Frequency Power Analysis", IEEE Photonics Technology Letters, Vol. 24, No. 17, September 1, 2012

Waiting for approval:

- **Ana Sousa**, Paulo André, "In line 40 Gb.s-1 group-velocity dispersion monitoring", submitted to Microwave and Optical Technology Letters
- **A. Sousa**, A. Shahpari., A. Teixeira, R. Nogueira and P. S. André, "Group-velocity dispersion monitoring for QPSK signals using direct detection", submitted to ETRI Journal

- **Ana O. P. Sousa**, C. A F. Marques, R. Nogueira, P. S. André, "Simplified method for passive optical network fibre-fault monitoring based on fibre Bragg gratings", submitted to Optics Communications

Publications in conferences:

- **Ana O. P. Sousa**, C. A. F. Marques, R. Nogueira, P. S. André, "OSNR Monitoring Using Hi-Bi FBG for 10 Gbit/s Optical Networks", International Conference on Transparent Optical Networks – ICTON, Stockholm, Sweden, June 2011
- **Ana O. P. Sousa**, C. A. F. Marques, R. Nogueira, P. S. André, "Optical Signal to Noise Ratio Monitoring with Hi-Bi Fiber Bragg Grating", 8th Conference on Telecommunications, Lisbon, Portugal, May 2011
- **Ana Sousa**, Carlos Marques, Paulo André, "Innovative OSNR Monitoring Technique Employing HiBi Fibre Bragg Gratings for 10Gb.s-1 Passive Optical Networks", Latin American Optics & Photonics Conference, São Sebastião, Brazil, November 2012
- **Ana O. P. Sousa**, Carlos A. F. Marques, Rogério Nogueira, Paulo André, "Fault Monitoring for Passive Optical Networks Based on Fibre Bragg Gratings", 9th Conference on Telecommunications, Castelo Branco, Portugal, May 2013

References:

[1] G. P. Agrawal, *Fiber-Optic Communication Systems*, Fourth Edition ed.: John Wiley & Sons, Inc., 2010.

[2] R. Ramaswami, K. Sivarajan, and G. Sasaki, *Optical Networks: A Practical Perspective, 3rd Edition*: Morgan Kaufmann Publishers Inc., 2009.

[3] E. Lach and W. Idler, "Modulation formats for 100G and beyond," *Optical Fiber Technology,* vol. 17, pp. 10-10, 2011.

[4] M. Cahill, G. Bartolini, M. Lourie, and L. Domash, "Tunable thin film filters for intelligent WDM networks," *Advances in Thin - Film Coatings for Optical Applications III,* vol. 6286, pp. F2860-F2860, 2006.

[5] C. Rottondi, M. Tornatore, A. Pattavina, and G. Gavioli, "Routing, Modulation Level, and Spectrum Assignment in Optical Metro Ring Networks Using Elastic Transceivers," *Journal of Opical Communications and Networking,* vol. 5, pp. 305-315, 2013.

[6] E. Ip, P. Ji, E. Mateo, H. Yue-Kai, X. Lei, Q. Dayou, B. Neng, and W. Ting, "100G and Beyond Transmission Technologies for Evolving Optical Networks and Relevant Physical-Layer Issues," *Proceedings of the Ieee,* vol. 100, pp. 1065-1078, 2012.

[7] F. J. Effenberger, J. I. Kani, and Y. Maeda, "Standardization trends and prospective views on the next generation of broadband optical access systems," *IEEE Journal on Selected Areas in Communications,* vol. 28, pp. 773-780, 2010.

[8] G. L, P. Garfias, M. D. Andrade, C. Cervelló-Pastor, and S. Sallent, "Next Generation Optical Access Networks: from TDM to WDM," in *Trends in Telecommunications Technologies*, ed, 2010.

[9] G. Kramer, M. De Andrade, R. Roy, and P. Chowdhury, "Evolution of Optical Access Networks: Architectures and Capacity Upgrades," *Proceedings of the Ieee,* vol. 100, pp. 1188-1196, 2012.

[10] Y. Luo, X. Zhou, F. Effenberger, X. Yan, G. Peng, Y. Qian, and Y. Ma, "Time and Wavelength Division Multiplexed Passive Optical Network (TWDM-PON) for Next Generation PON Stage 2 (NG-PON2)," *Journa of Lightwave Technology,* vol. 31, pp. 587-593, 2012.

[11] M. D. Edwards, Vanessa. (2011, 28/2/2013). Next Generation Optical Fibre: Making Your Broadband Network Go Further. *Corning White Papers*. Available: http://www.corning.com/WorkArea/showcontent.aspx?id=39421

[12] E. Desurvire, C. Kazmierski, F. Lelarge, X. Marcadet, A. Scavennec, F. A. Kish, D. F. Welch, R. Nagarajan, C. H. Joyner, R. P. Schneider Jr, S. W. Corzine, M. Kato, P. W. Evans, M. Ziari, A. G. Dentai, J. L. Pleumeekers, R. Muthiah, S. Bigo, M. Nakazawa, D. J. Richardson, F. Poletti, M. N. Petrovich, S. U. Alam, W. H. Loh, and D. N. Payne, "Science and technology challenges in XXIst century optical communications," *Comptes Rendus Physique,* vol. 12, pp. 387-416, 2011.

[13] G. Agrawal, *Nonlinear Fiber Optics*: Elsevier Science, 2010.

[14] (2008, July 17, 2013). Fiber Types in Gigabit Optical Communications. Available: http://www.cisco.com/en/US/prod/collateral/modules/ps5455/white_paper_c11-463661.html

[15] R. Wood, *Next-Generation Network Services*: Cisco Press, 2006.

Chapter 2: Optical Signal to Noise Ratio (OSNR) monitoring

2.1 Introduction

The noise is a major impairment in optical communication networks. The largest contribution of noise comes from the optical amplifiers deployed throughout the network that, besides amplifying the data signal, also amplify the effect of spontaneous emission (a phenomenon that occurs during the amplification process), generating the so called amplified spontaneous emission (ASE) noise.

While propagating through the network, the optical data signal is degraded by this effect. The generated ASE noise can reach a high power level, becoming very hard to distinguish the data signal from the noise. Therefore it is important to measure and control the amount of optical noise and compare it to signal power, the so called optical signal to noise ratio (OSNR).

The OSNR monitoring becomes more important in the core/metro regions than in the access networks, due to the use of EDFAs. In access networks the presence of EDFAs is not mandatory as the signals travel along a limited fibre span. However, due to attenuation, the OSNR can decrease along the propagation, because the noise may reach such a low level (as well as the signal) that the receiver thermal noise becomes predominant. Therefore, monitoring the OSNR enables the direct analysis on the quality of the signal, preventing that kind of signal quality loss.

2.1.1 Definition

The OSNR measures the ratio between the signal power and the amount of noise present in a given optical bandwidth and is defined by the following expression:

$$OSNR = 10 \cdot \log_{10}\left(\frac{P_{signal}}{P_{noise}}\right), \tag{2.1}$$

where P_{signal} is the data signal optical power and P_{noise} is the noise optical power. The OSNR can be determined through the analysis of the signal optical spectrum obtained usually with an optical spectrum analyser (OSA). In Figure 2.1 is shown a typical optical spectrum of a multiplexed signal and displays the definition used to estimate the OSNR.

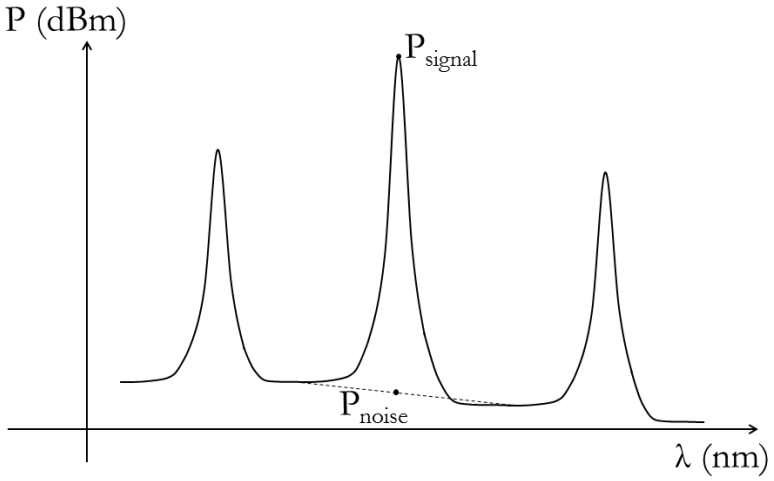

Figure 2.1 - Optical spectrum of a signal showing the optical power as function of the wavelength. The noise optical power is estimated by interpolation of the adjacent noise levels at the channel wavelength.

The noise power at the channel wavelength is determined by measuring the optical power present at a specific spectral distance and interpolating it to the wavelength of the channel (as illustrated in Figure 2.1).

To measure the OSNR using an OSA it is mandatory to take into account the resolution of the equipment. Through this method, spectra with different resolutions will give different noise levels and consequently different values for OSNR. So, in order to normalize the OSNR values given by different devices, a standard has been defined. This definition states that the OSNR is measured taking into account the amount of noise present in a 0.1 nm bandwidth [1].

Throughout this chapter, this standard definition has been used and all obtained results regarding the OSNR were compared to this standard.

2.2 State of the Art

Several techniques to monitor the OSNR of a signal have been introduced over the past years. Before describing our own approach to this issue, some of the most relevant methods introduced so far are presented here. All of them, as well as the one proposed, present their own advantages and disadvantages when it comes to the application in a real network.

Linear interpolation

This first method principle operation is very straight forward. Actually, most of the monitoring solutions commercially available apply this concept. Companies like *Optoplex* and *Aegis Lightwave* are examples that commercialize this type of monitors [2, 3].

This method is based on the application of a diffractive grating or a tuneable optical filter that sweeps the spectral region of measurement. Then, a photodetector collects the optical signal along the spectral band and the OSNR is estimated by linear interpolation of the noise level in between the channels, as is illustrated in Figure 2.1.

This solution can be very useful for static networks. However, in a dynamic network, each optical channel propagates through different paths and distances and ends up gaining different amounts of noise. The presence of optical filters, for instance in ROADMs, modifies the amount of noise present in the adjacent spectral components of the channel. So, this technique becomes erroneous for these scenarios, overestimating the value of OSNR. This overestimation is illustrated in Figure 2.2 where the OSNR measured through the conventional method is higher than the real one [4].

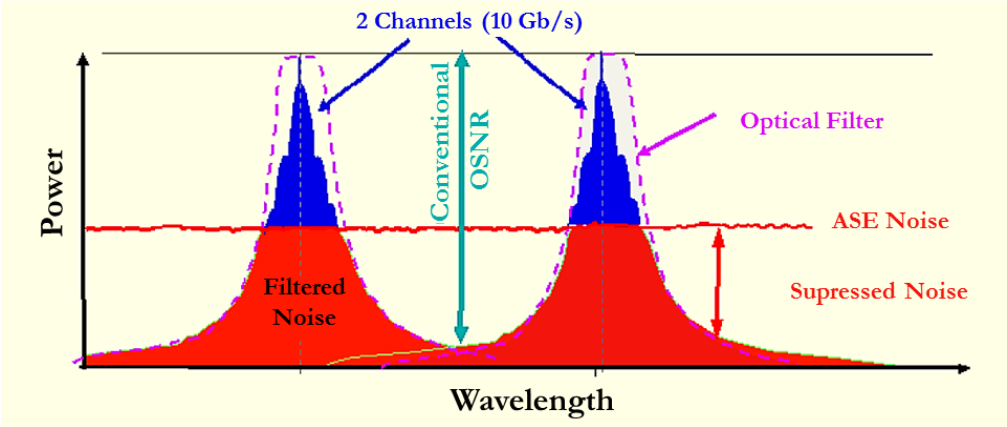

Figure 2.2 - Linear interpolation principle of operation. This method can overestimate the OSNR. In the illustrated situation the real OSNR is lower than the estimated through linear interpolation [4]

To overcome this issue other techniques more adequate for this kind of networks, which allow a more precise OSNR measurement, have been introduced [5].

Polarization-nulling

The polarization-nulling techniques make use of the signal polarization characteristic to distinguish it from the noise. By assumption that the signal is linearly polarized while the noise is totally depolarized, it is possible to measure the OSNR [6].

In Figure 2.3 is displayed a diagram that explains the principle of this method.

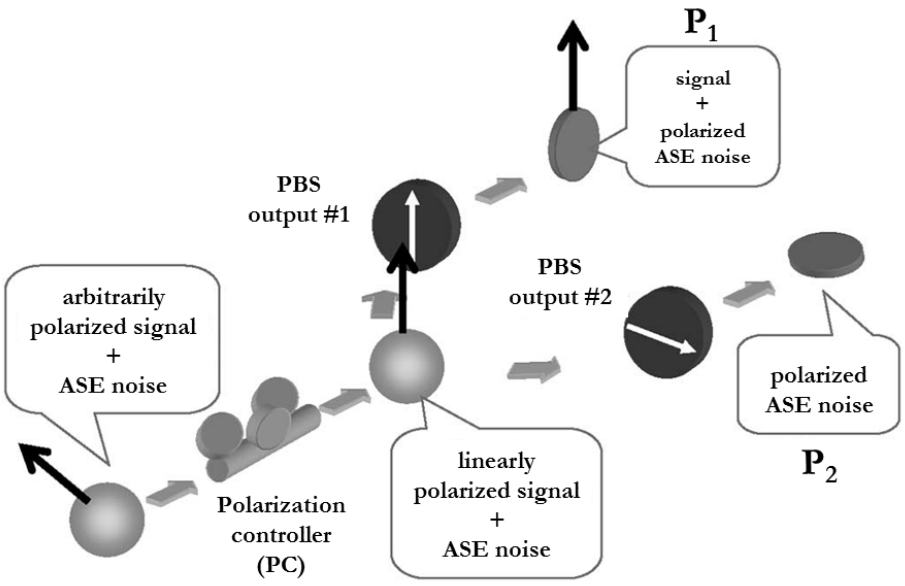

Figure 2.3 - Principle behind the polarization-nulling method [6]

A polarization controller (PC) and a polarization beam splitter (PBS) are used in order to split the incoming signal into two orthogonal components, where one (P_1) will contain the data signal plus 50% of the noise contribution and the other (P_2) will contain the remaining 50% of the noise. By measuring the optical power from both outputs is possible to estimate the OSNR of the signal:

$$P_1 = P_{signal} + \frac{1}{2} P_{noise} \ , \tag{2.2}$$

$$P_2 = \frac{1}{2} P_{noise} \ . \tag{2.3}$$

So, the OSNR will be given by:

$$OSNR = 10 \cdot \log_{10} \left(\frac{P_1 - P_2}{2P_2} \right) . \tag{2.4}$$

There are alternative methods to the previously described one. These take into account the fact that the signal might suffer depolarization from, for instance, polarization mode dispersion or birefringence. For these cases, the polarization of the signal will not be perfectly linear and the technique that was described just now will give inaccurate OSNR.

In Figure 2.4 is schematized the operation principle of an alternative method that takes into account the depolarization o the signal.

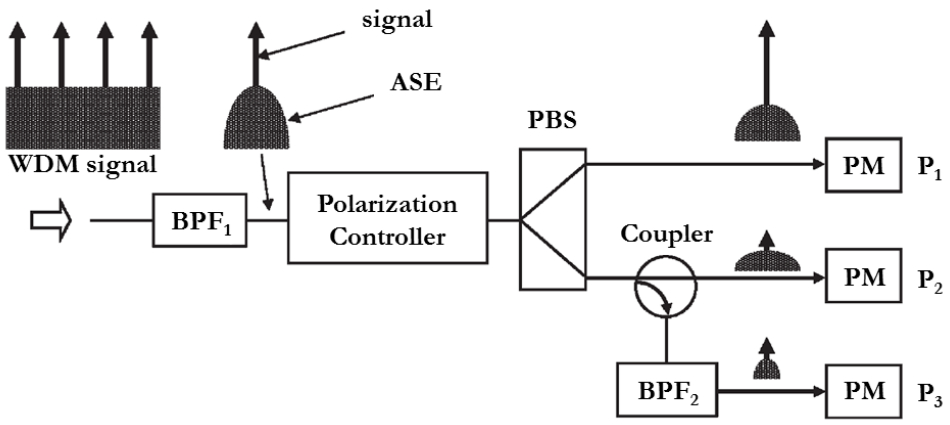

Figure 2.4 - Principle of operation of a polarization nulling technique that takes into account an eventual depolarization of the signal [6]

A bandpass filter (BPF_1), that allows the selection of the channel to be monitored, is placed before the signal enters the monitor. Then, the signal and ASE noise pass initially through polarization controller and a PBS which has orthogonal outputs. At one of those outputs the optical power is measured using a power meter (PM). The polarization controller is adjusted so that the measured power P_1 is maximized. If the signal is totally polarized, this situation is equivalent to the previous one. But in the scenario where the data signal gets depolarized, a portion of the signal power is forwarded to the other output of the PBS. A 3 dB coupler is placed at that output of the PBS and, at one of the outputs of the coupler, an optical filter is applied (BPF_2). This optical filter (BPF_2 in Figure 2.4) has a narrow bandwidth that allows the reduction on the noise bandwidth. This way:

$$P_1 = P_{signal} \cdot (1-\varepsilon) + \frac{1}{2} \cdot P_{noise} \ , \tag{2.5}$$

$$P_2 = \frac{1}{2} \cdot P_{signal} \cdot \varepsilon + \frac{1}{4} \cdot P_{noise} \ , \tag{2.6}$$

$$P_3 = \frac{1}{2} \cdot P_{signal} \cdot \varepsilon + \frac{1}{4} \cdot \alpha \cdot P_{noise} \ , \tag{2.7}$$

where ε is the depolarization factor and α is the reduction factor of the filter bandwidth. This method is able to return more reliable results than the one described previously. However, the synchronization between the two optical filters can become quite difficult.

In Figure 2.5 is shown the principle of operation of another technique that returns the OSNR of a channel taking into consideration the depolarization of the signal due to nonlinear birefringence.

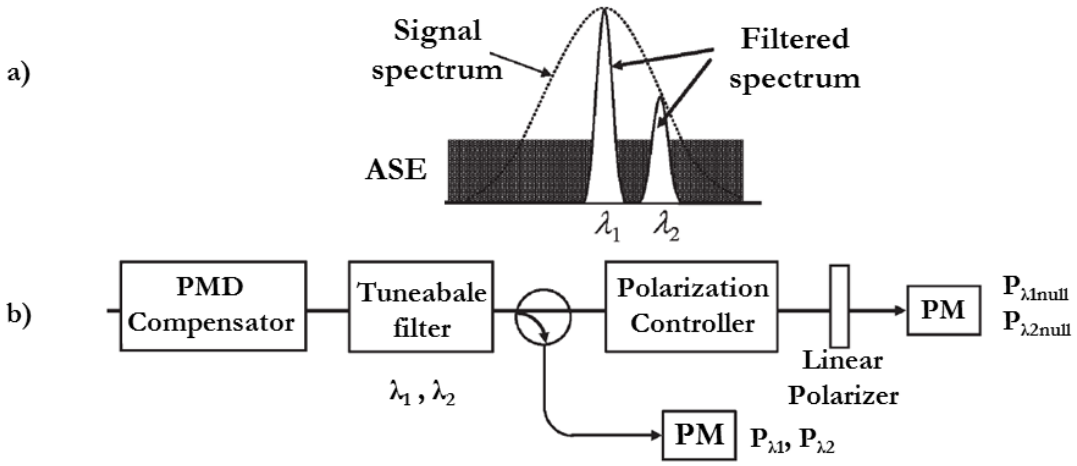

Figure 2.5 - Polarization-nulling technique: a) representation of the narrow bandwidth filters; b) experimental setup [6]

This technique applies a tuneable optical filter with a bandwidth much narrower than the signal spectrum as you can see in Figure 2.5 a); its experimental setup is displayed in Figure 2.5 b).

Initially, the signal passes through a PMD compensator in order to eliminate PMD effects on the OSNR measurement. At the output of the PMD compensator is used a filter that is tuned to the signal wavelength (λ_1) and the signal power is registered ($P_{\lambda 1}$). Then, the polarization controller and the linear polarizer are adjusted so that the components orthogonal to the signal are measured by the power meter ($P_{\lambda 1null}$). This procedure is repeated with the filter tuned to λ_2, a wavelength slightly deviated from the signal central wavelength, and the optical power values $P_{\lambda 2}$ and $P_{\lambda 2null}$ are registered:

$$P_{\lambda 1_{null}} = \left(P_{\lambda 1} - P_{noise}\right) \cdot \varepsilon_{NL} + \frac{1}{2} \cdot P_{noise} \ , \tag{2.8}$$

$$P_{\lambda 2_{null}} = \left(P_{\lambda 2} - P_{noise}\right) \cdot \varepsilon_{NL} + \frac{1}{2} P_{noise} \ , \tag{2.9}$$

where ε_{NL} is the depolarization factor due to nonlinear birefringence. So, P_{noise}, can be estimated by the elimination of ε_{NL} from the equation system:

$$P_{noise} = \frac{2 \cdot \left(P_{\lambda 1} \cdot P_{\lambda 2_{null}} - P_{\lambda 1_{null}} \cdot P_{\lambda 2}\right)}{P_{\lambda 1} - P_{\lambda 2} - 2 \cdot P_{\lambda 1_{null}} - 2 \cdot P_{\lambda 2_{null}}} \ . \tag{2.10}$$

The methods described in this section allow the monitoring of the OSNR of a channel even in scenarios of signal depolarization using entirely all optical processes.

Making use of the polarization characteristic of the signal provides an efficient method to measure the OSNR. With a more complex setup it is even possible to take into consideration eventual

depolarization of the signal. However those techniques require optical filters that increase the difficulty of the measurement losing its robustness.

Interferometry

Another set of measurement techniques is based on the application of an interferometer that, by assuming that the data signal is coherent, will induce interference at the output. As the noise is considered incoherent, those components will not interfere making it possible to retrieve the OSNR

In reference [7], a technique based on this basic principle is presented where an interferometer is applied, as it can be seen in Figure 2.6:

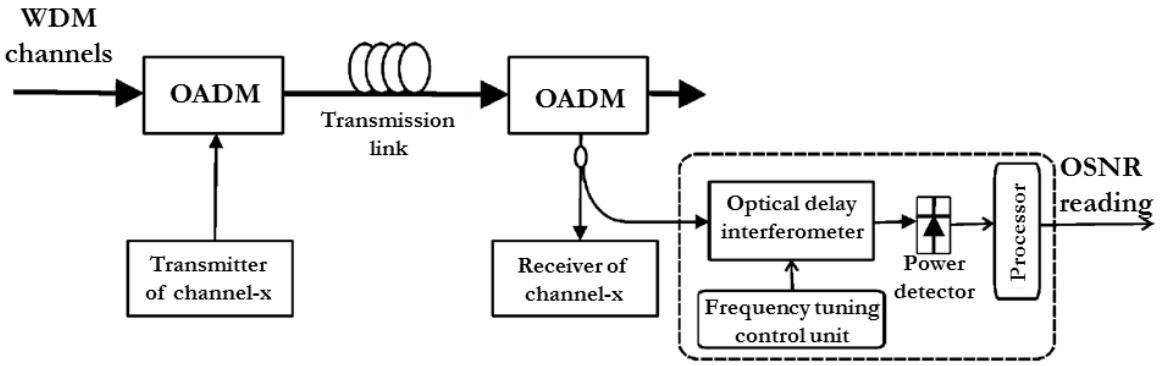

Figure 2.6 - Interferometer based OSNR monitor [7]

After selection of the channel by the optical add drop multiplexer (OADM), the signal passes through an optical delay interferometer whose response is sinusoidal and tuneable. A slow photodiode measures the optical power and extracts the maximum and minimum optical powers. It takes into account the ratio between the maximum and minimum signal power when noise is absent (*s*) and when the signal is absent (*n*). As the noise is considered to be white, *n=1*. The factor *s* is dependent of the signal extinction ratio (ER). For an OOK modulated signal the OSNR will obey the following expression:

$$OSNR = \frac{NEB}{0.1nm} \cdot \left(\frac{1+2\cdot\sqrt{\frac{1}{ER}-\frac{1}{ER^2}}}{R-1} - \frac{1-2\cdot\sqrt{\frac{1}{ER}-\frac{1}{ER^2}}}{2} \right)^{-1}, \qquad (2.11)$$

where *NEB* is the noise equivalent bandwidth and *R* is the ratio between the maximum and minimum optical power values. In Figure 2.7 is shown the results obtained in [7] using this technique.

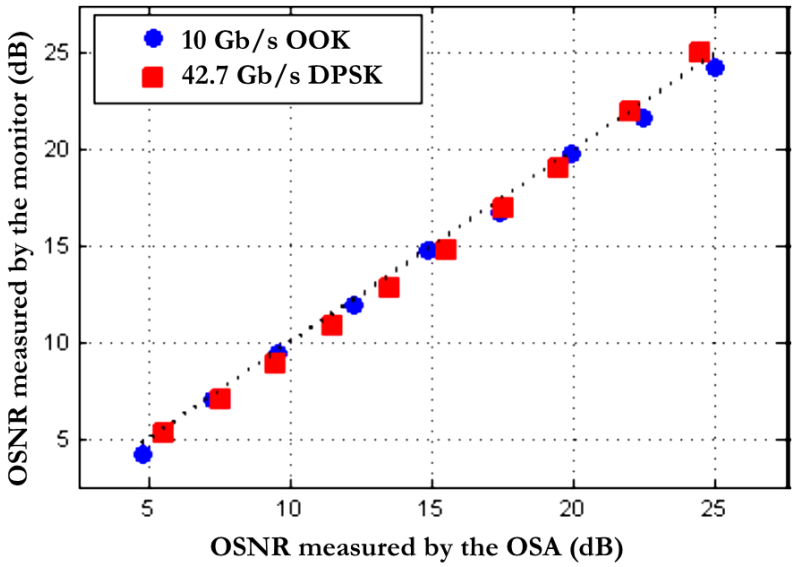

Figure 2.7 - Results obtained from the interferometer based method for OOK and DPSK modulated signals [7]

Figure 2.7 shows two sets of results: for an amplitude modulated signal (OOK at 10 Gb/s) and for signal modulated with differential phase shift keying (DPSK) format at 42.7 Gb/s. Both results (OOK and DPSK) show a good agreement (maximum error of 0.5 dB) with the reference OSNR which was measured with an OSA [7].

As the interferometer response is dependent on the wavelength, it functions as a filter that, in constructive mode, its maximum is centred at the signal wavelength and, in the destructive mode, is a notch filter centred at the signal wavelength. Depending on its free spectral range, in the destructive mode, components of the data signal can also be measured by the detector and induce measurement errors [8]. This issue can become more relevant in WDM systems, where the neighbouring channels aren't efficiently rejected.

Pilot tones

The pilot tone technique consists on adding a low frequency subcarrier, designated pilot tone, to the signal. This pilot tone is propagated along with the data signal suffering the same degradation as the signal. In Figure 2.8 is depicted the principle for this method [9].

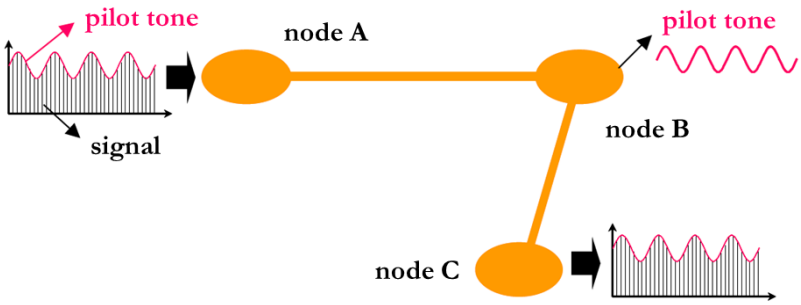

Figure 2.8 - Pilot tones technique basic principle of operation [9]

In this illustrative example, the data signal is generated at the transmitter (A) and is sent to the receiver (C) passing by the monitoring node (B). The pilot tone is added to the signal at the transmitter and travels along with it until it reaches the monitoring node (B), where it is extracted and analysed. The addition of the pilot tone can be accomplished by implementing dithering (application of a small, low frequency variation at the electric current level) electric current to the laser. In a multichannel system, a pilot tone with a different frequency can be added to each channel.

To measure the OSNR, a pilot tone with a frequency outside the bandwidth of the signal can be added. Then, analysing the radio frequency spectrum and measuring the carrier-to-noise ratio (CNR) of the pilot tone frequency component, the OSNR can be estimated. This can be seen in Figure 2.9.

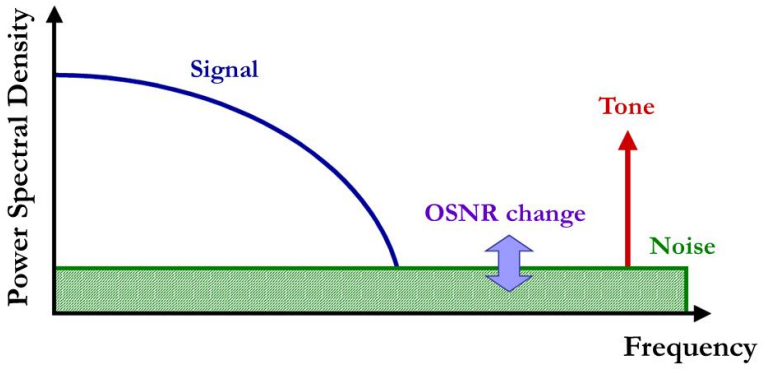

Figure 2.9 - OSNR estimation from the pilot tone electric spectrum [9]

Thus, the OSNR can be obtained by:

$$OSNR = \sqrt{\frac{B_{ESA}}{\Delta\nu}}\frac{CNR}{m^2}\ , \tag{2.12}$$

where B_{ESA} is the electric spectrum analyser resolution bandwidth; $\Delta\nu$ is the optical bandwidth; and m, the modulation depth of the subcarrier. With this technique it was possible to retrieve the OSNR in a range of [0-25] dB with an error smaller than 2 dB [10].

This technique presents several advantages such as the simplicity of the monitoring unit which provides a low cost solution. However, every transmitter must be slightly modified in order to add the subcarrier components [9].

Stimulated Brillouin Scattering

The stimulated Brillouin scattering (SBS) occurs due to the fact that materials have tendency to become denser in the presence of high power radiation (electrostriction). A signal propagating in a highly nonlinear fibre (HNLF) induces variations on the core density, which generate the scattering of the signal: an acoustic phonon with a certain frequency is created and the incident signal is backscattered suffering a spectral deviation [11]. Figure 2.10 illustrates this phenomenon showing the generation of the acoustic phonon and the consequent scattering of the incident signal.

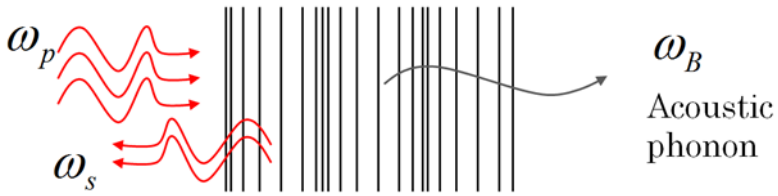

Figure 2.10 - Stimulated Brillouin scattering. ω_P is the incident pump signal frequency; ω_S the scattered frequency and ω_B the acoustic phonon frequency, so $\omega_P = |\omega_S| + |\omega_B|$.

The effectiveness of this effect is related to the peak spectral power density of the incident signal. Therefore, the amount of noise present in the channel will have an influence on this effect that will be directly related to power of the backscattered signal. So, it is possible to make use of this phenomenon to monitor the OSNR of a channel: when noise level is high, the reflected power will be lower than the one reflected when the channel is noise free.

This principle was tested successfully on a WDM of 3 channels, where the OSNR was measured in a range of [10-25] dB. Those results can be seen in Figure 2.11 [12].

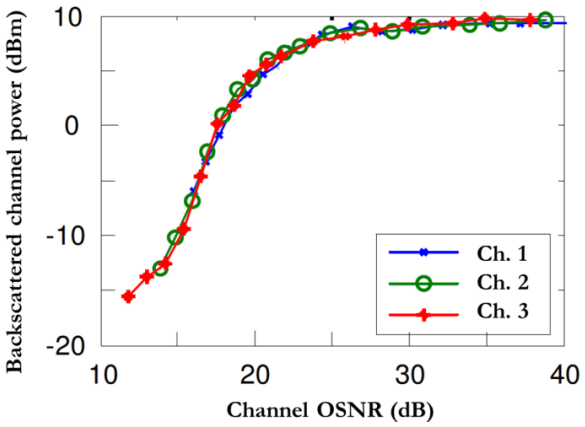

Figure 2.11 - Results for OSNR estimation through the SBS based technique [12]

However, one of the challenges faced was the Brillouin scattering generated by the presence of SPM and XPM. These two nonlinear effects induce attenuation on the signal reflected power, decreasing the OSNR measurable range. This effect can be even more aggravated with the presence of more channels. However, it is possible to overcome this limitation by inducing a slight dispersion to the signals, which will decrease the signal peak power and, consequently, eliminate the SPM and XPM effects [12].

Summary

In this section, the most relevant OSNR monitoring techniques introduced so far were described. It is shown that an optimal solution is difficult to achieve, with all techniques presenting their own advantages and disadvantages.

Linear interpolation is a simple method, but is becoming outdated due to the transition of WDM channels and the increase of routers in the network.

Polarization-nulling is, probably, the most efficient way to estimate the OSNR because of the polarization characteristic of the transmitted signals, which are linearly polarized on contrary to the noise. Even when the signal is slightly depolarized it is possible to measure the OSNR. However that requires more complex setups.

Interferometry based techniques also make use of a characteristic that differentiates the signal from the noise which is, in this case, the coherence. However, for the destructive interference situation, the interferometer will act as a notch filter centred at the channel wavelength, which may lead

to measurement errors, if it presents a short free spectral range, as some components from the signal can also be detected.

The methods based on pilot tones present a key advantage which is the fact that several parameters can be measured including such as the OSNR and the dispersion of the signal. By adding different "tones" to different channels, multi-channel monitoring is also possible. However, it requires a modification at the transmitter level in order to add the pilot tone, which can be a major drawback for the application of this method.

Stimulated Brillouin based technique also allows the monitoring of several channels, as the frequency of the scattered signal will be different for each channel. However, for this type of methods, the incident signal must have high intensity power in order to induce Brillouin scattering.

To illustrate the relevance of this topic, in Figure 2.12 is displayed the number of publications per year with the keywords "OSNR" and "monitoring" according to ISI Web of Knowledge, obtained on May 20th of 2013.

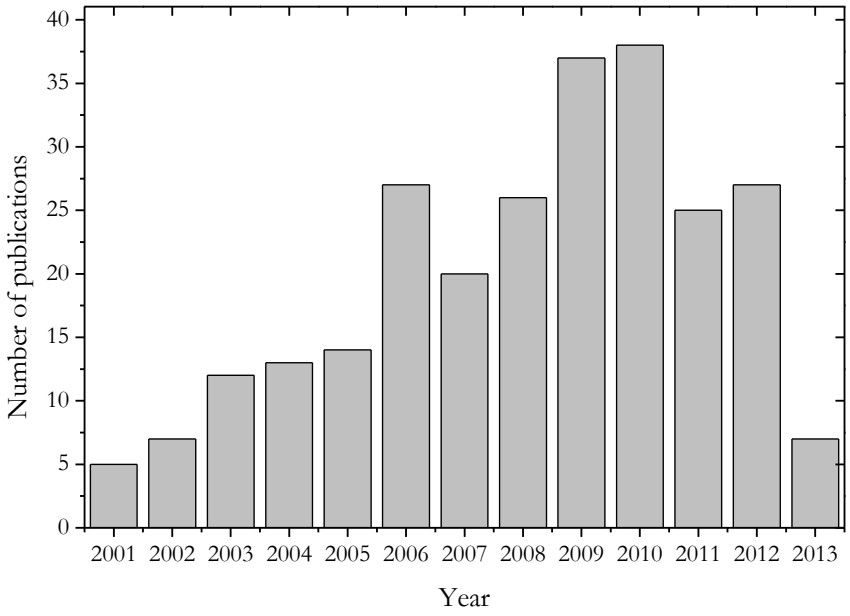

Figure 2.12 - Number of published works on the topic of "OSNR monitoring" throughout the past years

In the last seven years, this topic has been widely studied as it can be seen from the data in Figure 2.12. Up to 2010, the number of publications has increased and seems to stagnate after that. However, besides showing a small portion of 2013, this chart doesn't consider the works waiting for official publication of the past months (early 2013).

2.3 Implemented OSNR monitors

2.3.1 High Birefringent Fibre Bragg gratings (HiBi FBG)

The methods presented in this thesis are based on the application of Bragg gratings imprinted in high birefringent (HiBi) fibres. The main motivation for this approach was already mentioned and is two-fold: FBGs are relatively inexpensive and end up providing a cost-effective solution; and the imprinting process of the gratings is one of the flagship technologies in IT-Aveiro, which makes them easily available.

A Bragg grating is produced by imposing, in the core of the optical fibre, a periodic perturbation in the refractive index along the propagation axis. This perturbation will induce reflection of the incoming optical signal at spectral components centred in a specific wavelength, usually called the Bragg wavelength. The perturbation in the refractive index is accomplished by exposing the core of the optical fibre to a ultra-violet (UV) optical source. Using a phase mask, an interference pattern over the optical fibre is achieved, which will affect only the refractive index of the exposed zones as illustrated in Figure 2.13.

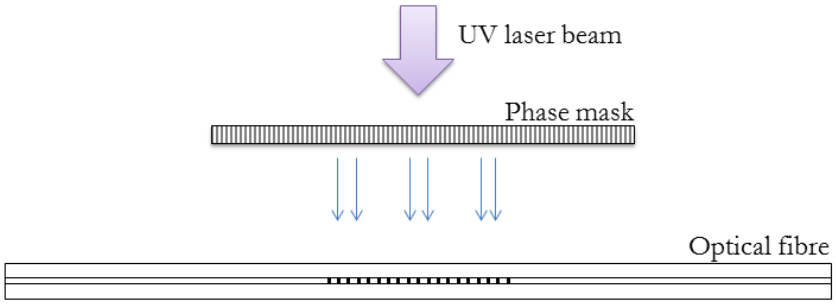

Figure 2.13 - Bragg grating imprinting process using the phase mask method.

When an incident signal reaches this zone, the spectral components around the Bragg wavelength (λ_{Bragg}), will be reflected according to following expression, which is the Bragg law.

$$\lambda_{Bragg} = 2 \cdot n_{eff} \cdot \Lambda \ , \tag{2.13}$$

where n_{eff} is the effective refractive index and Λ is the period of the refractive index perturbation.

In Figure 2.14 is shown the spectral reflection response of a typical uniform Bragg grating.

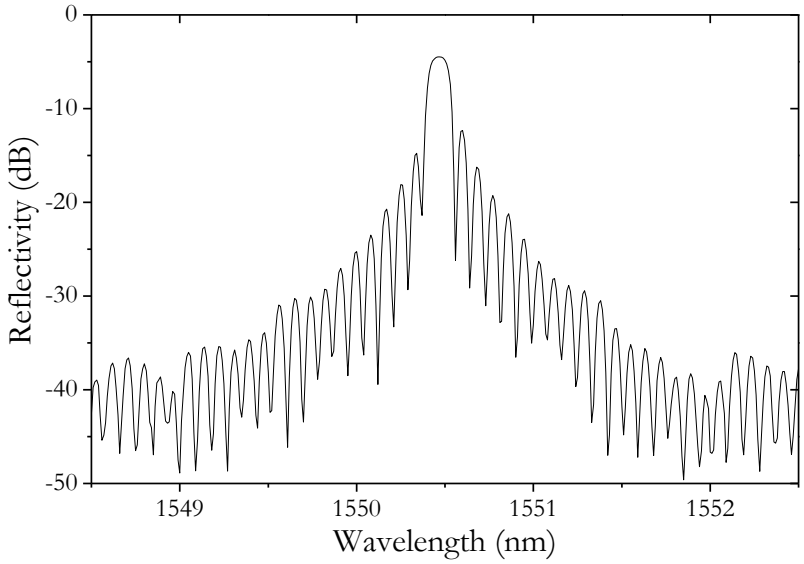

Figure 2.14 - Typical reflection response of a uniform FBG measured with an optical resolution of 0.01 nm

The uniform fibre Bragg grating whose spectrum can be seen in Figure 2.14 was imprinted by phase mask method using a 500 Hz pulsed KrF excimer laser (λ=248 nm), with an exposure time of 10 s. The used phase mask had a period of 1072.55 nm and the grating has a length of 6 mm with a Bragg wavelength of 1550.46 nm.

While the standard single mode fibres have a core with cylindrical symmetry along the propagation axis, for a high birefringent fibre this symmetry is lost. The geometry of the high birefringent fibre presents an asymmetry that will consequently affect the values of the effective refractive index, so it will present two different refractive indexes, one per optical axis, n_x and n_y. In Figure 2.15 is shown the example of a cross section from a typical high birefringent fibre.

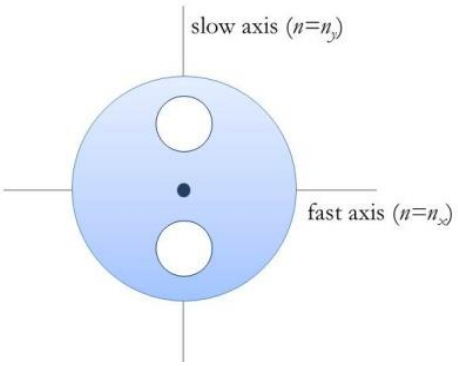

Figure 2.15 - Typical cross section of a high birefringent optical fibre

The white circles represent two holes that are in the cladding area. This structure induces the alteration of the refractive indexes at the core (blue small circle in the centre). When an incident optical signal, with orthogonal polarization components along the two optical axes, propagates along a

HiBi fibre, each of the orthogonal components will experience a different refractive index and consequently will propagate with different velocities causing the signal dispersion.

A Bragg grating imprinted on this type of fibre will then generate a spectral response dependent on the signal polarization resulting in two different Bragg wavelengths, one per optical axis, as it can be deduced from the Bragg law in the following expressions:

$$\begin{aligned} \lambda_{Bragg\_x} &= 2 \cdot n_x \cdot \Lambda \\ \lambda_{Bragg\_y} &= 2 \cdot n_y \cdot \Lambda \end{aligned} . \tag{2.14}$$

The reflection response of a HiBi FBG can be considered as the equivalent to the sum of two uniform Bragg gratings, centred at different Bragg wavelengths, each one corresponding to a different polarization state. The spectral difference between the two Bragg wavelengths is related to the birefringence (*B*) of the fibre:

$$\Delta\lambda = 2 \cdot B \cdot \Lambda, \qquad \text{where } B = \left| n_x - n_y \right| \tag{2.15}$$

Throughout the realization of this work and the experimental setups implementations, several HiBi FBGs were used. In Figure 2.16 are displayed the reflection responses of the used HiBi FBGs for a depolarized incident signal, measured with an optical resolution of 0.01 nm with an optical network analyser (ONA).

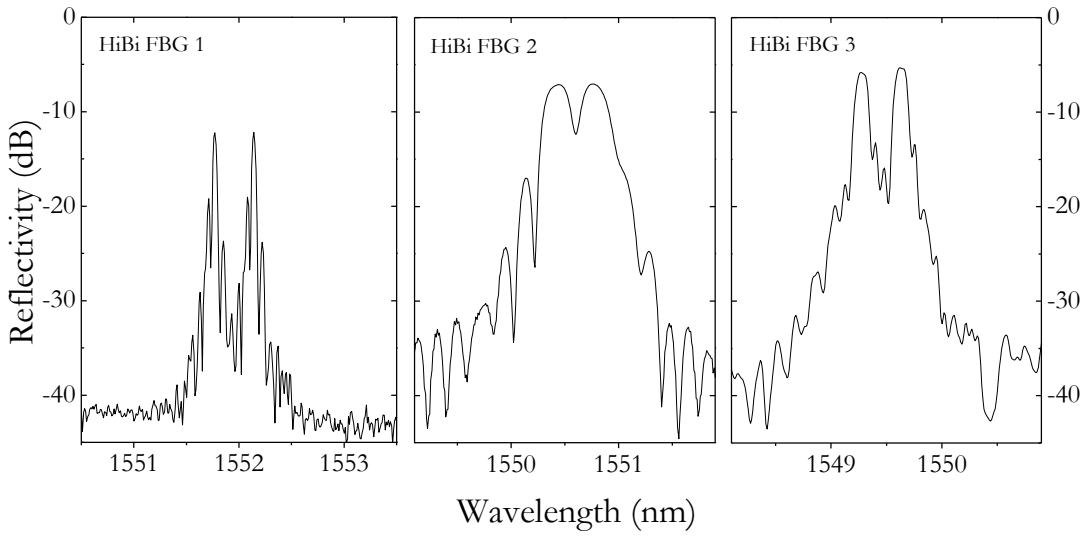

Figure 2.16 - Reflection spectral responses of the HiBi FBGs used in this work

The two reflection bands on each of the reflection spectra are clear in Figure 2.16. The spectral components reflected at each of these bands are linearly polarized along the direction of the corresponding optical axis and are orthogonal to each other.

All three HiBi fibres are Panda type optical fibres HP-1550 (Thorlabs) where the Bragg grating was imprinted using the phase mask method. The same UV source, which was a pulsed (500 Hz) KrF excimer laser signal, peaking at 248 nm was used on all of them for the imprinting process. However, in these cases, the laser is not static and sweeps the phase mask in order to expose a longer length of the fibre core.

The differences between these HiBi FBGs are clear when observing the spectrum on Figure 2.16. The parameters used for the imprinting process and the characteristics of their reflection spectral responses are summarized on Table 2.1.

Table 2.1 - Summary of the HiBi FBG imprinting parameters and spectral reflection characteristics

	HiBi FBG 1	**HiBi FBG 2**	**HiBi FBG 3**
Period of the phase mask	1073 nm	1071.45 nm	1070.34 nm
Length of the grating	35 mm	10 mm	32 mm
Sweeping speed	0.4 mm/s	0.14 mm/s	0.2 mm/s
Bandwidth (at -3dB)	0.05 nm	0.25 nm	0.15 nm
Spectral distance between the two reflection bands centres	0.37 nm	0.33 nm	0.37 nm
Sideband rejection	30 dB	33 dB	35 dB

The spectral distance between the Bragg wavelengths, which depends on the fibre birefringence, should be common to all the gratings. The variation verified is due to measurement errors associated to the large width of some of the reflection bands.

2.3.2 Description of the proposed techniques

To analyse the quality of service (QoS) in optical networks, a method to measure the OSNR of an optical signal was developed and different variations of the same basic principle were studied through simulations as well as experimentally.

All of the methods described here rely on the same assumption that the channel to be monitored is composed by a data signal that is linearly polarized and a noise component that is totally depolarized. So, we make use of the polarization properties of the HiBi FBG in order to distinguish the signal from the noise and consequently estimate a value for the OSNR.

As it was mentioned before, a HiBi FBG generates two reflection bands centred at different Bragg wavelengths. The reflected spectral components, from each of these bands, are linearly polarized along the direction of the corresponding optical axis and are orthogonal to one another.

By matching the Bragg wavelength to the signal wavelength and by aligning the signal state of polarization to the corresponding optical axis, the reflection condition is achieved and the signal is reflected. The noise is depolarized, resulting that only 50% of its contribution will be reflected at each of the two reflection bands. Therefore, in one of the reflection bands is present the data signal (P_S) and 50% of the noise (P_N), while the other reflection band will contain 50% of the noise contribution.

The first developed technique proposes the measurement of the two reflected spectral components optical powers (P_1 and P_2) separately in order to determine the OSNR which, through the following relations, is possible:

$$\begin{aligned} P_1 &= P_S + \frac{1}{2} P_N \\ P_2 &= \frac{1}{2} P_N \end{aligned} \quad . \tag{2.16}$$

So, the OSNR can be determined by:

$$OSNR = 10 \cdot \log\left(\frac{P_1 - P_2}{2 \cdot P_2} \right) . \tag{2.17}$$

This operation principle was tested primarily on a continuous wave (CW) single channel and then on a 10 Gb/s modulated single channel. The application of this method on a multi-channel system was tested as well, by mounting a two-channel system based on CW signals. The purpose of this last experiment was mainly to understand how the presence of a neighbouring channel would influence the measurement of the monitored channel OSNR and, in the case that it does, find a solution for this issue.

The second proposed technique varies from the latter in the fact that instead of analysing only the reflection side, we also take into account the transmission side of the HiBi FBG. This variation will provide a simpler setup than the previous one. By placing an optical filter, the selection of one of the HiBi FBG reflected bands, the one that matches the wavelength of the signal, is done. Then, both the reflected and the transmitted optical power of those spectral components are measured. The optical power values at the HiBi FBG reflection (P_{ref}) and transmission (P_{tr}) ports were measured with a power meter and the ratio between them (R) was defined as follows:

$$R(dB) = 10 \cdot \log\left(\frac{P_{ref}}{P_{tr}} \right) . \tag{2.18}$$

The signal OSNR is also determined through an OSA applying the standard definition, and by plotting the *R vs OSNR* it becomes possible to estimate the OSNR. This method was tested on a CW and then on a 10 Gb/s modulated single channel system.

2.3.3 Simulation Description

All the simulations presented in this document were performed in *Matlab*, where dedicated scripts were developed. The realization of these simulations has two main purposes. They give an extra validation to the experimental results and, once the simulation and experimental processes are in agreement, the simulation becomes a tool for future application of similar setups.

In the proposed methods, several tests were performed using both CW and modulated signals. To emulate the spectrum of the CW signal, a Gaussian function was used and, to represent the noise, a random function, whose level is controllable, is combined with the Gaussian. For the case of the modulated signal, a time domain signal is generated, to which white noise is added. Then, the time domain signal is converted into the frequency domain via Fast Fourier Transform (FFT) and the optical spectrum of the combined (data + noise) signal is determined.

The combined signal spectrum (data signal + noise) is divided into the two orthogonal components and each of them is multiplied to the corresponding spectral responses of the components used in the experiment, such as an optical filter or/and the reflection (or transmission) of the HiBi FBG. In all simulations, the real responses of the HiBi FBGs and optical filter, extracted previously from the ONA, were applied.

The output spectra are then determined and the corresponding optical powers are given by the integral of the respective spectrum.

2.3.4 Experimental Implementation and Results

2.3.4.1 Based on the HiBi FBG Reflection

The performance of this proposed monitoring technique was initially tested for a CW signal and then for a 10 Gb/s modulated signal using the experimental setup illustrated in Figure 2.17.

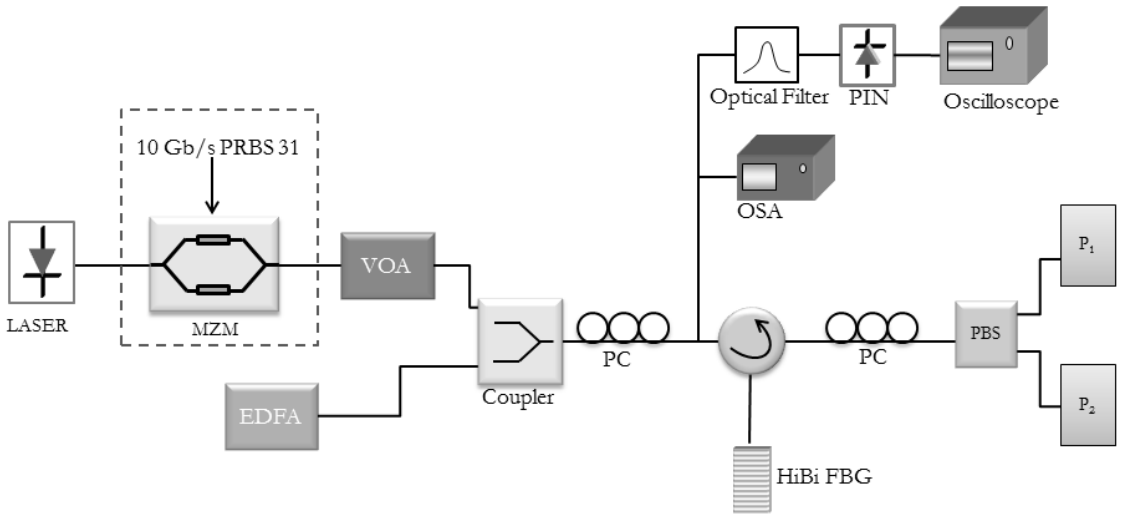

Figure 2.17 - Experimental setup implemented to test the method on a CW and 10 Gb/s signal

The test data signal is produced by a distributed feedback (DFB) laser peaking at a wavelength coincident with one of the HiBi FBG reflection bands. Then, in the scenario of a CW signal, it goes directly to a variable optical attenuator (VOA) which is used to adjust the data signal power and thus control the signal OSNR. For the modulated signal scenario, before reaching the VOA, the optical signal is externally modulated using a Mach-Zehnder modulator (MZM) with a pseudo-random binary sequence (PRBS) of 2^{31}-1 bits, at a bitrate of 10 Gb/s.

An EDFA is used as a white noise source which is added to the signal through an optical coupler. The combined optical signal passes through a PC, to adjust the data signal polarization with the corresponding optical axis of the HiBi fibre. Hence, the reflection of the data signal is maximized. The noise is totally depolarized and only 50% of its contribution will be reflected at each of the two bands. The spectral distance between the reflection bands is not large enough to observe changes in the noise power, so the amount of noise reflected at each bands is considered constant. The use of another polarization controller and a PBS allows the isolation of these two reflection bands. However, this could also be accomplished with an optical filter that would do the selection of the bands. The measurement of the optical powers P_1 and P_2 allows the determination of the OSNR using the expression in (2.17). The obtained OSNR values were compared to the real ones obtained with an OSA from Advantest (Model Q8384). The OSNR is determined by the standard definition that relates the power of the data signal with the power of the noise present in a bandwidth of 0.1 nm.

The attenuation set at the VOA is varied in order to have different values for the OSNR. In Figure 2.18 is shown the obtained results for the CW signal, showing the estimated OSNR as function of the real OSNR, measured with an OSA. This experiment was performed with two different HiBi FBGs (HiBi FBG 1 and HiBi FBG 2) and the results using the two HiBi FBGs are shown.

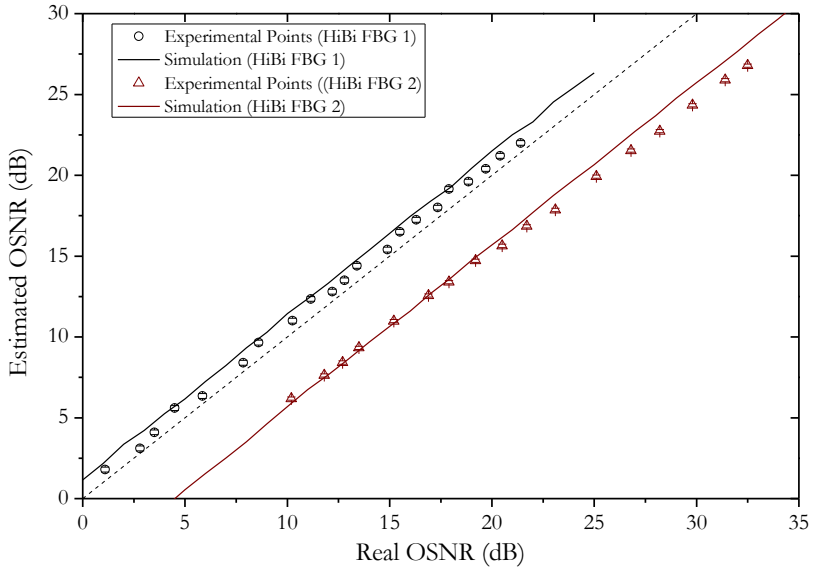

Figure 2.18 - Experimental (circles and triangles) and simulation (lines) results for the OSNR monitor using HiBi FBG. The dashed line represents the correct values of OSNR (estimated OSNR = real OSNR).

Analysing the results obtained with HiBi FBG 1, the estimated OSNR has always a value slightly higher than the real OSNR. This occurs due to the narrow bandwidth of the reflection bands. In this case, the HiBi FBG has reflection bands with a bandwidth of 0.05 nm, half of the bandwidth used to measure the OSNR in the OSA, which was 0.1 nm. So, measuring the optical power at the PBS outputs, the noise present in that measurement will be lower. So, this will increase the calculated OSNR. Nevertheless there's good agreement between the experimental data and the simulation.

When using HiBi FBG 2, the bandwidth of the reflection bands is larger than the standard noise bandwidth (0.25 nm *vs* 0.1 nm). So the estimated OSNR will present values lower than the real ones, as it can be verified from the results in Figure 2.18. However, the simulation and the experimental data are in agreement and this overestimation and underestimation of the OSNR can be compensated with an adequate calibration process. Through this method it was possible to estimate the OSNR of a continuous wave signal with a maximum error of 1.4 dB for a wide range of OSNR values: [1,22] dB with HiBi FBG 1 and [10,32] dB with HiBi FBG 2, which corresponds to the error between the estimated value obtained with simulation and the experimental one.

This method was tested in a more close to reality situation, that is, with an intensity modulated signal. In this case, only the HiBi FBG 2 was applied. The reason to use only the HiBi FBG 2 is related to the stability of the Bragg wavelengths with temperature fluctuations. Since HiBi FBG 1 has a very narrow bandwidth, a small temperature variation can shift the reflection spectrum and induce fluctuations in the measured optical power values. With the HiBi FBG 2, this temperature instability isn't problematic.

Nevertheless, throughout the realization of this work, both HiBi FBGs were mounted in a tuneable system that enabled an adjustment of the Bragg wavelengths. While HiBi FBG 1 was tuneable through a mechanical process, HiBi FBG 2 was placed on a temperature controlled tuneable system.

In Figure 2.19 are shown the eye diagrams of the monitored signal for different values of OSNR.

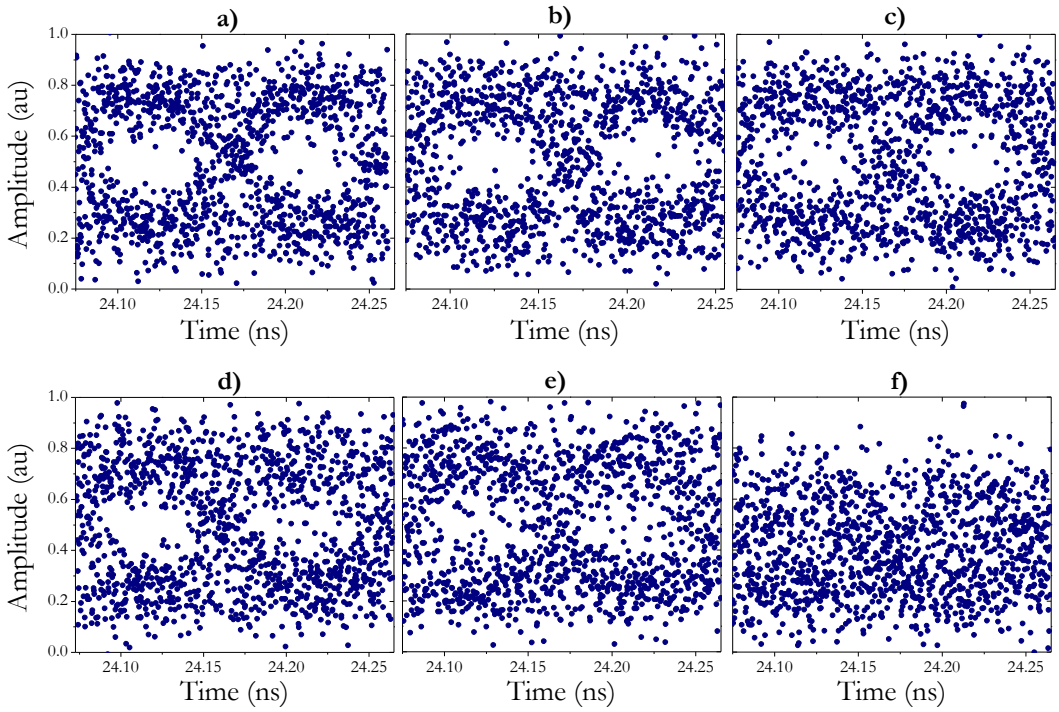

Figure 2.19 - Eyediagrams of the monitored signal for different values of OSNR: 30 dB (a); 25 dB (b); 22 dB (c); 20 dB (d); 18 dB (e); 14 dB (f)

The eye diagrams were taken using a photodetector (PIN in Figure 2.17 (HP 11982A)) and an oscilloscope from Agilent (Model 86100A). An optical filter with a -3 dB bandwidth of 0.3 nm (Santec – OTF 30M) was used to eliminate the noise present at different spectral components. It is clear that at lower values of OSNR the quality of the signal is degraded due to the presence of noise.

Figure 2.20 shows the obtained results for the estimated OSNR through the HiBi FBG monitor as function of the real OSNR, for the 10 Gb/s modulated signal.

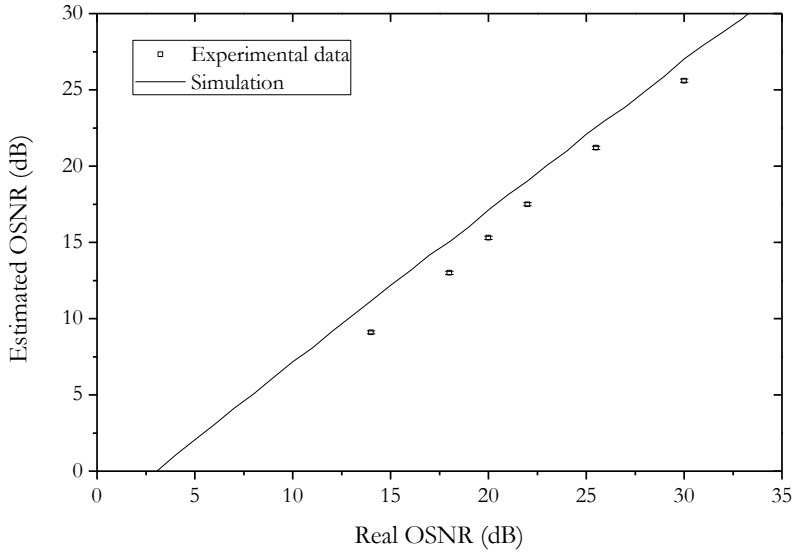

Figure 2.20 – Estimated OSNR as function of the real OSNR for a 10 Gb/s modulated signal

Once again the estimated OSNR values are lower (around 4 dB) than the real ones. As it was previously mentioned, this occurs due to the fact that the amount of noise present in both measurements is different, i.e., the real OSNR is measured considering a bandwidth of 0.1 nm while the reflection bands of the HiBi FBG have a bandwidth of 0.25 nm. Thus, in the latter case more noise will be detected in the measurement and consequently a lower OSNR is obtained. Nevertheless, both the experimental and simulation results show an identical linear behaviour from which we can predict the real OSNR value. The experimental data points fall close to the simulation line; a maximum difference between the simulation and experimental points of 2.2 dB, which is considered a reasonable error for the purpose of this work and can also be justified with eventual attenuations in the experiment that were not taken into account in the simulation.

This technique was also tested on a CW multi-channel system. In Figure 2.21 are shown the implemented setups which are a similar setup to the one in Figure 2.17, where two lasers peaking at two different wavelengths were used. The main goal of these tests was to understand how the presence of a neighbouring channel would influence the measurement of the monitored channel OSNR.

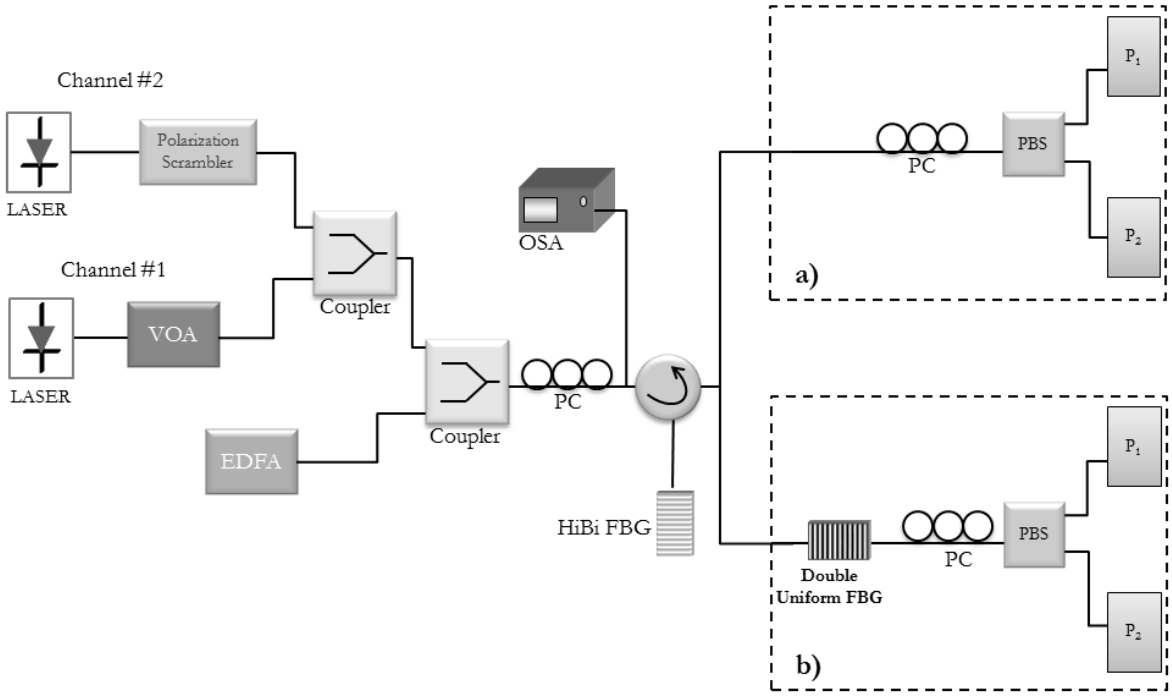

Figure 2.21 - Setup used to monitor the OSNR on a two-channel system

The channel to be monitored is designated as channel 1 and has a wavelength of 1551 nm corresponding to one of HiBi FBG Bragg wavelengths. Channel 2 peaks at 1550.2 nm with a fixed optical power while its polarization is varied with a polarization scrambler, so that the measurements are independent of its state of polarization. Both channels are coupled together and the noise, generated with an EDFA, is also coupled. Then, the signals reach the PC and PBS where the orthogonal polarization components are split and P_1 and P_2 are measured (scenario *a)*). In scenario *b)*, the composed signal passes through a double uniform FBG that rejects channel #2, before reaching the PBS. The reason subjacent to the application of the alternative scenario is explained later in this section.

In Figure 2.22 are shown the results that were obtained with scenario *a)* by fixing the OSNR of channel #2 at a determined value and by adjusting the VOA in order to vary the OSNR of channel #1.

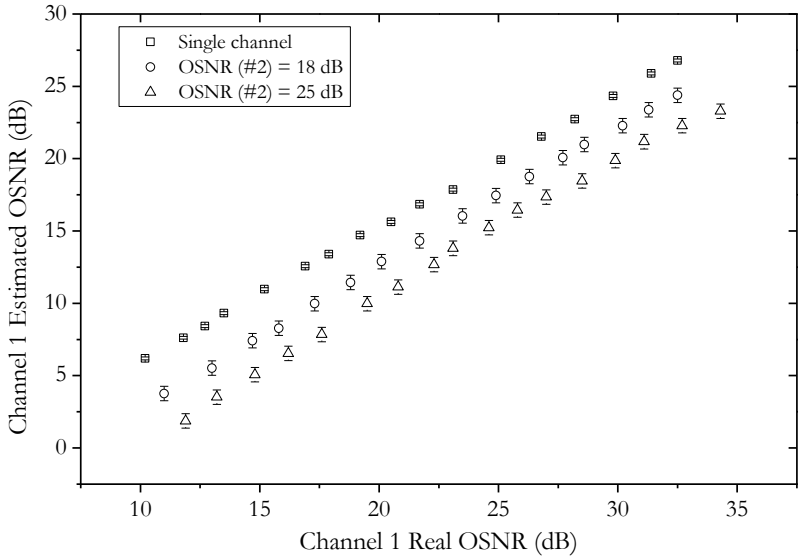

Figure 2.22 – Estimated OSNR of channel #1 as function of the real OSNR on a multi-channel system with the monitor of scenario a) from Figure 2.21

In Figure 2.22 are presented three sets of results (one of them corresponds to the single channel situation displayed in Figure 2.18, just for comparison purposes (open squares)). It is clear that, as the OSNR of channel 2 increases, the results get further away from the single channel case. This occurs because the HiBi FBG is not able to totally reject the signal from channel 2 and it influences directly the measurement of channel 1 OSNR. So, in order to measure the OSNR of a channel it is mandatory to filter out the neighbouring channels.

To improve these results, a rejection filter for channel 2 has been included (Figure 2.21 *b)*). This rejection filter is a double FBG, i.e., two identical FBGs whose Bragg wavelength matches the wavelength of channel 2 that is reflected (and rejected) while channel 1 is transmitted.

After the inclusion of the rejection filter, the power of the neighbouring channel was kept constant so that its OSNR was constant and approximately 34 dB, in order to test the worst-case scenario, i.e., the neighbouring channel presents a high OSNR making it difficult to be totally rejected. Figure 2.23 presents the optical spectra of the channels at the output of the HiBi FBG and at the output of the double FBG configuration, where channel 2 has an OSNR of 34dB and channel 1 has an OSNR of 21 dB, being clear that the presence of this rejection filter efficiently eliminates the neighbouring channel.

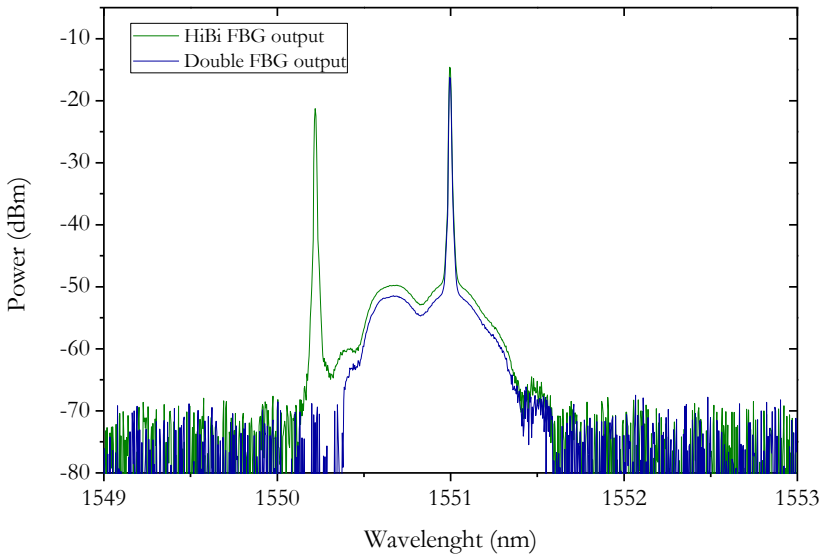

Figure 2.23 - Spectra obtained at the output of the HiBi FBG (green) and at the output of the double FBG (blue)

In Figure 2.24 are displayed the obtained results. The results from the single channel are also visible for comparison purposes.

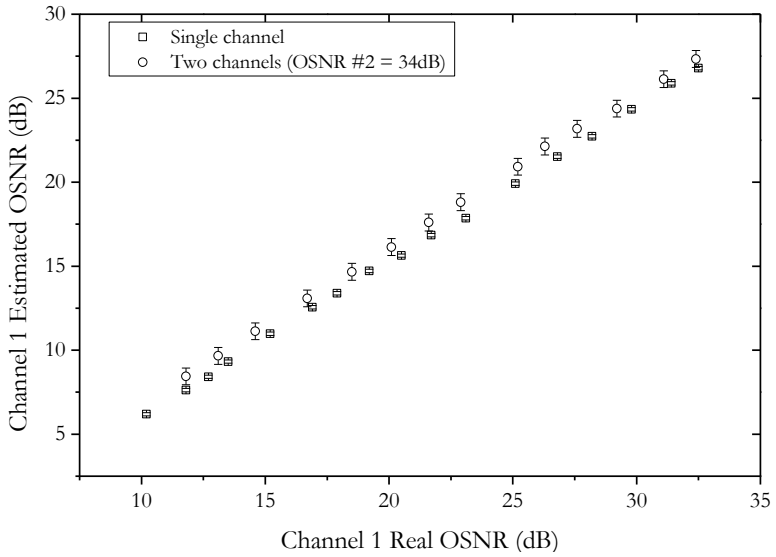

Figure 2.24 - Results obtained with the application of a rejection filter in a two-channel system

These results confirm that the inclusion of a rejection filter efficiently rejects the neighbouring channel and allows to accurately measure the OSNR of the monitored channel. Although this is an efficient way to accomplish the rejection of a neighbouring channel, it becomes unpractical when the number of channels increases. To implement a monitor, which measures the OSNR of channels individually, it is mandatory the presence of a high rejection filter in order to isolate the channel to be monitored.

2.3.4.2 Based on the reflection and transmission of the HiBi FBG

This experiment was performed on a CW single channel and, later, on a 10 Gb/s modulated signal according to the experimental setup displayed in Figure 2.25.

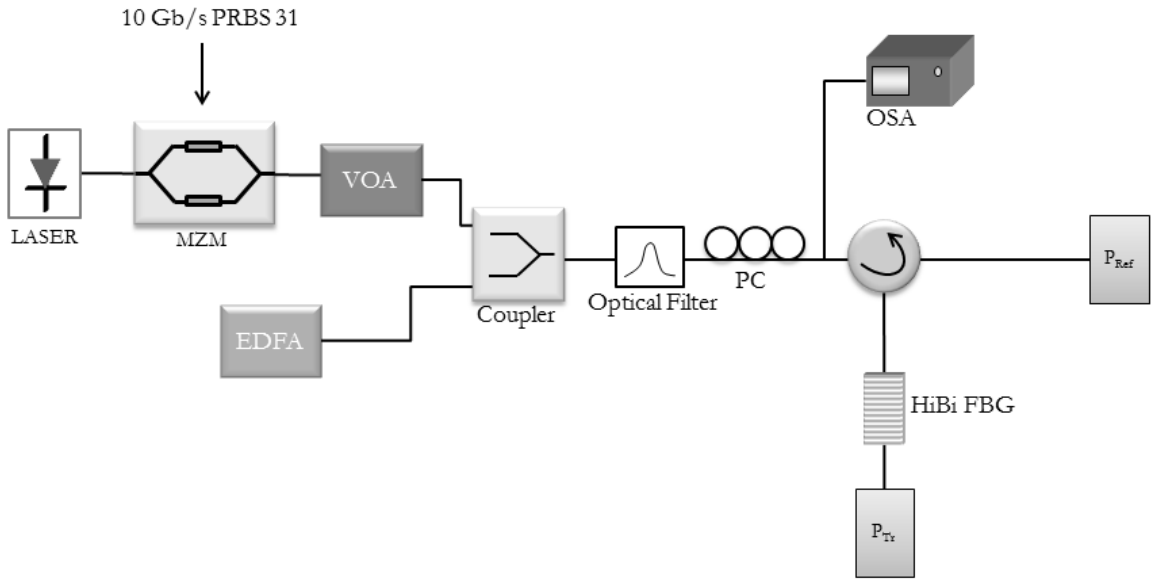

Figure 2.25 - Experimental setup of the alternative OSNR monitor where both the reflection and transmission components of the HiBi FBG are considered

In this case the monitoring unit comprises an optical filter (Santec OTF-30M), which allows the reduction of the noise bandwidth and also emulates a channel selection. Then a polarization controller is used to adjust the data signal polarization so that it matches the corresponding HiBi optical axis. The HiBi FBG used is in this test is HiBi FBG 3 (Figure 2.16).

The OSNR of the measured optical signal was varied by adjusting the applied attenuation at the VOA, for the continuous wave and modulated signal. Figure 2.26 displays the experimental and simulation results for the parameter R (dB) as function of the effective OSNR value.

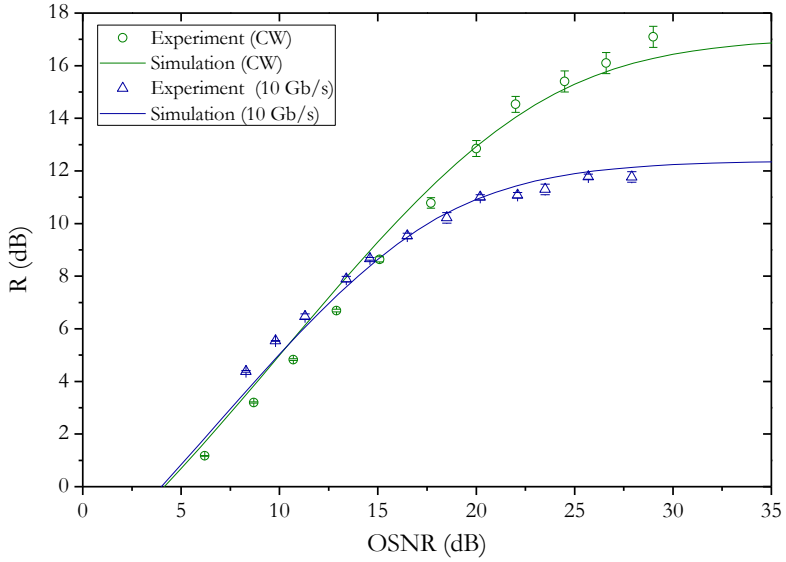

Figure 2.26 - Results obtained on a CW (green) and modulated (blue) signals

For both scenarios, the experimental data falls closely to the simulation one. It is verified a maximum error between the experimental and simulated results of 0.9 dB for the continuous wave case and 0.8 dB for the modulated one over a range of OSNR values of [5,20] dB.

However, for high OSNR, the reflection-transmission ratio stabilizes at a lower level in the modulated signal scenario. This occurs due to the presence of the lateral sidebands generated by the modulation process. This will result in an increase of both the reflection and transmitted integrated optical powers with the consequent decrease of the ratio *R*. Also the limited reflectivity of the used HiBi FBG imposes this limit on the *R* parameter. By using a HiBi FBG with higher reflectivity, this stabilization threshold will increase.

However, it is clear that the ratio between the reflecting and transmitting power values is univocally related with the OSNR of the channel in a significant range of values [0,20] dB.

2.4 Summary and conclusions

In this chapter, the work developed on OSNR monitoring was described and all results were presented. The techniques are based on the application of HiBi FBGs to isolate the data signal from the noise, through their polarization characteristics.

The first presented method, which analyses the reflected signal components by the HiBi FBG, works very well on a single channel system. Results show that the OSNR of a single channel modulated at 10 Gb/s is measurable through this method where a maximum error of 2.2 dB over a range of [14, 22] dB was obtained.

The application of this technique in a multi-channel system is challenging. The issue resides in the fact the optical power of neighbouring channels interfere in the measurement of a signal OSNR, because the used HiBi FBG is not able to totally reject the adjacent channels. So, the presence of a high rejection filter is mandatory in order to efficiently isolate the channel we want to monitor. This was accomplished with the presence of a double FBG that totally reflected (and consequently rejected) the adjacent channel. This way it was possible to measure the monitored channel OSNR accurately. This, however, in the presence of more channels can become unpractical.

An alternative to this method is also presented, which requires a slightly less complex setup. In this case both the reflected and transmitted responses of the HiBi FBG are considered and through their optical powers, the OSNR can be estimated. This however can also be accomplished with a FBG in a SMF. With this alternative technique the OSNR of a 10 Gb/s modulated channel was successfully measured with a maximum error of 0.9 dB over a range of [5,20] dB.

References:

[1] D. Gariépy and G. He. (2009, Measuring OSNR in WDM Systems - Effects of Resolution Bandwidth and Rejection Ratio. *EXFO Application Notes 98*.

[2] (July 17, 2013). *Optoplex Optical Channel Monitor*. Available: http://www.optoplex.com/Optical_Channel_Monitor.htm

[3] (July 17, 2013). *Optical Channel Monitor*. Available: http://www.photoptech.com/main/products_tx/Optical%20Channel%20Monitor.php

[4] W. Moench and J. Y. Larikova, "Measuring the Optical Signal-to-Noise Ratio in Agile Optical Networks," in *Optical Fiber Communication and the National Fiber Optic Engineers*, Anaheim, CA, 2007, pp. 1-6.

[5] Y. C. Chung, "Optical performance monitoring techniques; current status and future challenges," in *34th European Conference on Optical Communication*, 2008, pp. 1-3.

[6] J. H. Lee, H. Y. Choi, S. K. Shin, and Y. C. Chung, "A review of the polarization-nulling technique for monitoring optical-signal-to-noise ratio in dynamic WDM networks," *Journal of Lightwave Technology,* vol. 24, pp. 4162-4171, Nov 2006.

[7] X. Liu, Y. H. Kao, S. Chandrasekhar, I. Kang, S. Cabot, and L. L. Buhl, "OSNR Monitoring Method for OOK and DPSK Based on Optical Delay Interferometer," *Photonics Technology Letters, IEEE,* vol. 19, pp. 1172-1174, 2007.

[8] C. C. K. Chan, *Optical Performance Monitoring: Advanced Techniques for Next-Generation Photonic Networks*: Elsevier Science, 2010.

[9] H. Ji, K. Park, J. Lee, H. Chung, E. Son, K. Han, S. Jun, and Y. Chung, "Optical performance monitoring techniques based on pilot tones for WDM network applications," *Journal of Opical Networking,* vol. 3, pp. 510-533, 2004.

[10] G. Rossi, T. E. Dimmick, and D. J. Blumenthal, "Optical performance monitoring in reconfigurable WDM optical networks using subcarrier multiplexing," *Journal of Lightwave Technology,* vol. 18, pp. 1639-1648, Dec 2000.

[11] R. W. Boyd, "Chapter 9 - Stimulated Brillouin and Stimulated Rayleigh Scattering," in *Nonlinear Optics (Third Edition)*, ed Burlington: Academic Press, 2008, pp. 429-471.

[12] M. D. Pelusi, A. Fu, and B. J. Eggleton, "Multi-channel in-band OSNR monitoring using Stimulated Brillouin Scattering," *Optics Express,* vol. 18, pp. 9435-9446, Apr 26 2010.

Chapter 3: Group Velocity Dispersion Monitoring

3.1 Introduction

The dispersion of the optical fibre is also one of the main impairments suffered by the optical signals propagating in the medium, besides the attenuation. It emerges from material (silica) and waveguide dispersion as was previously explained.

When an optical pulse propagates along the optical fibre, each spectral component, of frequency ω, will arrive at the fibre output with a time delay [1]. This phenomenon is displayed in Figure 3.1.

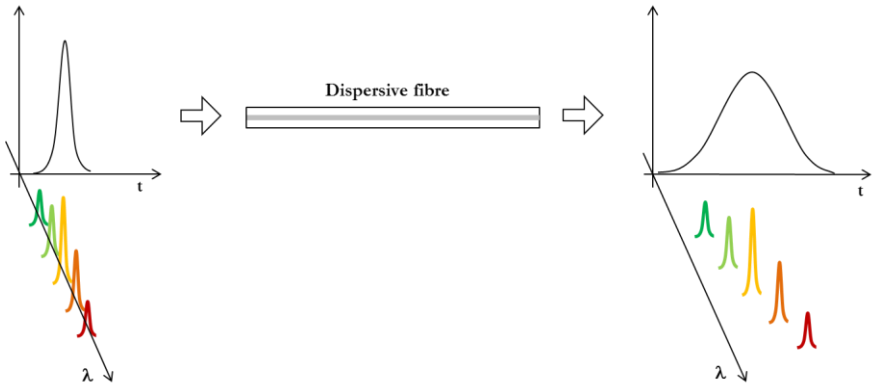

Figure 3.1 - Propagation of an optical pulse in a dispersive fibre.

The time delay between each spectral component will be $T=L/v_g$, where L is the fibre length and v_g the group velocity defined as:

$$v_g = \left(\frac{d\beta}{d\omega} \right)^{-1} \tag{3.1}$$

being β the propagation constant which is related to the wavenumber, k_0, and the propagation medium refractive index, n, by $\beta=n\cdot k_0=n\cdot c/\omega$. Therefore, a pulsed signal with a frequency bandwidth of $\Delta\omega$ will suffer a temporal broadening which will be:

$$\Delta T = \frac{dT}{d\omega}\cdot\Delta\omega = \frac{d}{d\omega}\left(\frac{L}{v_g}\right)\cdot\Delta\omega = \frac{d}{d\omega}\left(L\cdot\frac{d\beta}{d\omega}\right)\cdot\Delta\omega = L\cdot\frac{d^2\beta}{d\omega^2}\cdot\Delta\omega = L\cdot\beta_2\cdot\Delta\omega \tag{3.2}$$

β_2 is defined as the second derivative of β with respect to the frequency and is called the group velocity dispersion (GVD) parameter. Converting the frequency into wavelength, which is more usual in the optical communications domain, using $\omega=2\pi c/\lambda$ and $\Delta\omega=-2\pi c/(\lambda^2)\cdot\Delta\lambda$, we will have:

$$\Delta T = L \cdot \beta_2 \cdot \left(-\frac{2\pi c}{\lambda^2} \right) \cdot \Delta\lambda = L \cdot D \cdot \Delta\lambda \qquad with \quad D = -\frac{2\pi c}{\lambda^2} \beta_2 \tag{3.3}$$

D is designated as the dispersion parameter, commonly expressed in *ps/nm·km*, being specific for each type of fibre and wavelength dependent [1]. In Figure 3.2 is displayed the D parameter for a typical SMF.

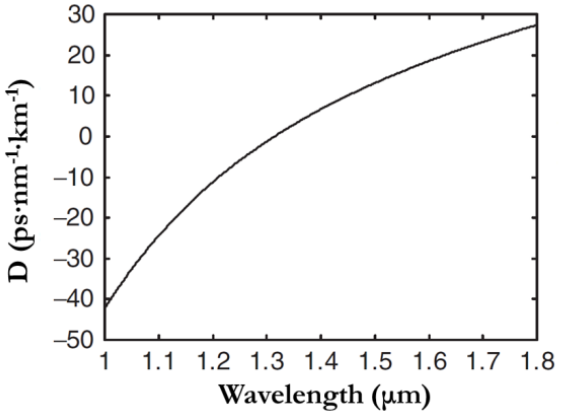

Figure 3.2 - Wavelength dependence of the dispersion parameter, D, in a standard SMF [2]

A pulsed signal with a wavelength in the C-band (near 1550 nm) will suffer a dispersion of approximately 18 ps/nm·km. The main consequence of this effect is the dispersion of the binary optical signal in the time domain, the consequent data distortion and the bit error rate (BER) increase. For an extreme situation, consecutive bits will overlap each other and the signal becomes undistinguishable.

Therefore, for direct detection systems, it is imperative to monitor this impairment and develop ways to measure dispersion and also compensate for it. During the realization of this work, the term group-velocity dispersion (GVD) is used instead of chromatic dispersion as the monitored parameter, as chromatic dispersion is mostly used to characterize the fibre and not the signal.

3.2 State of the Art

Several methods and techniques have been reported to compensate the GVD, allowing the recovery of the information. However, in order to perform the correct compensation for this effect, it is of most importance to accurately determine the accumulated dispersion suffered by the optical signal along the propagation. Therefore, it is imperative to implement an online monitoring method, which can measure the overhaul link dispersion and determine the required amount of dispersion

compensation to be applied. Moreover, methods that are able to perform these tasks quickly and without any interruption on the network service are highly desirable.

The state of the art techniques shown here are divided into four main categories, corresponding to the processes they're based on, namely: nonlinear effects, eyediagram analysis, pilot tones and radio frequency (RF) clock component measurement.

Nonlinear effects

Several techniques use nonlinear effects, such as FWM, SPM or XPM to measure the amount of dispersion suffered by the signal along the propagation.

The nonlinear process called FWM arises from the propagation of two high intensity signals (usually called signal and probe) which, under a phase matching condition, induces the generation of a third signal, called idler. The efficiency of this effect depends on the signal peak power, which is measurable through the optical power of the generated idler. As the group velocity dispersion induces broadening of the signal spectral bandwidth of the signal, its peak power will consequently decrease. So, the idler signal optical power will give information on the dispersion suffered by the signal. This is the principle of the techniques proposed in [3, 4]. In these works, after the propagation on the fibre link, the data signal is inserted onto a HNLF along with the probe continuous signal. Then, as the process of FWM takes place the optical power of the idler signal is measured and the dispersion is estimated. The main drawback of this method is that the signal must have high optical power in order to induce FWM (approximately a minimum average power of 15 dBm, for a 40 Gb/s return-to-zero (RZ) signal), so an amplifier, such as an EDFA, is mandatory. In reference [3] this technique was applied via simulation in a 40 Gb/s channel modulated with RZ format where a range of [0, 39] ps/nm of measurable dispersion is achieved. In reference [4] the technique was experimentally verified, achieving a range of [0, 40] ps/nm, for a 40 Gb/s RZ modulated signal.

Other techniques make use of SPM to estimate the dispersion. SPM is a nonlinear effect that occurs when high intensity modulated signals propagate through a highly nonlinear medium. For this medium, the refractive index depends on the intensity of the incident signal. Thus, the intensity modulated signal induces changes to the medium refractive index, which, on its turn, induces a phase shift in the signal. Consequently, the signal becomes spectrally broadened.

In this method, this spectral broadening effect is measured using an optical filter after the HNLF. This filter transmits only the longer wavelength components of the signal and its integrated optical power (measured with a photodetector) is directly related to the spectral broadening and, consequently, to the signal dispersion. The GVD induces a decrease in the signal peak power, so the

SPM is reduced and there will be less spectral broadening. In reference [5] this method is applied to estimate the dispersion of a 40 Gb/s RZ signal. The spectrum of the optical signal, after propagation through different amounts of GVD, is obtained at the output of a HLNF. Then, the integrated optical power at the longer wavelengths is calculated numerically and related to the signal GVD.

Another technique, presented in reference [6], uses XPM to determine the dispersion of a signal. The XPM occurs when two signals propagate in a HNLF and the intensity variation of one signal induces a change on the phase of the other signal. The modulated data signal propagates in a HNLF along with a probe signal. Without dispersion, the intensity modulated signal induces a phase modulation of the probe signal. Therefore the optical spectrum of the probe signal presents sidebands at a spectral distance (that corresponds to the bitrate of the signal) from its central wavelength. In the presence of dispersion, the signal peak power decreases and the XPM does not occur as efficiently, so the peak power of the sidebands components also decrease. In Figure 3.3 is shown the obtained spectra for different amounts of dispersion, where the sideband peak variation is clearly visible.

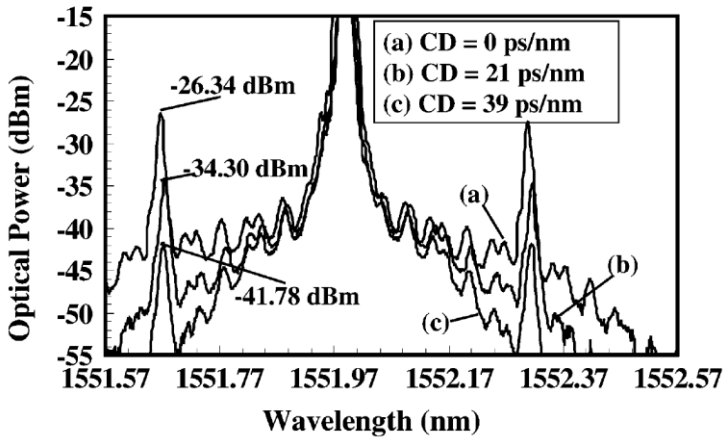

Figure 3.3 - Spectra of the probe signal while measuring the GVD with the XPM effect [6]

This technique was experimentally tested in a 40 Gb/s RZ data signal and a range of measurable dispersion of [0, 40] ps/nm was achieved.

These techniques, which are based on the optical fibre nonlinear effects, present one major advantage: they are totally optical processes and do not require any electronic circuitry. However, there are also some drawbacks, such as the necessity of high intensity signals and the consequent requirement of amplification before the monitoring process.

Eyediagram analysis

Other monitoring techniques are based on the observation of the signal eyediagram, amplitude histogram or other data derived from the time domain signal. The shape of the analysed diagram gives information on the distortion of the signal and consequently on its group velocity dispersion. Some parameters can be extracted from the diagram in order to give a more objective and quantitative analysis.

Some works regarding this method and several variations have already been introduced. Here, some of the most relevant ones are described.

The method presented in reference [7] consists of extracting the power of the data signal at two different instants of the bit length. These two sampling instants are separated by an interval defined as Δt and this pair of measurements is performed with a period T_s. The measurement pairs are then plotted in a two dimension *(x,y)* plot and, by analysing its shape, the group velocity dispersion can be estimated. Varying the interval Δt, this method can be optimized in order to find the value that is more sensitive to dispersion. This technique was studied by simulation in reference [7] and in Figure 3.4 are shown two examples of the obtained diagrams: one without dispersion and another with a dispersion value of 800ps/nm for different Δt values: bit period (*B*), half bit period (*B/2*) and quarter bit period (*B/4*).

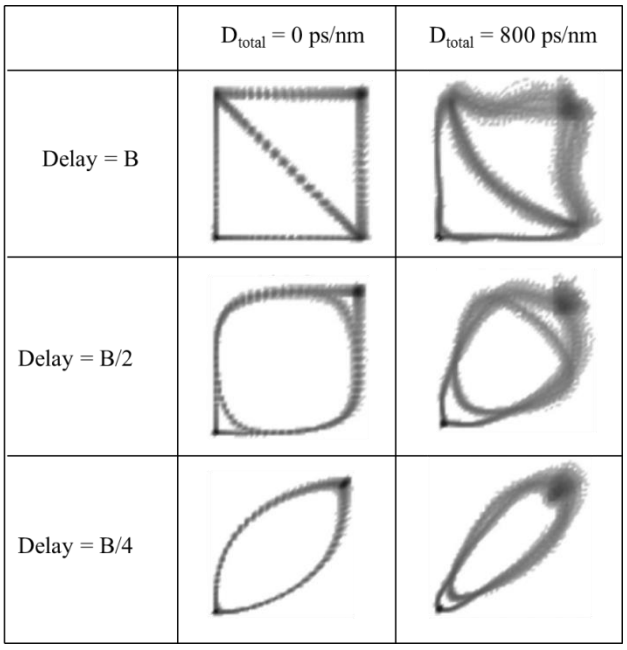

Figure 3.4 - Obtained diagrams, from which the GVD can be estimated, where *B* is the bit period bit [7]

In reference [8], the eyediagram of the signal is extracted and the signal power is sampled at two different instants: at -40 ps and +40 ps relatively to the centre of the eye opening. The amplitude

histograms of these samples are then determined and from each of them, two points are extracted whose positions depend on the distortion of the signal. In Figure 3.5 is shown this principle of operation for two different eyediagrams: one without dispersion (Figure 3.5 a) and c)); and one with high distortion (Figure 3.5 b) and d)).

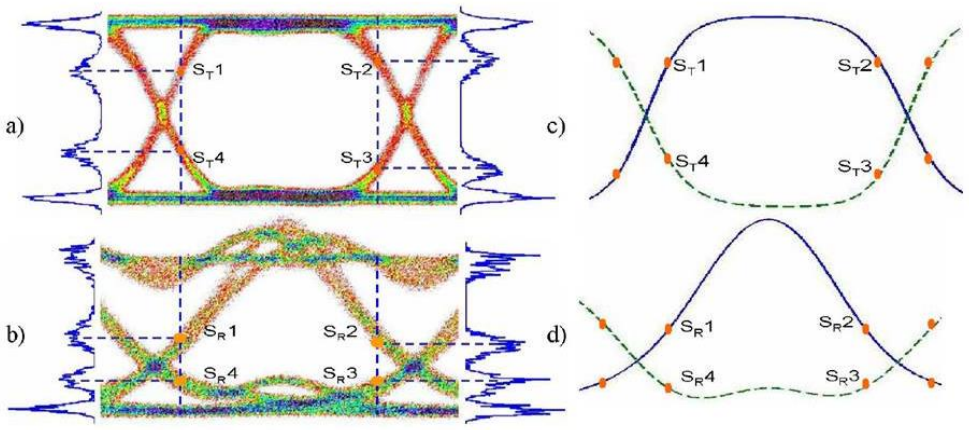

Figure 3.5 - Principle of operation of a technique based on the extraction of data from the signal eyediagram: eyediagram without dispersion (a) and the respective approximation to a hyperbolic tangent (c); eyediagram with dispersion (b) and the hyperbolic tangent approximation (d) [8]

The histograms are plotted vertically aside the eyediagrams on the left of Figure 3.5. From each histogram, two points that correspond to the mean of the inner distributions are extracted. The position of this set of four points (two per histogram) is dependent on the GVD of the signal. Varying the dispersion of the signal, those points are retrieved and a database for posterior access is created. This database will then give an approximate estimate of how much dispersion the monitored signal has. This technique has been experimentally tested in reference [8] with a 10 Gb/s non-return-to-zero (NRZ) data signal, where the database is created with a resolution of 8.5 ps/nm, i.e., the set of four points are determined for every 0.5 km of propagation. Experimental results show that the GVD can be measured through this method for a maximum fibre span of 103 km (approximately 1800 ps/nm) with a maximum error of 110 ps/nm.

Other monitoring techniques use a process called artificial neural networks (ANN). These ANN's are computational algorithms that have the ability of learning the relationships that relate the inputs to their outputs. In optical performance monitoring, its inputs can be, for instance, parameters derived from the eyediagram and the outputs are signal impairments to be monitored such as OSNR or GVD. This algorithm learns from observing its inputs, establishing the relations and finally determines its outputs. The obtained values for the outputs are then compared to the desired ones and the process is repeated until the error between them reaches a predetermined value.

This method involves complex computational processes that vary from technique to technique. Some are able to measure not only the GVD, but also other impairments such as PMD and OSNR.

They can also be applied to different modulation formats like DPSK [9]. In Figure 3.6 is displayed a diagram concept of an ANN concept where its complexity is clear.

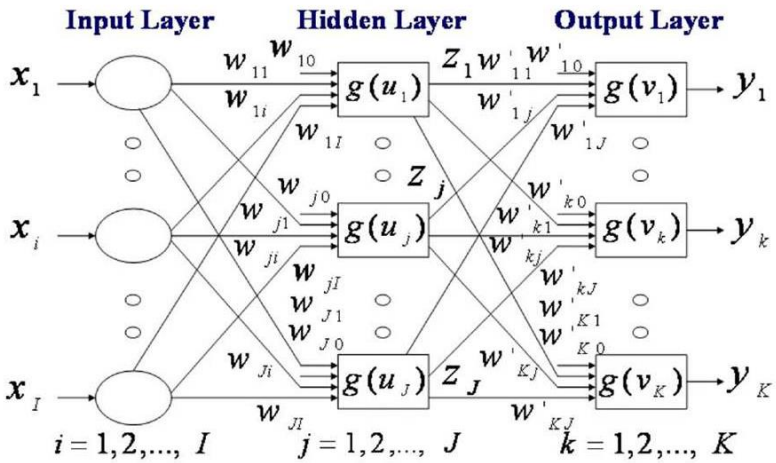

Figure 3.6 - Example of an ANN operation principle [9]

An ANN is composed by several layers: the input layer, where the input parameters extracted from the eyediagram are inserted into the ANN process; one or more hidden layers, where several computational operations take place in order to produce the outputs; and the output layer which returns the values of the calculated impairments we wish to implement. This method was tested through simulation in reference [9] where selected combinations of different impairments (OSNR, GVD, PMD) were imposed on the signal. To test the accuracy of the method, the GVD was varied between the predetermined values of 10 ps/nm and 30 ps/nm (which were then combined with the other impairments). The signal GVD was extracted with an average error of 3.98 ps/nm [9].

The main benefit of this type of techniques is its low cost, requiring a setup based on electronic processing which can be quite inexpensive. However, these systems have usually a very complex operation principle and their measurement process is not as fast as the optical based ones.

Pilot tones

These methods are based on the addition of a radio-frequency (RF) tone to the data signal at the transmitter and analysing it after propagation. This additional tone propagates along with the data signal, through the fibre, undergoing the same impairments. Posterior analysis of the added RF tone will give information on the impairments suffered by the signal.

When added to the data signal, the RF tone induces sidebands in the optical spectrum of the data signal. These sidebands are located at a spectral distance from the carrier which corresponds to the tone frequency. When detected by an electronic spectrum analyser, these sidebands are summed

and squared resulting in a single frequency component on the electric spectrum. The peak power of this frequency component is dependent on the phase difference between the two sidebands, which is directly related to the signal dispersion.

In reference [10], the experimental proof of concept for dispersion monitoring applying RF tones is demonstrated, where a subcarrier is added to a data signal modulated at 2.5 Gb/s with the setup shown in Figure 3.7.

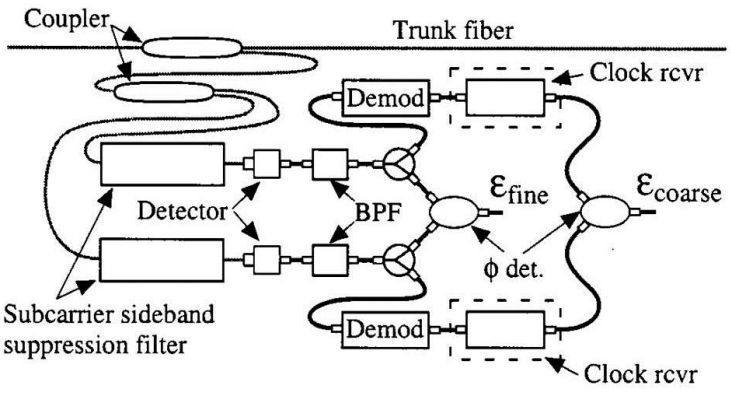

Figure 3.7 - Setup implemented to measure the group velocity dispersion using pilot tones [10]

In this scheme the signal is divided in two branches and, at each one, an optical filter is used in order to suppress one of the generated sidebands and isolate the other one. These are then divided, where one output is forwarded to a phase detector and the other an amplitude demodulator. The phase detector returns a signal that is proportional to the phase difference between the inputs, which, on its turn, depends on the accumulated dispersion. The outputs of the amplitude demodulator are also forwarded to a phase detector which will give a coarser estimate of the dispersion. The purpose of this coarse measurement is to resolve phase ambiguities from the first measurement. The simulation results show that a measurement range of 9167 ps/nm can be achieved where a low frequency (410 MHz) subcarrier is used as the pilot tone.

One alternative is proposed in [11], which follows the same principle, as it makes use of the phase difference between the sidebands to estimate dispersion, but introduces a slight enhancement. The power of the frequency component, in the electric domain, correspondent to the subcarrier tone, obeys the following expression:

$$P = A \cdot e^{-\alpha L} \cdot \cos^2\left(\frac{\pi D L \lambda^2 f^2}{c}\right), \tag{3.4}$$

where α is the attenuation coefficient; L the fibre length; D the dispersion coefficient; λ the carrier wavelength; f the pilot tone frequency; c the speed of light; and A is a constant that takes into account the loss and gain experienced by the signal. This method proposes to eliminate the dependency on the

constant by adding to the signal two subcarriers at different frequencies. Then, the power ratio between these two frequency components is determined and the dispersion is estimated. This ratio, *R*, between the two frequencies, follows this expression:

$$R = \frac{\cos^2\left(\frac{\pi D L \lambda^2 f_1^2}{c}\right)}{\cos^2\left(\frac{\pi D L \lambda^2 f_2^2}{c}\right)}, \quad f_1 < f_2 \tag{3.5}$$

In Figure 3.8 are shown two results: one obtained with a single subcarrier; and another with two subcarriers, where the ratio R was determined and plotted as function of the dispersion.

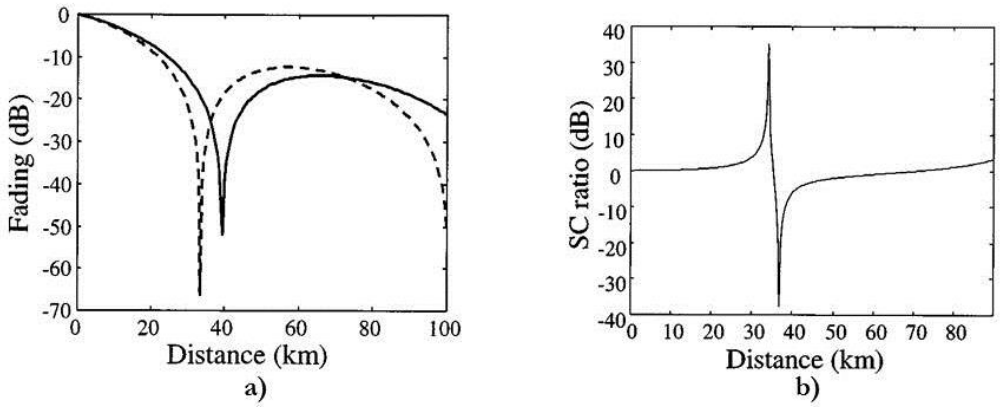

Figure 3.8 - Comparison between the two methods using one pilot tone (a) and two pilot tones (b) [11]

In Figure 3.8 a), the fading, which is a measurement relative to the peak power, is plotted as function of the fibre length. In Figure 3.8 b), is the calculated subcarrier ratio (SC ratio) as function of the fibre length, for λ=1550nm, D=18ps/nm.km, where f_1=9.6GHz and f_2=10.4GHz. This measurement is independent of the peak power.

In reference [12] a technique is proposed and experimentally tested with a data signal modulated at 10 Gb/s with an RZ format. The added tone used in this experiment has a varying frequency from 7 to 9 GHz. The goal is to observe how different tone frequencies affect the final outcome. Without dispersion the generated sidebands will be in-phase and so, at the electric spectrum, the RF tone frequency component will present a high peak power component. As the signal propagates and suffers dispersion an additional phase difference between the sidebands is accumulated and the peak power decreases.

In Figure 3.9 is shown the results for the tone power as function of the dispersion for two different subcarrier frequencies.

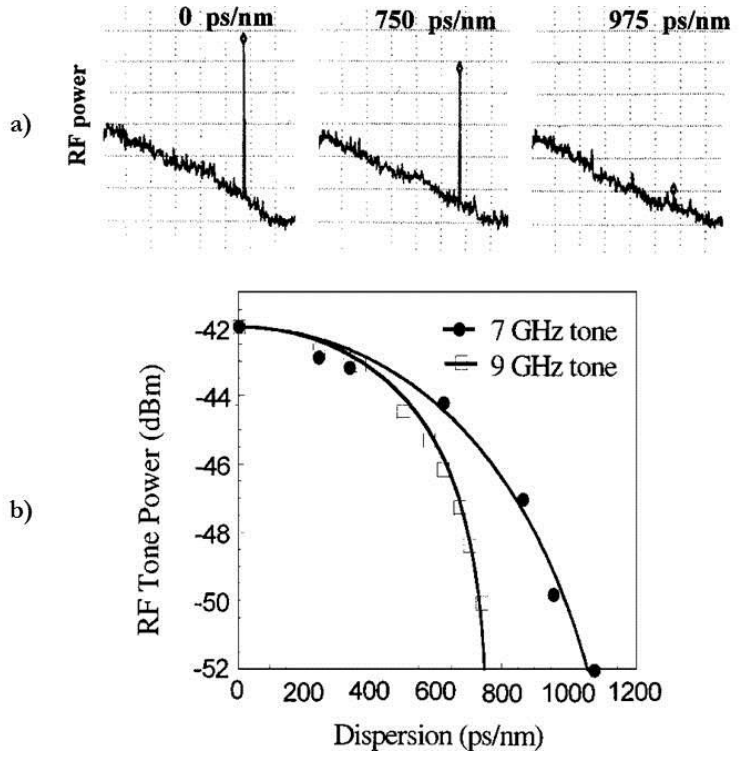

Figure 3.9 - Dependence of the RF tone power with the dispersion (a) and the obtained results for two different tone frequencies (b) [12]

With a lower frequency, a wider range of dispersion is reached: with the 7 GHz tone, a range of 1200 ps/nm is achieved, while with 9 GHz only a 675 ps/nm range is measurable. However, for the lower frequency tone, the sensitivity is also lower, so a compromise must always be met.

These techniques present a good solution for optical performance monitoring. They're able to perform multi-impairment monitoring as well, and regarding GVD monitoring, they provide accurate resolution for a wide range of dispersion (600-1000 ps/nm for a 10 Gb/s signal). However, these methods imply one major drawback which is the mandatory alteration of the transmitter in order to add the pilot tone to the signal.

RF Spectrum Analysis

Other class of techniques involves the analysis of the signal RF spectrum and the measurement of the clock frequency component power. For some modulation formats, when an optical signal is modulated, the clock component sidebands appear in the optical spectrum. When observing the RF spectrum, these sidebands are summed and squared by the detector and the peak power of the clock component will depend on the phase difference between the sidebands and give information on the signal dispersion.

Several variations of this method have been proposed recently; the most important ones are described here.

In reference [13] is presented a method that relies on the fact that the clock frequency component either fades or regenerates, depending on the modulation format. When a signal is modulated with a NRZ format, its optical spectrum presents sidebands that correspond to the clock frequency. However, these sidebands are initially out of phase and cancel each other during the photo detection process. So, the clock component does not appear in the electric spectrum. With propagation in the fibre, the signal suffers dispersion, which induces an extra phase difference between the sidebands. Consequently, the clock component is regenerated and its peak power is directly related to the fibre dispersion. If the signal is modulated with an RZ format, the opposite occurs: the sidebands are initially in phase and the clock component is at its maximum power on the electric spectrum; with dispersion and consequent accumulated phase difference, the clock component fades.

This technique was tested experimentally in [13] with a data signal modulated at 10 Gb/s considering the two modulation formats: NRZ and then RZ. In Figure 3.10 are displayed the results obtained for both situations where the regenerating/fading effect is clearly visible as well as its dependence on the signal dispersion.

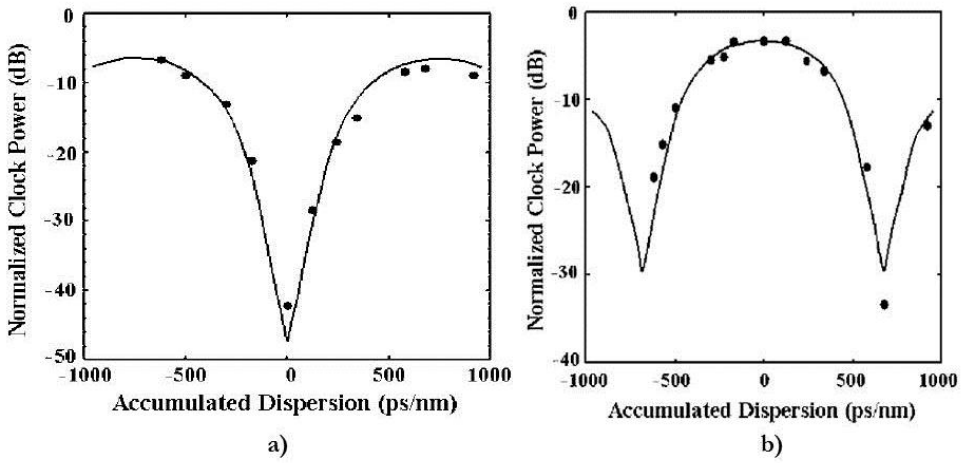

Figure 3.10 - Clock frequency peak power as function of the dispersion of the signal modulated with a NRZ (a) and an RZ (b) formats [13]

On signals modulated with phase shift keying, this type of techniques can also be applied. Due to the fact that a phase modulated signal presents also a slight amplitude modulation, the clock frequency component power will also depend on the signal GVD [14, 15].

In [16] is proposed a variation of this method that allows the monitoring of chromatic dispersion throughout a wide range (over 2300 ps/nm) for a 10 Gb/s data signal.

It is also based on the evolution of the clock frequency component. However, this measurement system has an interferometer that applies a time delay in one of the arms causing the appearance of a sideband of frequency $f_{RF}=1/(2\tau)$ (τ being the delay), whose power depends on the signal dispersion. With $\tau=100ps$, the generated sideband will appear at 5 GHz.

The dispersion range is defined by:

$$D = \frac{c}{2\lambda^2 f^2} \tag{3.6}$$

Therefore, for a lower frequency component a wider dispersion range is achieved. With a signal of λ=1552 nm and a sideband component at f=5GHz, the dispersion range will theoretically reach a 2491 ps/nm value.

This work also proposes a setup to differentiate the sign of the dispersion that is displayed in Figure 3.11.

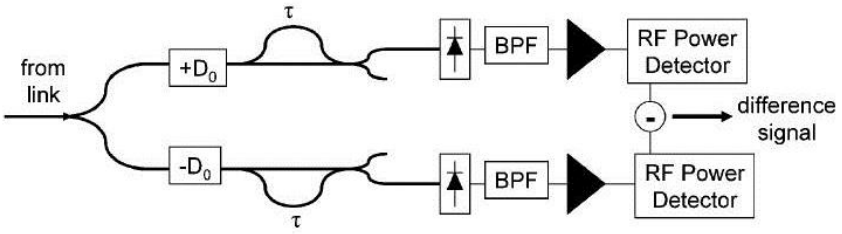

Figure 3.11 - Experimental setup of a technique that allows the measurement of both the magnitude and sign of dispersion by measuring the clock component peak power [16]

The signal is initially divided onto two branches, where each has a known dispersive element of $+D_0$ and $-D_0$ of dispersion, respectively. This design implies the application of two interferometers, whose outputs will then be detected and the difference between the powers (at interference frequency component) is determined. Therefore, it is possible to distinguish the sign of dispersion: if the dispersion is positive, the difference will also be positive and vice-versa.

The idea of using an interferometry to create a lower frequency sideband and increase the range of measurable dispersion is also explored in the work presented in [17]. In Figure 3.12 is shown the setup and measurement module applied.

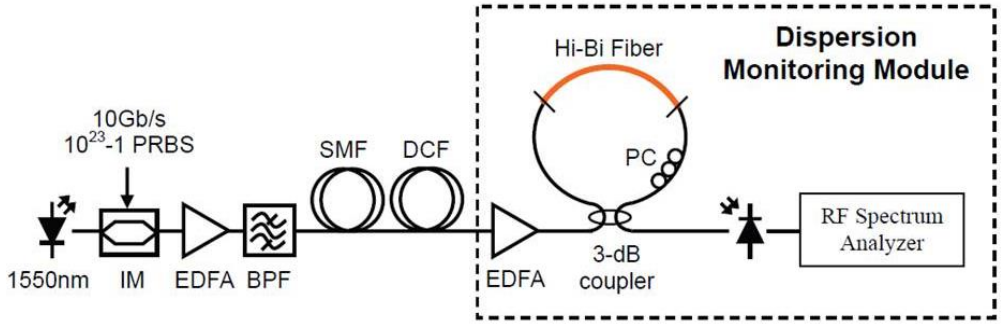

Figure 3.12 - Setup to measure the dispersion of a signal using a HiBi fibre loop as an interferometer [17]

The interference is generated with a 3 dB coupler, a polarization controller (PC) and a HiBi fibre that altogether form a loop. At the coupler the signal is divided into two branches that have orthogonal polarization states that are obtained by adjusting the polarization controller. The two components propagate with different velocities in the HiBi fibre and, once they reach the coupler, interference is created. The delay between the components is controlled by the length of the HiBi fibre, which has 56.8 m to produce a 100 ps delay and thus induce phase modulation at the 5 GHz frequency component.

This kind of techniques, based on the evolution of an RF component, provides the monitoring of GVD using a simple setup [13]. However, if we want to increase the range of the measurable dispersion, some alterations can be made to the setup and still have a reliable method that returns the GVD.

The work presented in [16] introduces an alternative modified setup that allows the extraction of the GVD sign. To distinguish whether the dispersion is positive or negative can be a very important factor when performing compensation. On one hand we could be introducing extra broadening to the signal and turn the data undistinguishable; on the other we could erroneously compensate the dispersion by decreasing the pulse duration and induce the occurrence of undesired nonlinear effects.

Summary

As a summary we can say that all the methods presented here have their strengths and weaknesses.

Nonlinear effects based techniques provide an all-optical based monitoring system that is fast as well as reliable. Their main drawback is the requirement of high intensity signals, in order to induce the nonlinear effects. This can become unpractical if we want a tap based monitor that only uses a small percentage of the signal power so that the transmission in the network doesn't get interrupted.

Eyediagram analysis techniques implement some complex setups and the application of the ANN concept, which basically functions a black box with inputs and outputs, require some degree of electronic and computational processing. A monitoring system of this kind, however, can provide a very cost-effective solution, as well as a multi-impairment monitoring.

Pilot tones based techniques and the analysis of the RF spectrum evolution provide simple and effective solutions. Pilot tones require a modification to the transmitter making the method less viable. The measurement of the clock component in intensity modulated signals can provide a cost-effective solution with reliable results.

In our work, we chose to develop a technique based on the clock component evolution. It's an alternative to the ones presented in this chapter as it requires a simple setup to retrieve not only the magnitude of signal dispersion but also its sign.

Similarly to what was presented in the previous chapter, it is also shown on Figure 3.13 a distribution of the published works along the past years on this topic. A search using the terms "chromatic dispersion" (which is a much more used term than GVD) and "monitoring" was performed on the ISI Web of Knowledge website on July 29th of 2013.

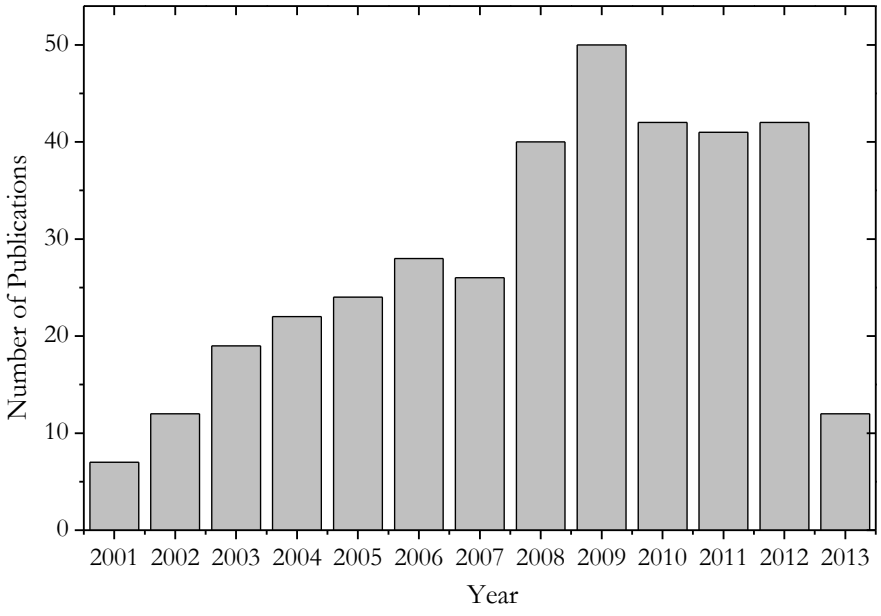

Figure 3.13 - Number of published works on a per year basis, about GVD monitoring. The data from the year 2013 only contains the works published so far (until July 29th of 2013).

As expected, this topic has gained relevance in the research world over the past five years, when the number of published papers has stabilized on a high number of publications (about 40 to 50 published works per year).

3.3 Implemented GVD monitor

In this section we present the technique proposed in this thesis to measure the GVD of a channel. It is based on the clock component evolution and its analysis on the RF domain.

3.3.1 Theoretical Demonstration

Amplitude modulated optical signals can be modulated according to two different formats: RZ and NRZ. For the first case, the bit "1" is represented by an optical pulse with duration shorter than the bit slot, always returning to the zero state before the end of the bit duration. The NRZ optical pulses remain in the "on" state as long as the sequence of bits "1" lasts; it only returns to zero when a bit "0" appears in the bit stream. In Figure 3.14 is illustrated the generated bit streams for these modulation formats.

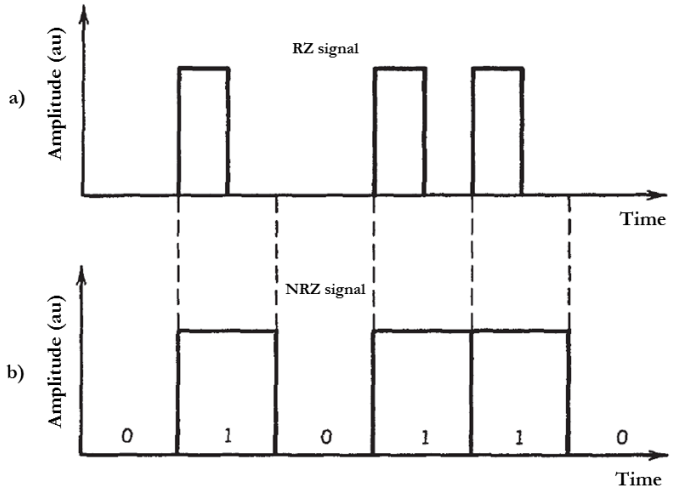

Figure 3.14 - OOK bit stream: a) RZ signal; b) NRZ signal [1]

It is clear that the NRZ format requires fewer transitions between the on-off states (in average about 50% of the times) that the RZ does. This presents an advantage on the application of NRZ signals over RZ, because they will occupy a smaller bandwidth in the spectrum and are most used in optical communication networks. In Figure 3.15 is shown the optical spectra for a signal modulated at 10 Gb/s with NRZ and RZ formats where the difference in the occupied bandwidth is visible.

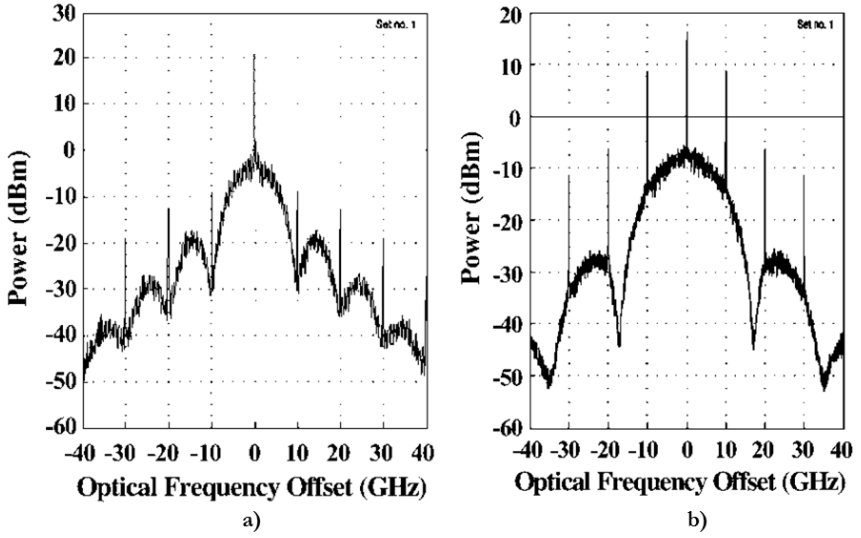

Figure 3.15 - Optical spectra of OOK modulated signals: NRZ (a) and RZ (b) [13]

Both spectra present power peaks every 10 GHz from the optical carrier frequency, which corresponds to the clock frequency. In Figure 3.16 is shown the RF spectra obtained for the same signals after detection with a photodiode.

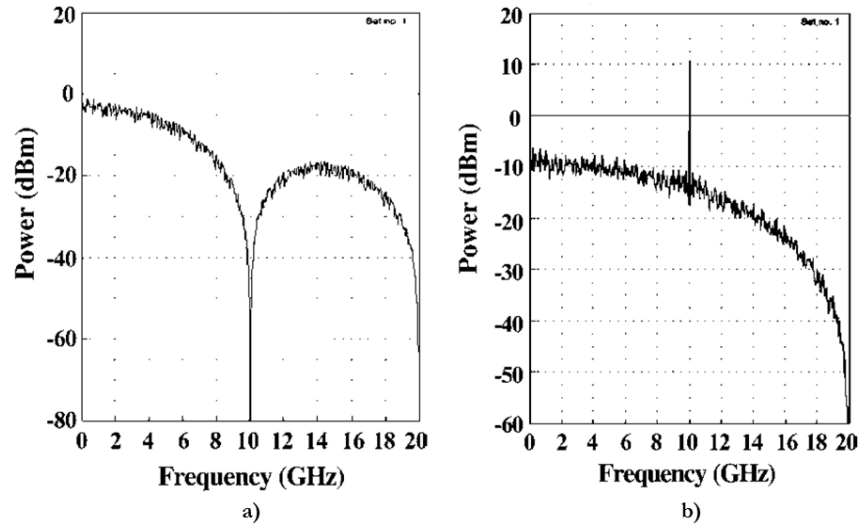

Figure 3.16 - RF spectra of OOK modulated signals: NRZ (a) and RZ (b) [13]

The differences between the two spectra are clear: while in the NRZ case the clock component vanishes, in the RZ situation there is a peak component at the clock frequency. The reason why this happens can be explained by the modulation process that was already described in the previous section (section 3.2 under the "RF spectrum analysis" subsection), where the dependence of the clock component peak power on the dispersion was stated.

What we propose is an alternative technique, where a well-known dispersive element is added to the optical signal path, so that the power at the clock frequency component generated by this

dispersive element accumulates with the overall link dispersion to monitor. By calculating the difference between the power at the clock component before and after the reference dispersive element it is possible to determine the sign of the overall group velocity dispersion.

The dependence of the clock component peak power on dispersion can be described according to the following expression [16]:

$$P \propto \sin^2\left(\frac{\pi\lambda^2 f_{RF}^2}{c} GVD\right), \tag{3.7}$$

where λ is the carrier wavelength, f_{RF} the clock frequency and GVD the overall group velocity dispersion.

While in the future, access networks will remain to be based mostly on OOK modulated signals, in the core network field new systems modulate the signals using the phase, as was already mentioned in the first chapter.

In these systems the information is encoded on the phase with, for instance, QPSK or DP-QPSK. When a signal is modulated with these formats, phase changes are imposed by the modulator. This, however also induces slight modulation on the signal amplitude. This can be observed in the direct detection eyediagram of a back-to-back QPSK (10 Gbaud/s) signal in Figure 3.17.

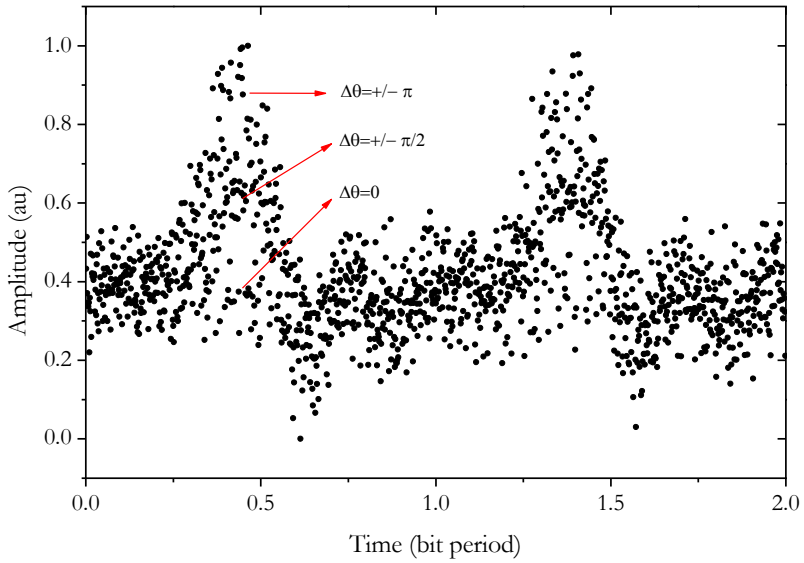

Figure 3.17 - Eyediagram obtained with direct detection of signal modulated with QPSK

This eyediagram was measured using an oscilloscope from *Agilent* (*Model 86100A*). It's clear that phase modulated signals also present a modulation on the amplitude and its variation depends on the phase change imposed by the modulator. The RF spectrum will then present a component at clock frequency whose peak will be dependent on the dispersion of the signal.

The proposed method was experimentally tested on an OOK NRZ signal modulated at 10 and 40 Gb/s as well as on a QPSK 10 Gbaud/s signal.

3.3.2 Simulation description

The simulations developed for this work were written using Matlab scripts. Here, a brief description of the developed script is presented.

Initially, the signal in the time domain is generated by creating a vector with a stream of bits with rectangular shape. This vector is then transformed into a Gaussian like waveform applying the following expression [1].

$$A(0,T) = A_0 \cdot e^{\left(-\frac{1+iC}{2}\cdot\left(\frac{t}{T_0}\right)^{2m}\right)}, \tag{3.8}$$

where A_0 is the peak amplitude; C the chirp factor; T_0 the impulse half-width at $1/e$ intensity and m controls the pulse shape and in this situation takes the value 3, which is the value for super Gaussian pulses and adequate for this scenario.

To obtain the signal in frequency domain, a FFT is applied. Finally, to induce the dispersion effect into the signal, the following expression is used [18]:

$$B(z,\omega) = B(0,\omega)\cdot e^{\left(\frac{i}{2}\beta_2\omega^2 z\right)}, \quad \beta_2 = -\frac{D\lambda^2}{2\pi c}, \tag{3.9}$$

where $B(0,\omega)$ is the optical signal at the optical fibre input, ω is the frequency of the optical carrier, z the total span of the fibre, D the dispersion coefficient, λ the wavelength of the carrier and c the speed of light in vacuum. From this, the RF spectrum is calculated and the peak power of the clock component is extracted.

3.3.3 Experimental setup and results

3.3.3.1 Implementation on OOK signals

Figure 3.18 shows the schematic of the experimental setup used to validate the proposed monitoring technique for a single channel modulated at 10 Gb/s.

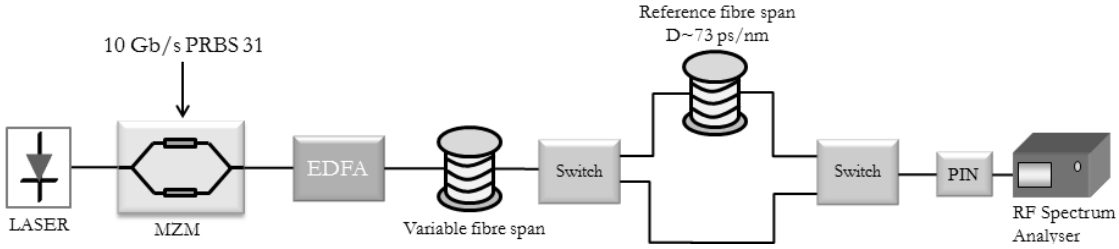

Figure 3.18 - Setup implemented to monitor the GVD in a 10 Gb/s OOK signal

A distributed feedback laser is used to generate a continuous wave signal, peaking at 1550.12 nm that is modulated by a MZM at a bitrate of 10 Gb/s, with a 2^{31}-1 PRBS bit sequence in a NRZ data format. The optical signal is then injected into a SMF, where several spans of fibre (from 5 km to 40 km) were considered in order to get a wide range of GVD values. A dispersion compensation fibre (DCF) with an overall dispersion of - 680 ps/nm was also used in order to get negative dispersion values. An EDFA is used to amplify the signal and compensate the optical fibre propagation losses, assuring a constant average optical power value in the photodiode. Then an optical switch enables the selection between two paths before conversion to the electrical domain by a photodiode PIN (HP 11982A): i) straight to RF spectrum analyser (R&S FSP40), resulting in the measurement of the clock component power designated as P_1; ii) through a reference dispersive element that induces an extra amount of dispersion (in this case 73 ps/nm), resulting in a clock component power designated as P_2.

The incorporation of the reference dispersive element and the measurement of P_2 enable the determination of the GVD sign, by taking the difference between P_2 and P_1. If the optical signal has suffered a positive dispersion during propagation, the extra (positive) dispersive reference element will distort the signal even more and P_2 will be higher than P_1, so the difference P_2-P_1 will be positive; if the signal has been under negative dispersion, the extra element will compensate it and difference P_2-P_1 will be negative. Therefore, by measuring P_2-P_1 we can fully characterize the dispersion.

The same procedure was repeated for a signal modulated at 40 Gb/s. The implemented setup was similar to the one presented in Figure 3.18. In this case the laser is modulated by the modulator (*SHF 12100B*) at a bitrate of 40 Gb/s, with a 2^{31}-1 PRBS bit sequence in a NRZ data format. The tolerance to GVD on a signal modulated at this bitrate will be much lower, so the spans of fibre used for this experiment were much shorter. Spans from 0 to 5 km were used, as well as a DCF of D~-54 ps/nm. The reference dispersive element was a span of fibre that imposes a positive GVD of 17 ps/nm.

In Figure 3.19 we show the eyediagrams of the detected signal modulated at 10 Gb/s for different values of dispersion obtained for both experimental and simulation scenarios. The experimental eyediagrams were measured with an oscilloscope (*Agilent 86100A*), where an optical filter

(*Santec OTF30M* - BW(3 dB)=0.3nm) is placed before the PIN receiver, in order to eliminate the out of band noise generated by the EDFA.

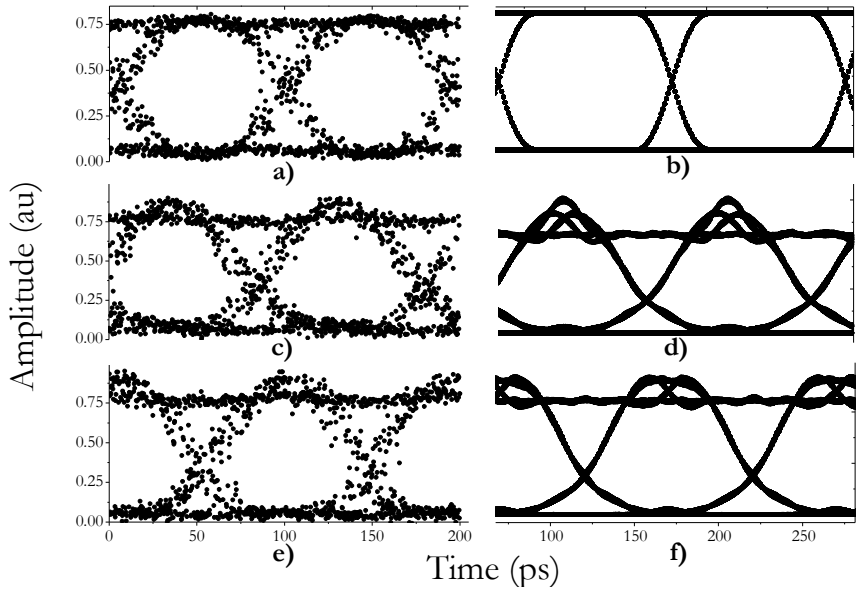

Figure 3.19 - Eyediagrams for different imposed dispersion values. (a) Back to back experimental values; (b) Back to back simulated values; (c) GVD ~ 408 ps/nm experimental values; (d) GVD ~ 408 ps/nm simulated values; (e) GVD ~ −352 ps/nm experimental values; (f) GVD ~−352 ps/nm simulated values.

The shapes of the experimental and simulated eyediagrams are similar to each other, confirming that the simulation describes accurately the laboratorial scenario.

In Figure 3.20 is shown the obtained power at 10 GHz (P_f) as function of the GVD, for the simulation and experimental scenarios, showing the capacity to predict the group velocity dispersion value from this measurement.

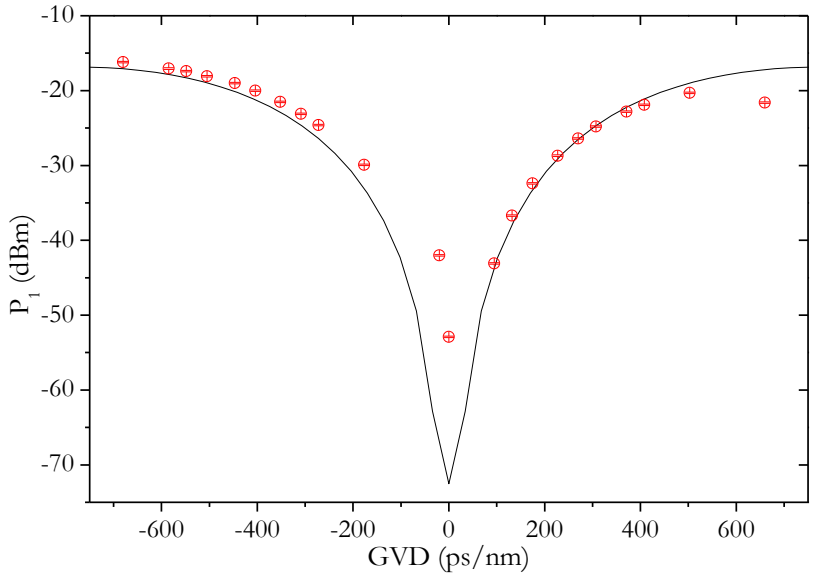

Figure 3.20 – Power of the clock frequency component as function of the GVD for the 10 Gb/s OOK modulated signal. Circles are experimental points and line is simulation. The error bars represent the oscillations verified during the measurement process.

The measurement of P_1 gives information about the dispersion absolute value, but the sign remains unknown. This can be obtained with the reference dispersive element. In Figure 3.21 and Figure 3.22 are shown the RF spectra obtained via simulation and experimentally, respectively, for different values of the overall group velocity dispersion: back to back (B2B), 408 ps/nm and -352 ps/nm, before and after the propagation on the extra dispersive element.

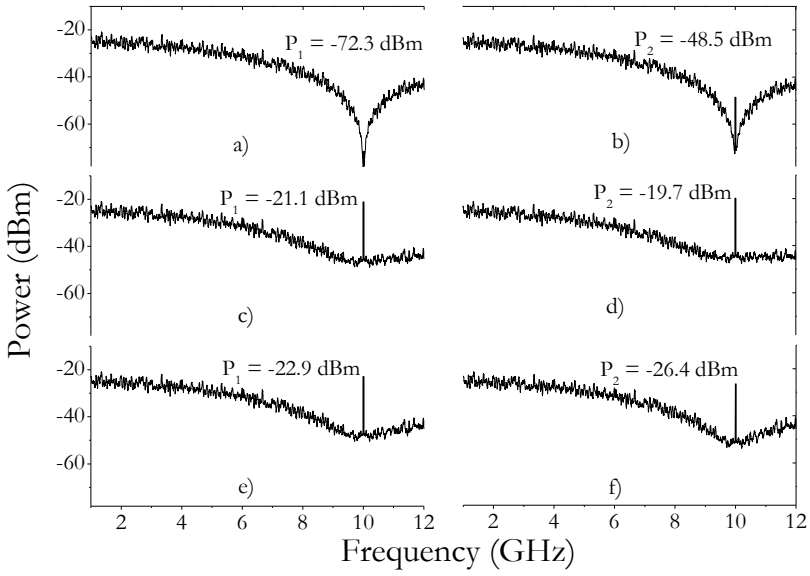

Figure 3.21 - Simulation of the RF spectra of the signal (OOK 10 Gb/s) for different GVD values, before (left) and after the reference dispersive element (right). Back to back (top); GVD ~ 408 ps/nm (middle); GVD ~ -352ps/nm (bottom).

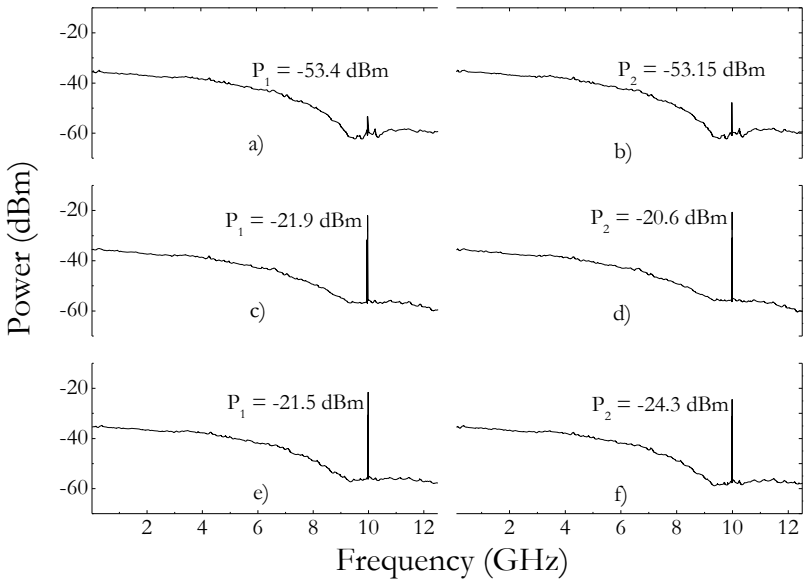

Figure 3.22 - RF spectra of the signal (OOK 10 Gb/s) for different GVD values, measured with the RF spectrum analyser, before (left) and after the reference dispersive element (right). Back to back (top); GVD ~ 408 ps/nm (middle); GVD ~ -352ps/nm (bottom).

When the dispersion is positive, a positive difference between P_2 and P_1 is observed (middle graphic). For a negative dispersion the opposite situation occurs (bottom graphic). This occurs for both plots (the simulation and the experiment) confirming the good agreement between these two sets of results. Therefore, the measurement of P_2 gives information on the dispersion sign. In Figure 3.23 are displayed the final results where P_1 returns the value of dispersion and P_2-P_1 returns the sign.

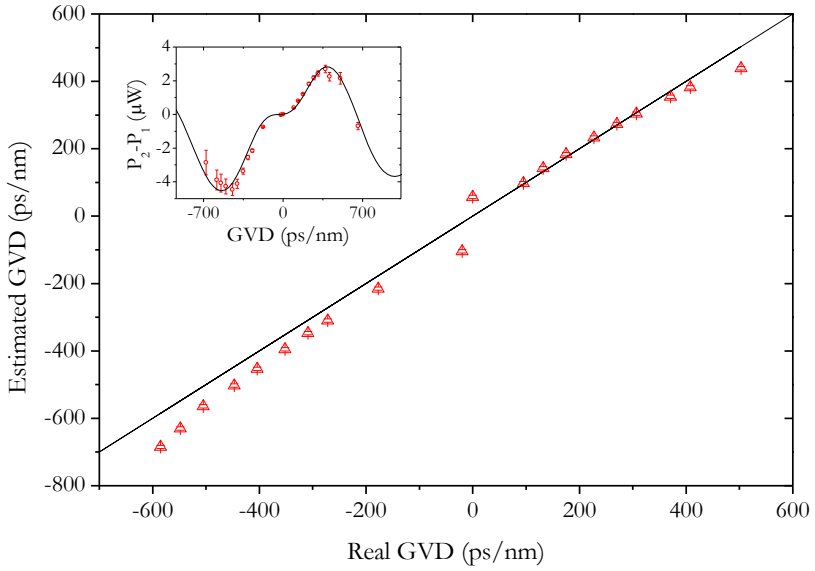

Figure 3.23 - Estimated GVD as function of the actual GVD for a 10 Gb/s OOK signal. Inset shows P_2-P_1 as function of the GVD. The error bars represent the uncertainty interval when measuring the GVD through visual inspection using Figure 3.20.

By resorting to the calculation of P_2-P_1 it was possible to distinguish the sign of the GVD. The inset of Figure 3.23 shows the obtained values of P_2-P_1 as function of the GVD, where dots are experimental points and line is the simulation. Using this technique it was possible to retrieve the GVD of a signal with a maximum error of 100 ps/nm in a range of [-600,600] ps/nm.

As it was previously mentioned, this method was also applied on a 40 Gb/s OOK signal. In Figure 3.24 is shown the eyediagrams of the signal modulated at 40 Gb/s OOK for different amounts of dispersion for both experimental (left) and simulation (right) scenarios.

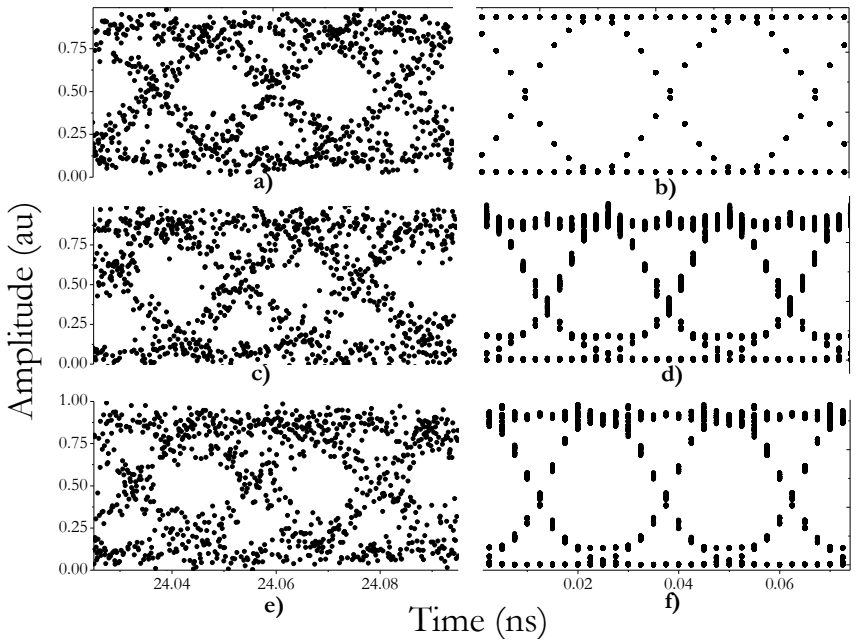

Figure 3.24 - Eyediagrams of the signal modulated at 40 Gb/s with OOK NRZ format for different dispersion values. Back to back (top); GVD~-54 ps/nm (middle); GVD~34ps/nm (bottom)

As the dispersion was varied, by changing the fibre spans, the peak power of the clock component was retrieved from the RF spectrum analyser. In Figure 3.25 is shown the obtained curve of P_1 as function of the imposed GVD.

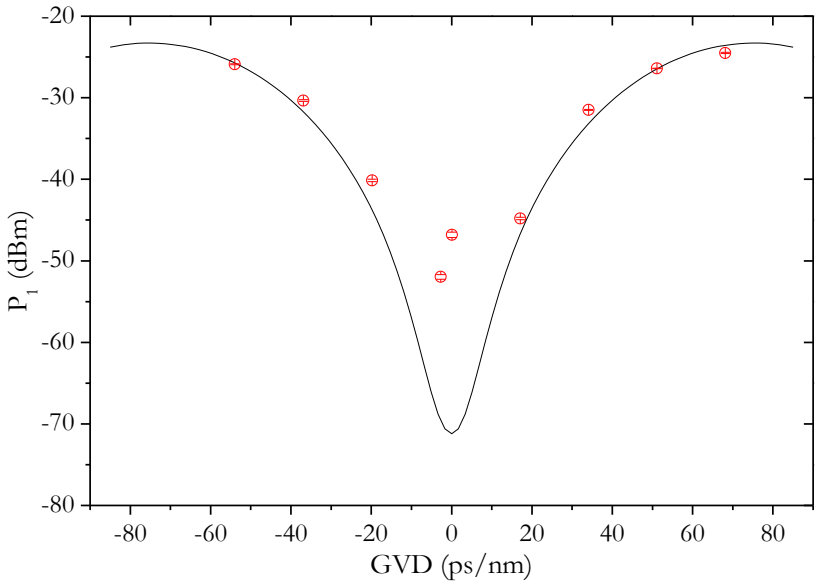

Figure 3.25 - Results obtained when measuring P_1 as function of the GVD on 40 Gb/s OOK signal. Circles are experimental points and line is simulation

Excluding the measurement range, the dependence of P_1 to the dispersion is similar to the one obtained in the 10 Gb/s situation, as expected. Near the B2B scenario (GVD~0) it was very difficult to get an accurate value of GVD using this method. However for values |GVD|>15 ps/nm the experimental points fall closely to the simulation curve.

In Figure 3.26 and Figure 3.27 are displayed the RF spectra obtained through the simulation and experimentally, for different values of dispersion, where both P_1 and P_2 are identified.

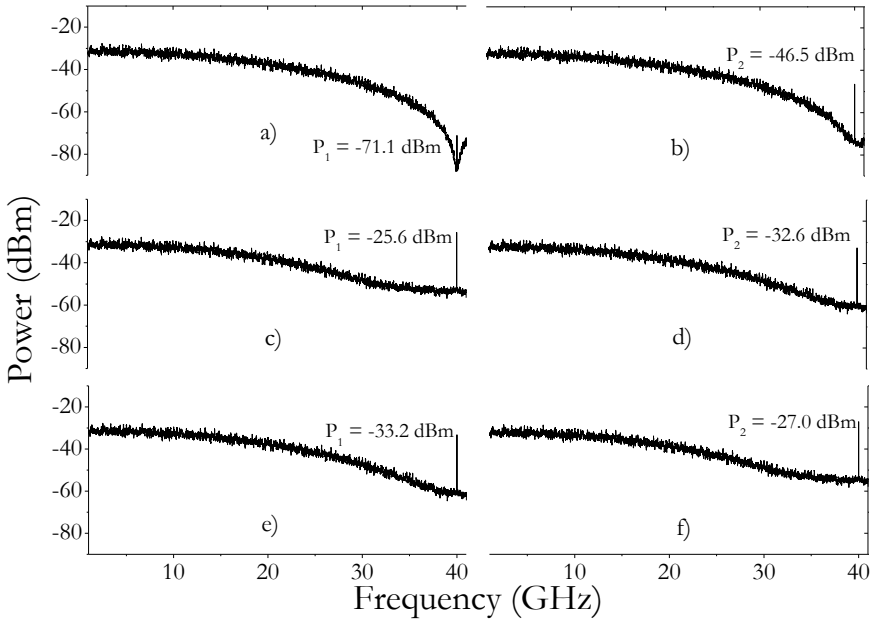

Figure 3.26 - Simulation of the RF spectra of the signal with different GVD values: a) Back to back (B2B); b) B2B after the extra dispersive element (17 ps/nm); c) GVD ~ -54 ps/nm before the extra dispersive element and d) after the extra dispersive element; e) GVD ~ 34 ps/nm before the extra dispersive element and f) after.

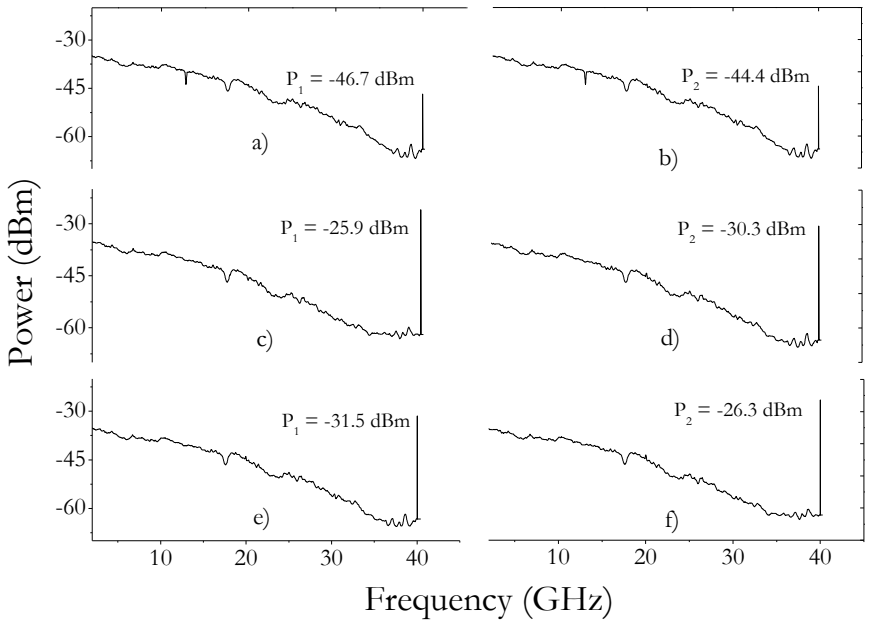

Figure 3.27 - RF spectra of the signal, obtained experimentally, with different GVD values: a) Back to back (B2B); b) B2B after the extra dispersive element (17 ps/nm); c)GV D ~ -54 ps/nm before the extra dispersive element and d) after the extra dispersive element; e) GVD ~ 34 ps/nm before the extra dispersive element and f) after.

The same behaviour as the one verified in the 10 Gb/s case, is observed here and the difference between P_2 and P_1 will give the sign of dispersion. In Figure 3.28 is shown the estimated GVD (considering already its sign) as function of the real one. The inset shows the difference between P_2 and P_1 as function of the GVD, from which the sign is extracted.

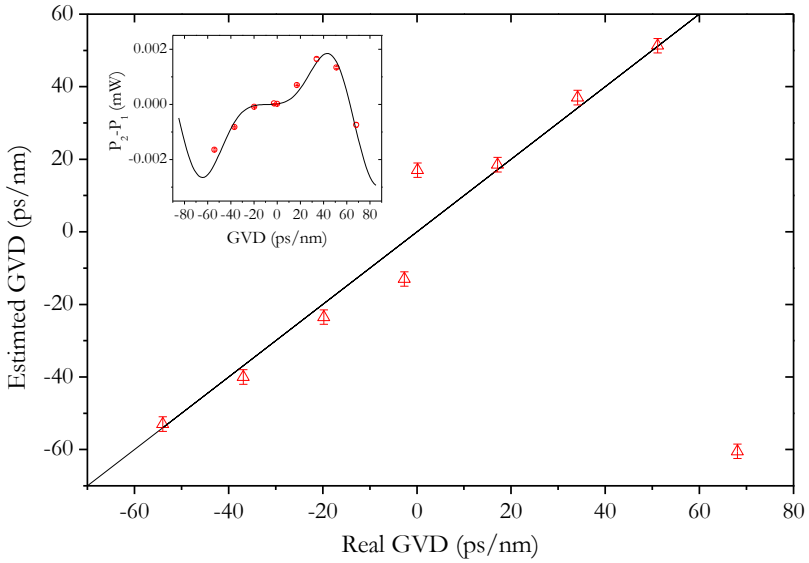

Figure 3.28 - Obtained results of the GVD monitoring technique applied on a 40 Gb/s OOK signal

The application of this method on a 40 Gb/s is also possible as the results show. However the measurement range is obviously shortened. With this technique it was possible to determine the signal GVD in a range of [-60,60] ps/nm with a maximum error of 17 ps/nm, but as the GVD gets increases (|GVD| > 15 ps/nm) this error decreases drastically to 3 ps/nm.

3.3.3.2 Implementation on a QPSK signal

The proposed method was extended to a QPSK modulated signal with 10 Gbaud/s, which corresponds to 20 Gb/s. In this case, no simulation was performed, thus only experimental results are shown.

The experimental setup applied in this case is, on the essential, very similar to the previously described ones and is shown in Figure 3.29.

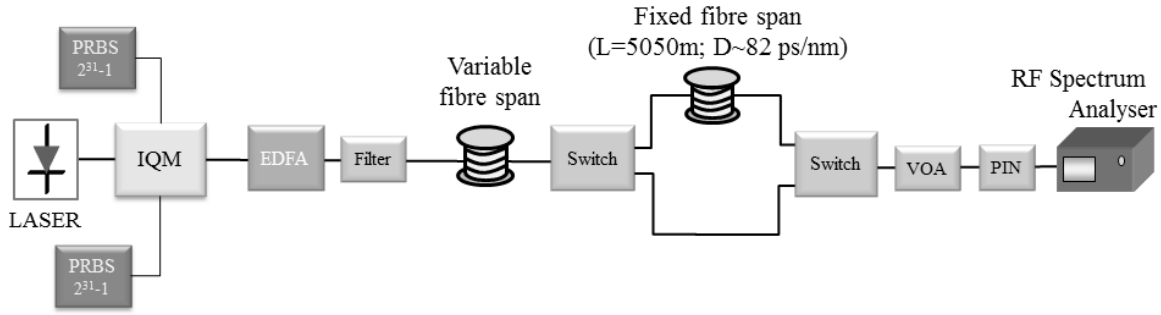

Figure 3.29 - Experimental setup implemented to test the method on QPSK signal

The transmitter is based on an external cavity laser source (peaking at 1549.3 nm), modulated using an IQ Modulator (IQM, from *YYlabs*, model D0156DQ MBC) fed with two 10 Gb/s - NRZ electrical signals encoded with 2^{31}-1 PRBS. An EDFA is used as a pre amplifier in order to compensate the attenuation imposed by the fibre. The noise generated by the EDFA at the adjacent spectral regions is filtered out by an optical filter centred at the signal wavelength. The remaining part of the setup is similar to the one in the OOK scenario and was already described.

Figure 3.30 shows the constellation of the QPSK signal with different amounts of dispersion. These constellations were obtained with an oscilloscope (Tektronix MS072004C) and processed with a Matlab based application.

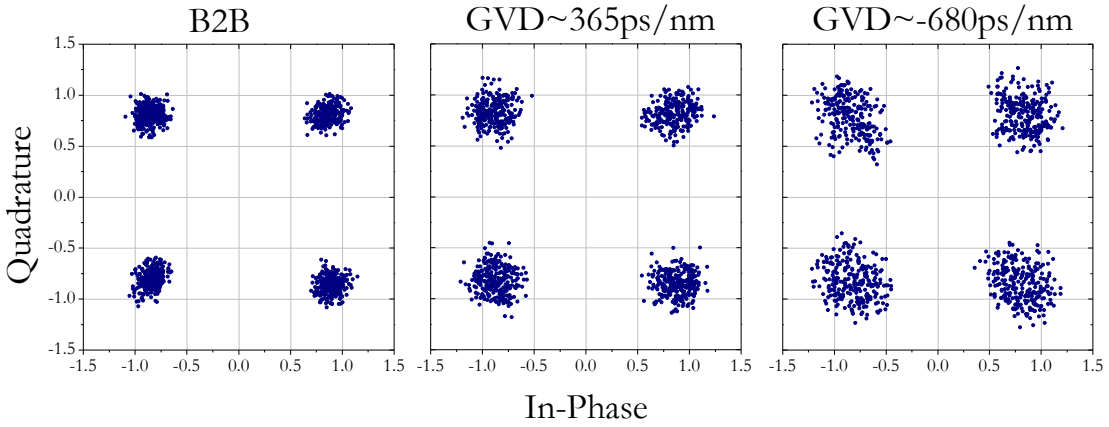

Figure 3.30 - Constellations of the QPSK signal with different dispersions

The effect of dispersion is evident in these constellations. As GVD value increases the quality of the received signal is clearly degraded. Also it's not possible, from this data, to distinguish the sign of dispersion.

The eyediagrams via direct detection of the same signals were retrieved as well and are displayed in Figure 3.31.

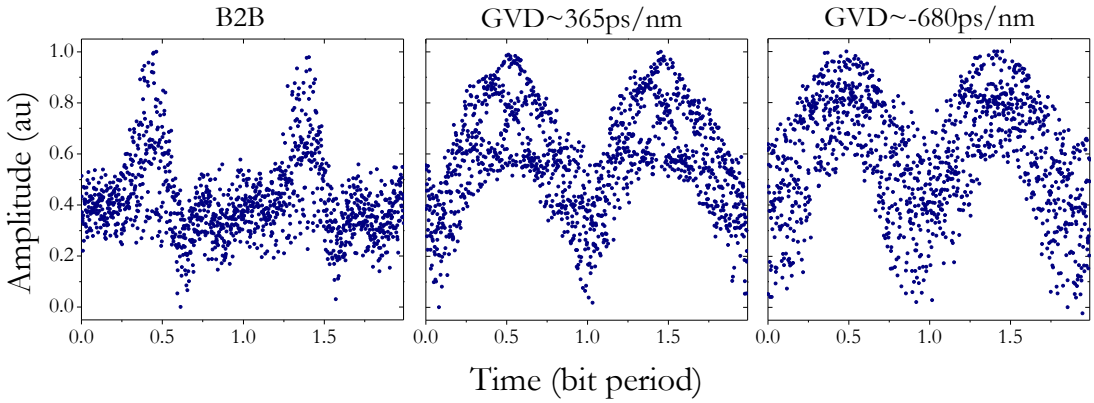

Figure 3.31 - Direct detection eyediagrams of the QPSK signal with different amounts of dispersion

Although the eyediagrams suffer modification, not much information can be taken from them. Resorting to the RF spectra, the peak power at the 10 GHz component was measured and in Figure 3.32 the obtained results as function of the GVD are shown.

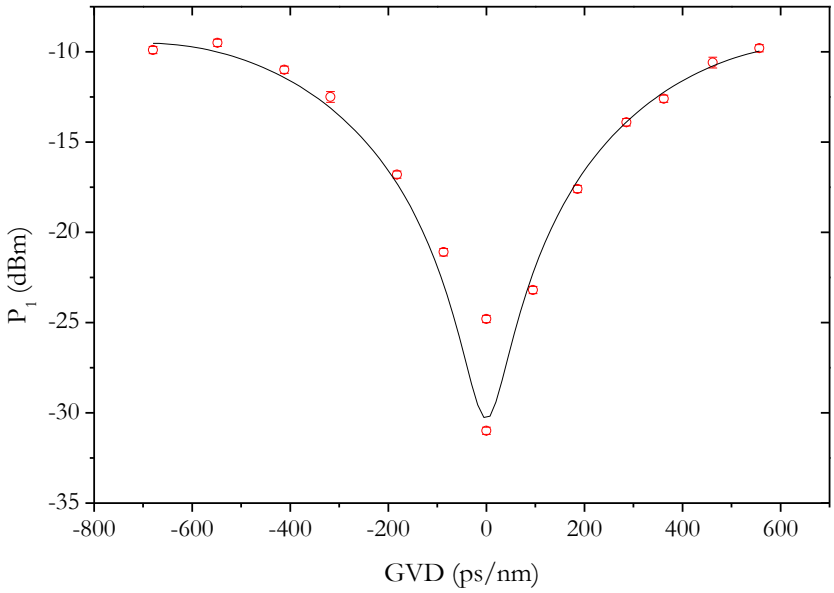

Figure 3.32 – Measured P_1 as function of the GVD for the 10 Gbaud/s QPSK signal: circles are experimental data and line is a theoretical fit

It is clear that the peak power of the clock component presents a dependence on the dispersion which is similar to the one verified in the OOK NRZ signal. This means that, although it is a phase modulated signal that is propagating, it is possible to use direct detection to estimate the dispersion suffered by the signal, using the same methods applied on amplitude modulated signals. A theoretical fit was calculated, which is represented by the line in Figure 3.32 and determined based on equation (3.7) using the following expression:

$$P_1 = P_0 + A \cdot \sin^2\left(k \cdot \frac{\pi \cdot \lambda^2 \cdot f_{RF}^2}{c} GVD\right) \tag{3.10}$$

The obtained parameters are shown in Table 3.1 and were calculated by chi square minimization.

Table 3.1 - Fit parameters

P_0 (dBm)	A (dBm)	K	r^2
$(9.28 +/- 2.05)\cdot10^{-4}$	0.111 +/- 0.002	1.12 +/- 0.16	0.92

The results from Figure 3.32 show that the fit describes the real scenario very well as the experimental points fall closely to the fit curve. Also, the value of R^2 from the fit calculation is close to the desired 1, confirming the goodness of the fit.

Figure 3.33 displays the RF spectra of the signal, from which P_1 (left) and P_2 (right) were extracted, for different amounts of GVD.

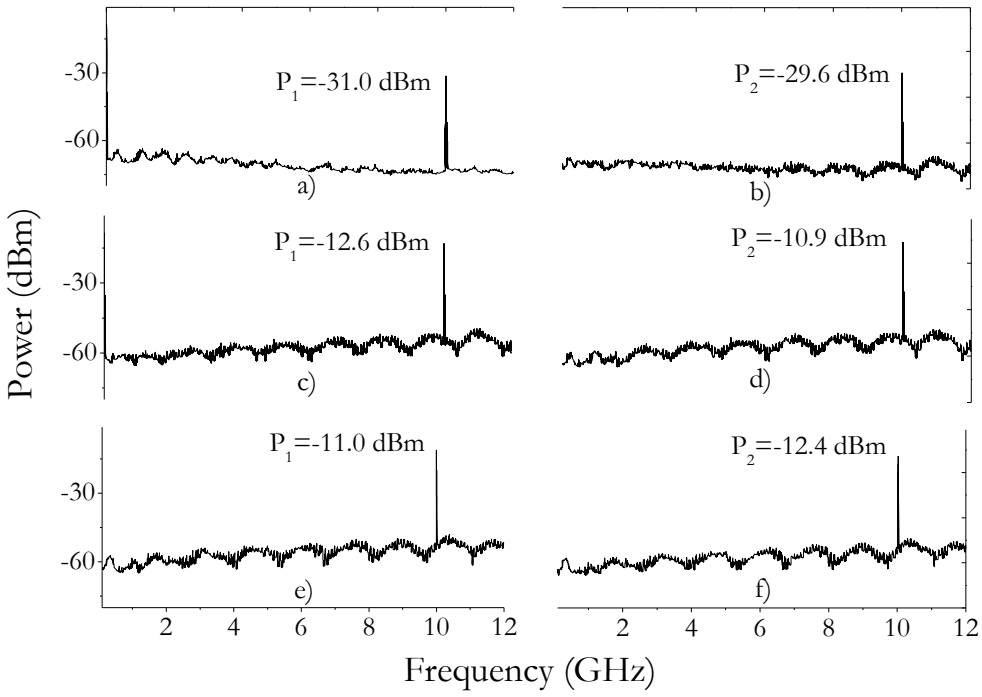

Figure 3.33 - RF spectra of the QPSK signal with different dispersions: Back to back (top left); B2B after the extra dispersive element (82 ps/nm) (top right); c) GVD ~ 360 ps/nm before the extra dispersive element (middle left) and after the extra dispersive element (middle right); GVD ~ -412 ps/nm before (bottom left) and after (bottom right)

These spectra are quite different from the previous ones (from the OOK signals). There's some periodical variation at the noise level that arises as the GVD increases, which doesn't occur in the OOK scenarios. However, that doesn't affect the final result and the peak power at the clock component still varies with dispersion and the measurement of the difference between P_2 and P_1 will give information on the sign of dispersion as well.

In Figure 3.34 are shown the final results where we have the estimated GVD already taking into consideration its sign) as function of the actual GVD. The inset shows the difference between P_2 and P_1 as function of the dispersion, from which the sign is extracted.

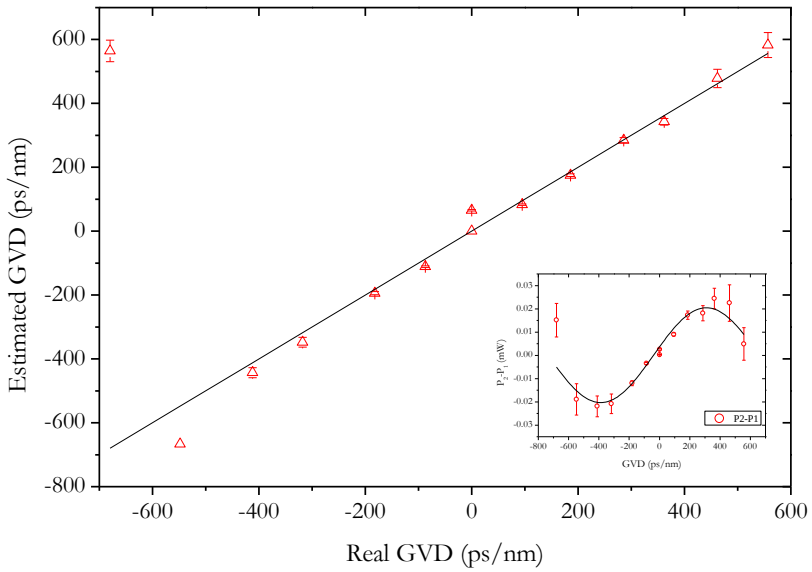

Figure 3.34 - Final results of the GVD monitoring technique applied on a 20 Gb/s QPSK signal. Triangles are experimental data and line is GVD calculated from the fit shown in Figure 3.32.

Results show that this technique can also be applied to a phase modulated signal. The achieved measurement range is [-600,600] ps/nm, like in the OOK 10 Gb/s scenario and the maximum measurement error within that range was 120 ps/nm.

3.4 Summary and conclusions

In this chapter, a GVD monitoring method was presented and its implementation was thoroughly described.

The proposed method is based on the analysis of the signal RF spectrum and the measurement of the power at clock frequency component. It is known that this power is dependent on the signal GVD, but through this measurement it is not possible to distinguish the sign. By applying an extra dispersive element the determination of the sign becomes possible using a simple setup.

This technique was applied on signals with different modulation bitrates and formats such as: OOK (10 and 40 Gb/s) and QPSK (20 Gb/s). For the OOK 10 Gb/s signal the GVD was experimentally measured in a range of [-600,600] ps/nm with a maximum error of 100 ps/nm. Similar results were obtained for the QPSK signal with a bitrate of 20 Gb/s. Although the signal is modulated on the phase, there are amplitude fluctuations imposed by the modulation process, resulting in the variation of the signal amplitude, with a frequency of 10 GHz. Thus, the GVD measurement range is the same as the one in OOK 10 Gb/s. Results show and confirm that it is possible to measure the

GVD of a QPSK (20 Gb/s) in a range of [-600,600] ps/nm with a maximum error of 120 ps/nm. To the experimental data a fit based on Equation (3.7) was calculated with a r^2 value of 0.92.

This method was also tested on an OOK signal modulated at 40 Gb/s. With this high bitrate, the GVD degrades the signal more prematurely, because the bit duration is one fourth shorter. This has also an effect on the GVD measurable range, as is confirmed from the obtained results. A measurable range of [-60,60] ps/nm was achieved. Near the origin (GVD~0 ps/nm) the measurement is quite difficult presenting high error. But as the GVD increases ($|GVD| > 15$ ps/nm), the error decreases drastically and GVD was estimated with a maximum error of 3 ps/nm.

The measurement of the clock frequency component provides a reliable and simple way to determine a signal GVD. And, with a simple modification on the setup it's possible to identify its sign. The main drawback of this technique is maybe the range of measurement, mainly on high bitrate signals. However, this method presents one important advantage which is the fact that is applicable on both amplitude and phase modulated signals.

References

[1] G. P. Agrawal, *Fiber-Optic Communication Systems*, Fourth Edition ed.: John Wiley & Sons, Inc., 2010.

[2] R. Hui and M. O'Sullivan, *Fiber Optic Measurement Techniques*: Elsevier Science, 2009.

[3] C. Sheng, L. Li, S. Simin, L. Jun, Y. Quan, and L. Deming, "Highly sensitive chromatic dispersion monitors based on phase-matched four-wave mixing," in *International Conference on Information Photonics*, 2011, pp. 1-2.

[4] L. Shenping and D. V. Kuksenkov, "A novel dispersion monitoring technique based on four-wave mixing in optical fiber," *Photonics Technology Letters, IEEE,* vol. 16, pp. 942-944, 2004.

[5] P. S. Westbrook, B. J. Eggleton, G. Raybon, S. Hunsche, and H. Tsing Hua, "Measurement of residual chromatic dispersion of a 40-Gb/s RZ signal via spectral broadening," *Photonics Technology Letters, IEEE,* vol. 14, pp. 346-348, 2002.

[6] T. Luo, C. Yu, Z. Pan, Y. Wang, J. E. McGeehan, M. Adler, and A. E. Willner, "All-optical chromatic dispersion monitoring of a 40-Gb/s RZ signal by measuring the XPM-generated optical tone power in a highly nonlinear fiber," *Photonics Technology Letters, IEEE,* vol. 18, pp. 430-432, 2006.

[7] S. D. Dods and T. B. Anderson, "Optical performance monitoring technique using delay tap asynchronous waveform sampling," *Optical Fiber Communication Conference/National Fiber Optic Engineers Conference,* pp. 2139-2141, 2006.

[8] Y. Benlachtar, R. I. Killey, and P. Bayvel, "Chromatic dispersion monitoring using synchronous sampling," *Optical Fiber Communication Conference/National Fiber Optic Engineers Conference,* pp. 837-839, 2006.

[9] X. Wu, J. A. Jargon, R. A. Skoog, L. Paraschis, and A. E. Willner, "Applications of Artificial Neural Networks in Optical Performance Monitoring," *Journal of Lightwave Technology,* vol. 27, pp. 3580-3589, 2009.

[10] T. E. Dimmick, G. Rossi, and D. J. Blumenthal, "Optical dispersion monitoring technique using double sideband subcarriers," *Photonics Technology Letters, IEEE,* vol. 12, pp. 900-902, 2000.

[11] G. Rossi, T. E. Dimmick, and D. J. Blumenthal, "Optical performance monitoring in reconfigurable WDM optical networks using subcarrier multiplexing," *Journal of Lightwave Technology,* vol. 18, pp. 1639-1648, Dec 2000.

[12] M. N. Petersen, Z. Pan, S. Lee, S. A. Havstad, and A. E. Willner, "Online chromatic dispersion monitoring and compensation using a single inband subcarrier tone," *Ieee Photonics Technology Letters,* vol. 14, pp. 570-572, Apr 2002.

[13] Z. Pan, Y. Xie, S. A. Havstad, Q. Yu, A. E. Willner, V. Grubsky, D. S. Starodubov, and J. Feinberg, "Real-time group-velocity dispersion monitoring and automated compensation without modifications of the transmitter," *Optics Communications,* vol. 230, pp. 145-149, Jan 15 2004.

[14] C. Chang-Joon, T. B. Anderson, and A. Nirmalathas, "OSNR-independent chromatic dispersion monitoring on 40Gb/s DPSK signals using two RF filters," in *OptoElectronics and Communications Conference*, 2009, pp. 1-2.

[15] Z. Jian, L. Chao, L. Zhaohui, H. Y. Tam, and P. K. A. Wai, "Optical signal monitoring of DPSK signals using RF power detection," in *Joint conference of the Opto-Electronics and Communications Conference and the Australian Conference on Optical Fibre Technology*, 2008, pp. 1-2.

[16] A. L. Campillo, "Chromatic dispersion-monitoring technique based on phase-sensitive detection," *Ieee Photonics Technology Letters,* vol. 17, pp. 1241-1243, Jun 2005.

[17] Y. C. Ku, C. K. Chan, and L. K. Chen, "Chromatic dispersion monitoring technique using birefringent fiber loop," *Optical Fiber Communication Conference/National Fiber Optic Engineers Conference,* pp. 2603-2605, 2006.

[18] M. Khafaji, H. Gustat, F. Ellinger, and C. Scheytt, "General Time-Domain Representation of Chromatic Dispersion in Single-Mode Fibers," *Ieee Photonics Technology Letters,* vol. 22, pp. 314-316, Mar 1 2010.

Chapter 4: Access Network Infrastructure Monitoring

4.1 Introduction

This chapter addresses the monitoring of the physical integrity of the network and the detection of failures in the fibres.

As described previously, access networks keep evolving into more complex architectures that provide a constant increase in transmission capacity. With the advent of PONs, the signal travels from the central office to the clients' premises entirely on passive elements, providing a cost effective solution for access networks. However, usually the physical infrastructure of a PON network is not monitored and an eventual fault can cause the interruption of service and impose losses in business for the service operator.

The occurrence of faults in the fibre network can be originated on several factors, for instance, accidental cuts or even voluntary ones; weather conditions such as temperature variations or the occurrence of floods which can give rise to the deterioration of the network. Another factor that must be taken into consideration is the fact that usually, when a network is installed, it is not fully operational. Usually the clients subscribe to the network progressively, and so several "dark" fibres, that are already installed, are activated only then. It is essential to take this into consideration and make sure that those early inactive lines are in order and can be activated [1].

The ideal monitoring system would somehow continuously supervise the deterioration of the network in order to prevent the occurrence of failures. In the eventuality of a failure, the monitoring system should be able to detect its occurrence and also locate it quickly and with minimal interruption of the data traffic service [2].

Optical time domain reflectometry (OTDR) is a technique, commercially available, commonly used to monitor point-to-point (P2P) networks such as long-haul links. As it will be described in the next section, its application on point-to-multipoint architectures is challenging, so other alternative methods have been under research [2].

In this thesis, a proof of concept of a simple method to monitor the physical integrity of an optical network is tested and its applicability in a real network is discussed. The proposed method is based on the application of FBG's as monitoring units distributed along the network.

4.2 State of the Art

Several solutions that perform the monitoring of the physical integrity of a network have been proposed over the years. Some present high advantages such as the capacity of accurately locate the failure as well as disadvantages such as the high implementation cost. A technique that satisfies all the requirements has been proven very difficult to achieve, so all techniques present their strengths and weaknesses.

Optical time domain reflectometry

Optical time domain reflectometry is the most studied technique for network monitoring. Its operation principle is based on the injection of an optical pulse to the network where, due to the presence of connectors and splices, it will undergo several reflections originating backscattering. This backscattered signal is then collected and its temporal trace is registered. In Figure 4.1 is shown a schematic of the OTDR setup and an example of the obtained temporal trace.

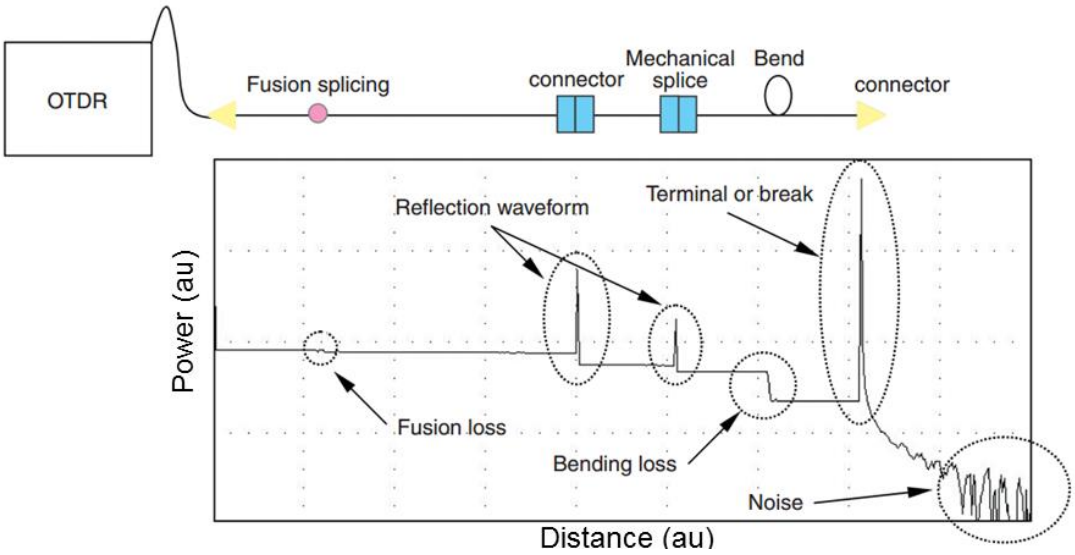

Figure 4.1 – Scheme of the OTDR operation principle: the operation setup (above) and the resulting trace (lower figure) [3]

Some companies, like *EXFO* or *JDSU*, commercialize OTDR solutions adequate for P2P architectures which are mostly used to monitor long-haul networks. The application of these devices is much more challenging in the access network field. In the presence of optical splitters at the remote nodes, the OTDR signal is split and the backscattered trace will contain the accumulated information from all the drop fibres making the identification of an eventual fault difficult or even impossible.

In order to monitor the physical state of these point-to-multipoint networks, some works with OTDR based techniques have been published and some of these will be described in the following sections.

Tuneable OTDR

In WDM PON's, the remote node may include an array waveguide (AWG), where individual wavelengths are split so that they propagate along the different drop fibres. These AWG's are cyclic, i.e., the outputs are periodic regarding the wavelength. This allows for both downstream and upstream to enter and exit the respective input/output of the AWG. One way to perform monitoring in this kind of networks is to use, in the OTDR, a tuneable source such as a tuneable laser or a broadband light source with a bandpass filter. Using the cyclic property characteristic of the AWG it is possible to send wavelength dependent signals to each branch and thus identify the faults at the OTDR. In Figure 4.2 is shown a setup that was experimentally tested, using this operation principle.

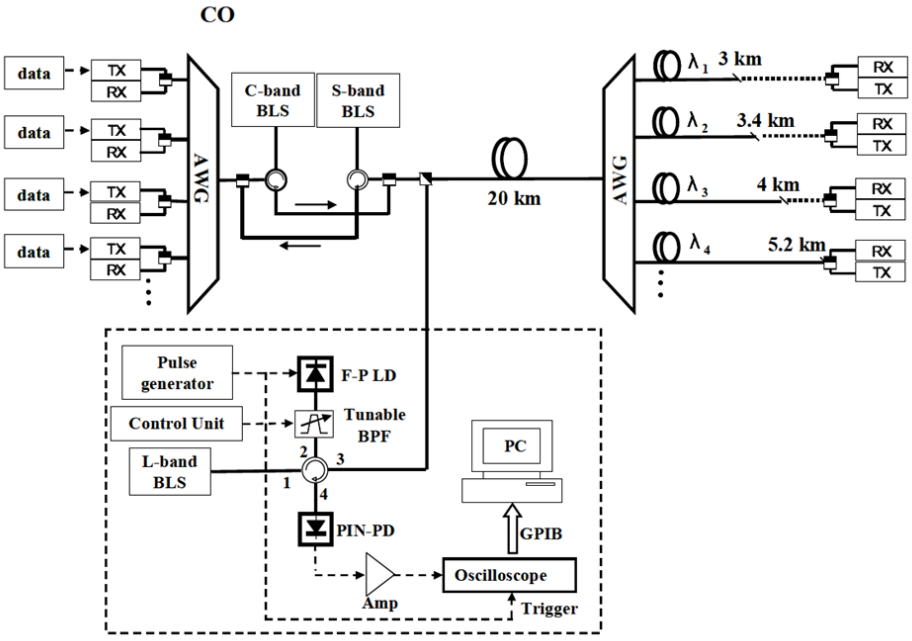

Figure 4.2 - Experimental setup of tuneable OTDR system on a WDM PON [4]

At the central office (CO), the signals with the transmission data (TX in Figure 4.2) are generated and the upstream data is received (RX in Figure 4.2). The dashed box represents the monitoring unit where the transmission side is composed by a broadband light source (BLS) with a Fabry-Perot laser diode (FP-LD) and tuneable bandpass filter (BPF) that form the tuneable optical pulsed signal. The detector side is composed by PIN photodiode (PIN-PD), an oscilloscope and a

signal processor unit that registers the incoming OTDR signal. Selecting the correct wavelength at the OTDR source it is possible to monitor the corresponding branch of the PON network individually.

In this experiment, some faults were imposed at different distances from the AWG and the results, displayed in Figure 4.3 show that the identification of the fault location is possible.

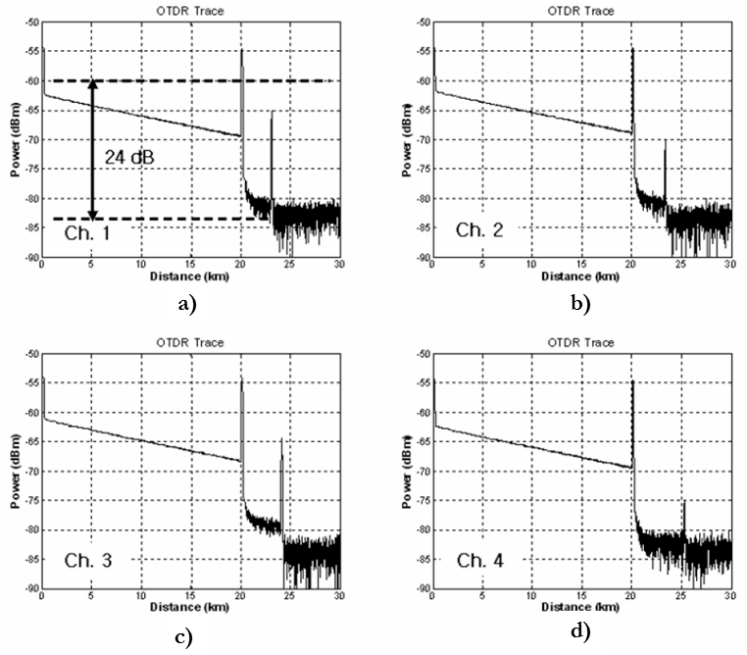

Figure 4.3 - Obtained OTDR traces for each of the drop fibres: λ_1 (a); λ_2 (b); λ_3 (c); λ_4 (d) [4]

Each plot shows the OTDR trace for a different branch. In each branch it is clear the presence of two high peaks: the first one, corresponding to the connection at the AWG (at 20 km) and another, corresponding to the failure in the branch (at different distances). The main advantage of this method is its capacity to identify the failure's location with high accuracy. This method offers a resolution of 100 m, which, in a PON with several kilometres of span, is considered acceptable.

Brillouin OTDR

Another interesting approach is the application of a Brillouin OTDR. In this case, the signal sent to the network induces fluctuations in the refractive index of the fibre which, on its turn, gives origin to backscattering of the signal with a frequency shift from the original one. This phenomenon (Brillouin scattering) has also been described in section 2.2. This frequency shift can be tailored so that it is unique for each drop fibre. In order to accomplish that, the fibres are doped with Germanium and Fluor with different concentrations. This method has been proposed by a researcher group at NTT

(Nippon Telegraph and Telephone Corporation) in Japan and in Figure 4.4 is shown the implemented experimental setup.

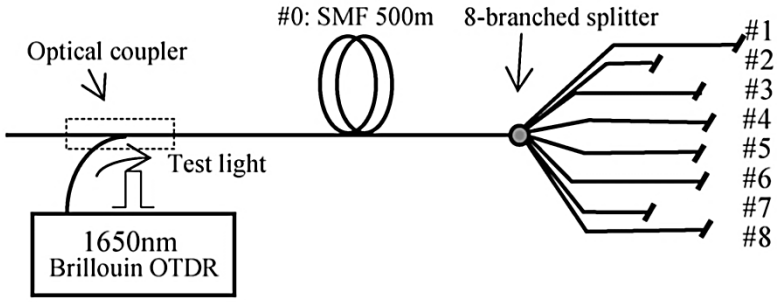

Figure 4.4 - Implemented setup of a Brillouin OTDR [5]

Analysing the OTDR trace at each of the Brillouin shifted frequencies, it's possible to identify an eventual defect in the network. In Figure 4.5 are shown some of the obtained traces.

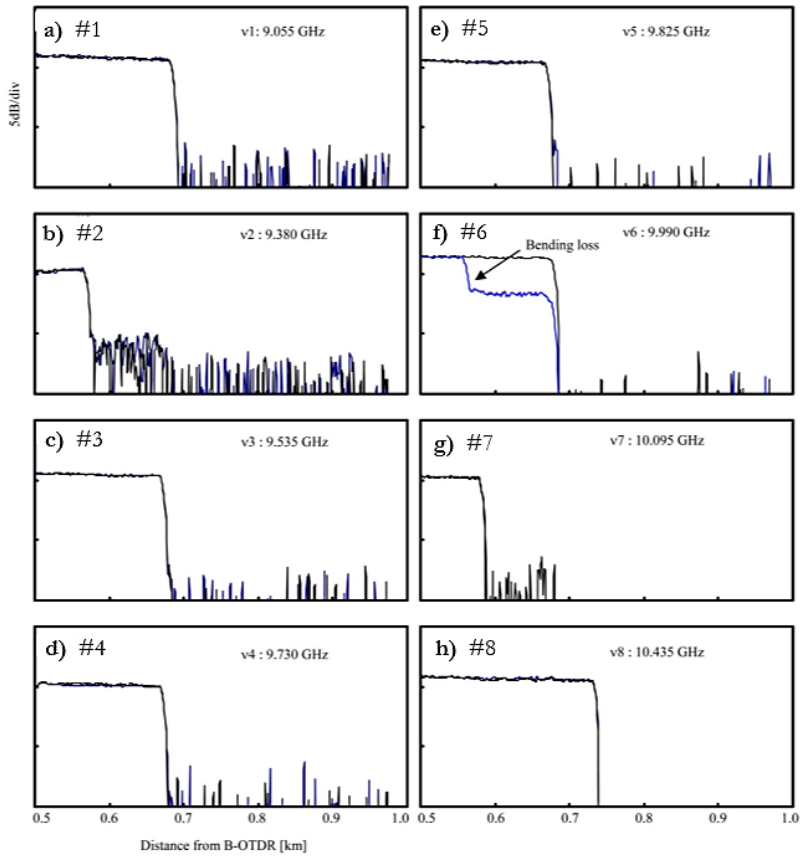

Figure 4.5 - Obtained Brillouin OTDR traces from the different drop fibre fibres where each is identified by different Brillouin shifted frequency [5]

The end of the fibre is easily identifiable when there are no failures along the pathway. In branch #6, the fibre is bent in order to observe its effect on the Brillouin OTDR trace. As it can be

seen in Figure 4.5 f), an attenuation of the signal is observed, indicating that there is a failure at that location.

Therefore, by detecting the signal from the correct Brillouin frequency, it is possible to analyse the health of that branch. This technique, however, presents one major drawback, which is the mandatory doping of the drop fibres, which is unpractical in many situations.

Optical Frequency Domain Reflectometry (OFDR)

Optical frequency domain reflectometry (OFDR) is a method that has been recently introduced to perform monitoring in PONs. Its operation principle is displayed in Figure 4.6.

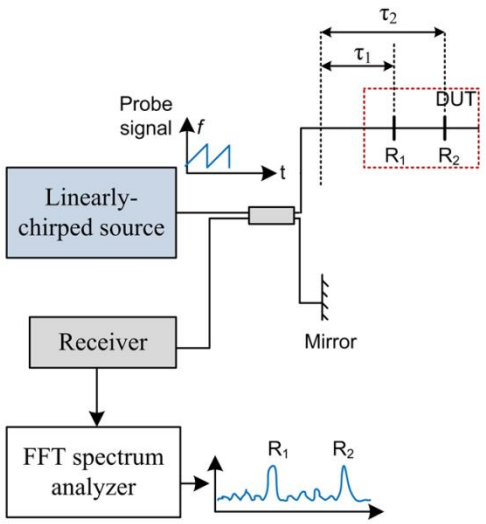

Figure 4.6 - Operation Principle of OFDR [6]

At the source, an optical signal (probe signal in the Figure 4.6) is frequency modulated. This signal is then divided, by an optical coupler, into two components. In one of the outputs the signal suffers reflections due to the device under test (DUT); on the other output the signal is also reflected by a reference mirror. The reflected signals are combined at the coupler which generates an interference signal with beat frequencies. This signal is then converted to frequency domain, via FFT, at the receiver side and the different beat frequencies are observed in the spectrum.

A diagram of the application of this principle in PON monitoring is shown in Figure 4.7.

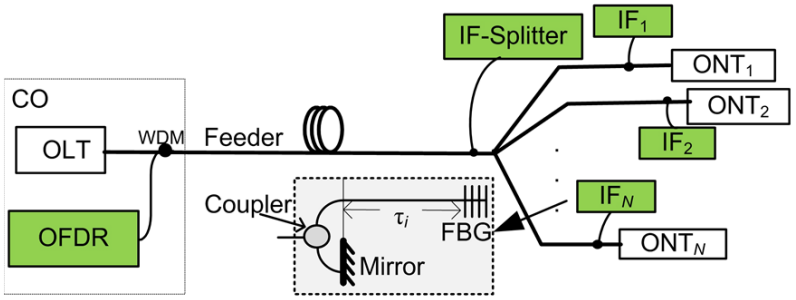

Figure 4.7 - Scheme of the OFDR monitoring system implemented on a PON [7]

To apply this technique in PON monitoring, several interferometer (IF in Figure 4.7) units are placed along the network. Each interferometer is attached to the network by a coupler. At one of the outputs of the coupler a FBG is placed at a pre-determined distance from the coupler (this distance is specific for each interferometer unit) that results in a time delay τ_i; at the second output will be the reference mirror. The interference and beat frequencies generated are then characteristic of each interferometer unit and can be identified when analysing the spectrum at the OFDR module.

In Figure 4.8 is shown the obtained spectrum from the setup shown in Figure 4.7.

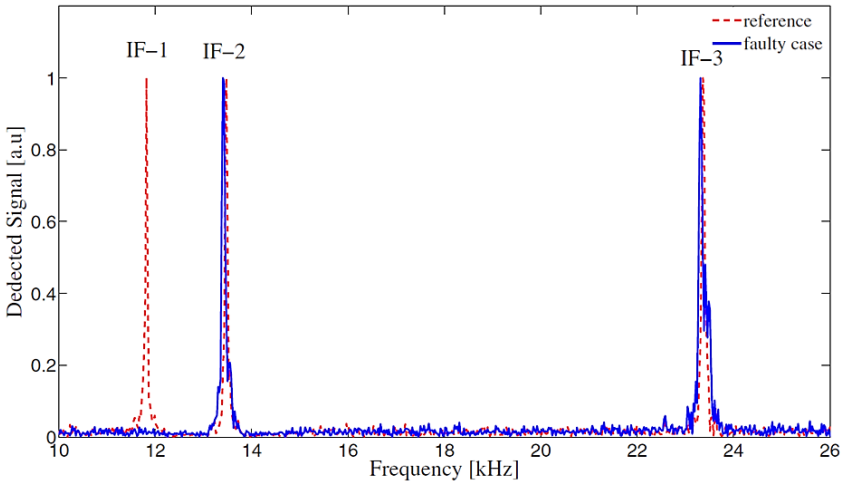

Figure 4.8 - Observed spectra from the OFDR fault monitoring system [7]

The red dotted is a reference and from it, it's possible to identify three interferometer units. The blue one only shows two peaks, representing two interferometer units, meaning that there is a failure on the branch of the IF-1.

This technique is only able to identify which branch is the faulty one. The knowledge of the failure's exact location is not possible this way.

FBG based techniques

As it was previously referred, FBG's are a cost effective component with many applications. So, it is without surprise that their application on PON monitoring is found on several different approaches. In the previous described technique, for instance, they are used as a component of the interferometer unit.

In another published work, a tuneable laser source is used at the OTDR and a FBG is placed at each of the termination points, so that the reflection trace is unambiguously observed at the OTDR [8]. In Figure 4.9 is shown the applied experimental setup.

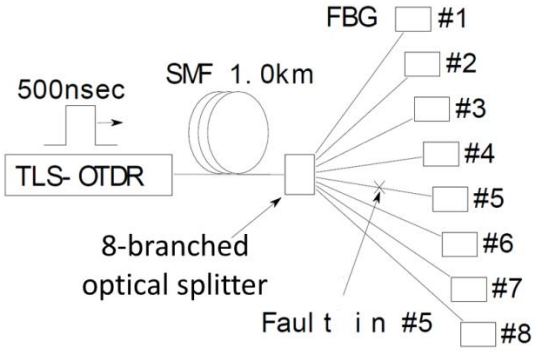

Figure 4.9 - Implemented setup of an OTDR based on the presence of FBGs [8]

A tuneable light source (TLS) OTDR sends a pulsed signal with a wavelength coincident to one of the FBGs. The FBGs are located at the end of each branch, at different distances from the splitter. The remote node is an optical splitter, without any kind of spectral filtering, so, once the signal leaves the OTDR, it is divided through all the drop fibres. Besides the reflection at the corresponding FBG, the measured trace will also include information on reflections that occur in the other branches. By analysing the collected traces (using different wavelengths), the OTDR trace corresponding to the events that occur in each individual branch is calculated and, from that, the localization of a fault is possible to obtain. This method shows a way of using different monitoring wavelengths (one per drop fibre) without the need of filtering component at the remote node, which represents a high advantage cost wise.

Another approach was explored in [9] by simulation and, in Figure 4.10, is displayed the scheme of its setup.

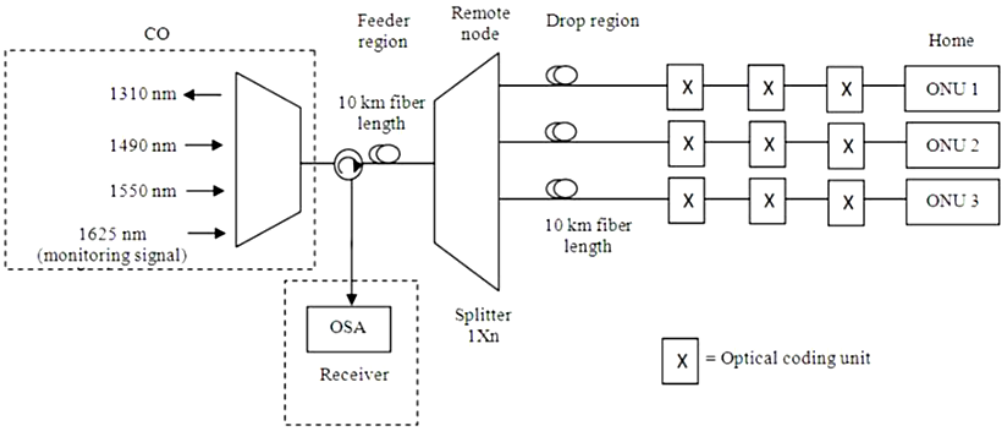

Figure 4.10 - Simulation operation setup of a fibre fault monitoring method based on FBGs [9]

Here, a monitoring signal (at 1650 nm) is sent to the network. The FBGs, are placed (represented by X) on each arm of the PON and will generate a unique spectral reflection pattern that is detected by an OSA. A failure in the network will alter this pattern and the identification of the faulty branch is possible. In Figure 4.11 are shown the simulated spectra.

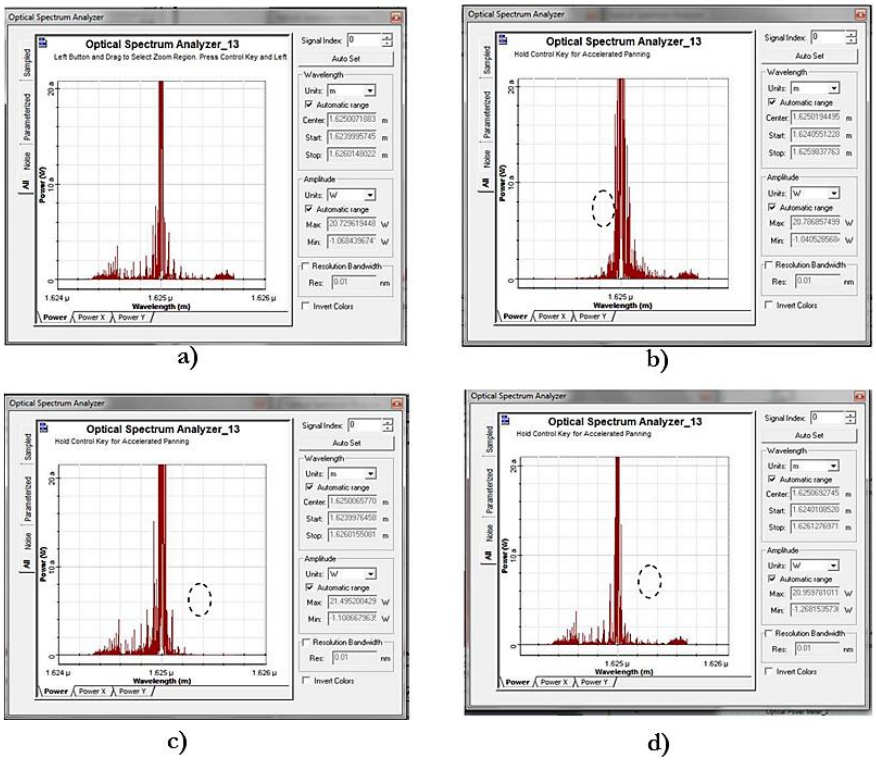

Figure 4.11 - Simulated spectra of the FBG reflections from the different drop fibres [9]

It is visible that a failure on one of the arms will modify the reflection spectrum and by comparison to the reference (Figure 4.11 a)), the faulty branch is identifiable. This method has only been tested via simulation and its proper application in the laboratorial environment is unknown. The

differences between the spectra in Figure 4.11 are very subtle, so it's expected that the application in an experimental setup to be quite challenging.

One other technique, explored in [10], also uses FBG's as reflectors at each one of the branches. However in this case, a semiconductor optical amplifier (SOA) is used as an optical source that will reach all FBGs. In Figure 4.12 is displayed the schematic setup.

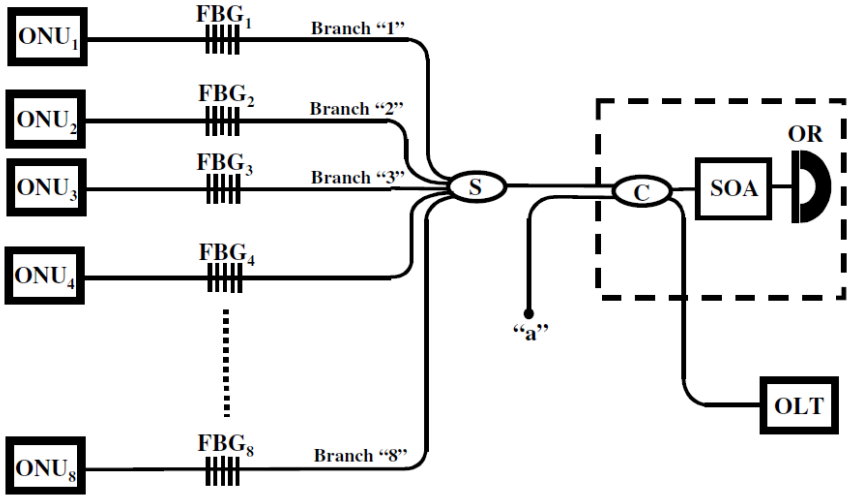

Figure 4.12 – Scheme of the experimental setup used to monitor a network using FBGs as end reflectors and a lasing cavity [10]

The SOA generates a broadband optical signal that is injected into the network and that will be reflected by the FBGs. Each FBG has a different Bragg wavelength and will reflect different spectral components of the incoming signal. The reflected signals re-enter the SOA where amplification occurs and are reflected by an optical reflector (OR in Figure 4.12). This cycle is equivalent to an optical cavity which generates a lasing effect at the reflected components. The coupler (C) allows the extraction of a portion of the signal, which is then analysed by an OSA (placed at monitoring point *"a"*). Observing the spectrum and the lasing peaks, one can guarantee the health of the network. If a missing peak is verified, means that the corresponding drop fibre has a failure.

The method that was proposed in this thesis, and studied in the next section, is similar to this one. In the work presented by Yeh et al [10], this technique is tested on a back-to-back scenario, with only 5 m of fibre span between the splitter and the FBGs. We explore the applicability of a method of this kind taking into account the attenuation that the signals are subjected to when propagating in the PON.

Summary

The need to supervise the integrity of passive optical networks is more than evident. As the typical OTDR device becomes unpractical for this kind of networks, so it is mandatory to find alternative solutions to perform this task.

The tuneable OTDR technique provides the supervision of individual drop fibres, where to each branch is assigned a different monitoring wavelength. The individual OTDR trace gives accurate information on the location of an eventual failure. However, one of the main drawbacks of this kind of techniques is at the tuneable source used, which usually is not cost effective.

Also based on the OTDR principle, there's another interesting approach that makes use of Brillouin scattering. In this method the monitoring induces backscattering at a wavelength slightly shifted from the incident. This shift is tailored by doping the drop fibres with different concentrations of Germanium and Fluor. This technique shows potential, however in order to implement it, all drop fibres must undergo a doping process, which is quite unrealistic.

OFDR has been introduced more recently and appears to be an interesting alternative to the OTDR. The interferometer units can be cost effective components such as FBG's. This technique allows the identification of the faulty branch, but not the failure's exact location.

The use of FBG's in this kind of application is becoming quite common. The analysis of their reflection spectrum can give information on the presence of a failure. In reference [9] is proposed the analysis of the reflection pattern of combined FBG's. A failure gives rise to a subtle alteration of that pattern. However this method has only been explored through simulations.

In reference [10] a more realistic approach is studied. Here a SOA is used as an optical source and the FBG's function as end reflectors of a cavity, generating a lasing state which is observable by an OSA.

Figure 4.13 shows the number of published papers along the past years, from a search using the terms "passive optical networks" and "monitoring", performed on July 29th of 2013 through the ISI Web of Knowledge database.

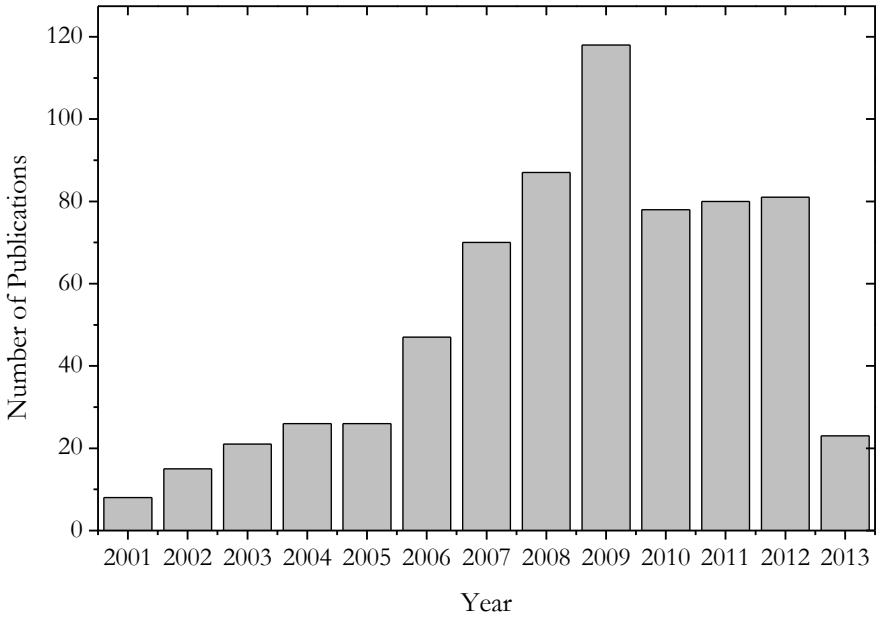

Figure 4.13 - Number of works about PON monitoting that were published over the past years. The data from the year 2013 only contains the works published so far (until July 29th of 2013).

The research on this topic is very strong and has grown in the past ten years and stabilized for the last four (with about 80 published works per year), confirming the importance that this topic has gained over the years.

4.3 Monitor based on FBG reflectors

4.3.1 Brief Description

The method here proposed consists on distributed FBGs along the network pathway, so that regions that may be more vulnerable are monitored, such as: near the client premises, remote nodes or other areas more propitious to failures. In Figure 4.14 is shown a hypothetical PON showing the monitoring FBGs distributed along the network pathway.

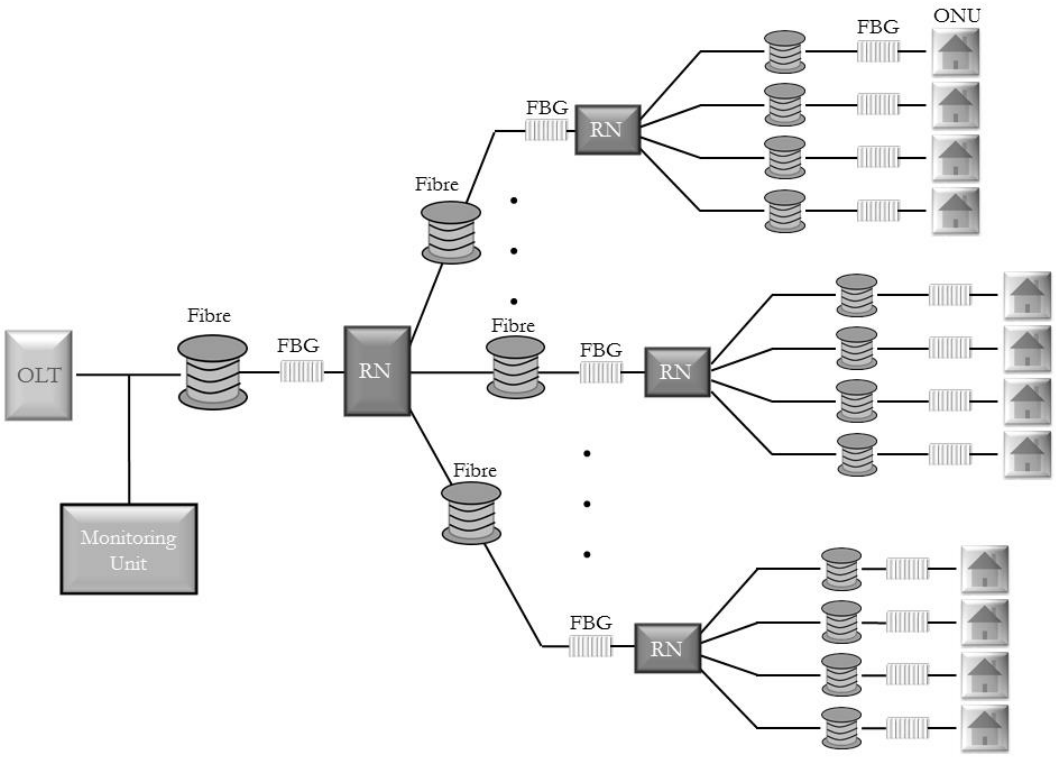

Figure 4.14 - PON with monitoring FBGs spread throughout the network

The data signals generated in the optical line terminal (OLT) are directed to the corresponding optical network unit (ONU) via an optical splitter in the remote node (RN). The monitoring unit sends also a signal that will be reflected by the FBGs, each one with a different Bragg wavelength and, by analysing the reflected spectrum, it is possible to identify a fault in the network and in which branch it is located. Including an amplifying medium such as a SOA at the monitoring unit, it is possible to form a cavity with the FBGs acting as end reflectors and, this way, induce a laser state to the reflected signals.

In this work the limits of this method were tested, regarding the attenuation of the fibres on the generation of lasing. Then an alternative scenario without any amplification was tested.

4.3.2 Setup

Figure 4.15 shows the two scenarios that were implemented in order to test and study this method: one with amplification, that allows lasing to occur, and another one without amplification of the reflected signals at the monitoring unit.

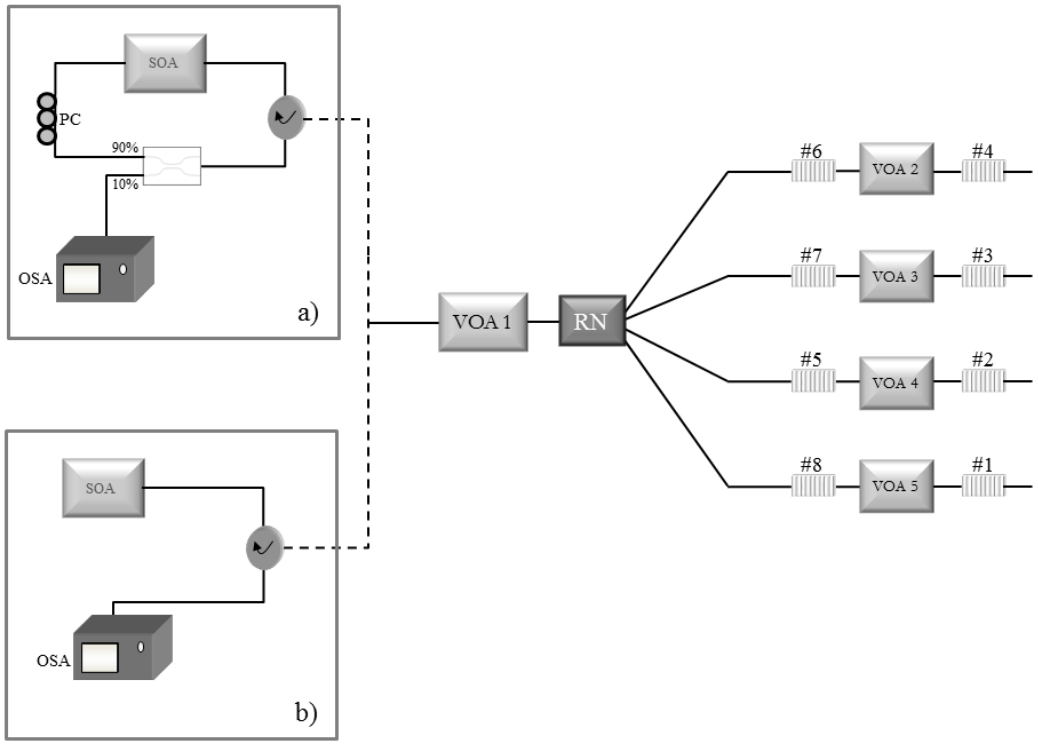

Figure 4.15 - Implemented experimental setups: a) monitoring unit with amplification; b) simplified monitoring unit

In both scenarios, a SOA, model *SOA-NL-OEC-1550* from *CIP*, is used as a broad optical source. The signal from the SOA is forwarded to a first variable attenuator (VOA1) via a circulator. The bias current of the SOA was set at 300 mA, having an output power of 11.5 dBm. The VOAs are placed in order to emulate the spans of fibre inducing a specific amount of attenuation. The application of the VOAs is adequate for the purpose of this work as the attenuation is the only effect considered. Throughout this work, it was considered an attenuation coefficient of 0.2 dB/km, which is the standard for single mode fibres at the spectral range of the Bragg wavelengths.

A coupler at the remote node splits the signal that propagates into four branches. Each of these branches is composed by a FBG, a VOA followed by a second FBG, where the latter would be near the client's ONU. The FBGs were designed with different Bragg wavelengths, so the reflections occur at different spectral components of the incoming signal. In the first situation (Figure 4.15 a)), the FBG reflected signal is directed back to the circulator and to the optical ring. At the coupler, 10% of the signal is analysed by an optical spectrum analyser (OSA), while the remaining 90% pass through a polarization controller and is inserted back into the SOA where it's amplified. This way a lasing effect is generated with the reflections from the FBGs, which can then be detected with the OSA. At the lower setup (Figure 4.15b)), the reflected signals go directly to the OSA and are not amplified at the SOA.

For a normal operation, without any faults in the network, all the FBGs are detected by the OSA. In the presence of a fault, the signal won't be able to reach every FBG and the missing reflection will give the information on the branch the fault is located. By placing the FBGs in strategic places in the network, it becomes easier to identify faults in the structure.

4.3.3 Results

The uniform fibre Bragg gratings used in the experimental implementation of this work have a length of 6 mm and were imprinted with the phase mask method using a 500 Hz pulsed KrF excimer laser (248 nm), with an exposure time of 10 s. All the FBGs used in the monitoring units have different Bragg wavelengths values, within the range of [1533, 1554] nm, being possible to identify unequivocally the several network elements.

All the produced FBGs have a sideband rejection higher than 35 dB and a maximum bandwidth at 3 dB smaller than 0.2 nm. These FBG parameters, sideband rejection and bandwidth, are crucial in the monitoring planning service, since they will limit the maximum extension of the monitored network and the maximum number of allowed monitors.

In Figure 4.16 is shown the spectral responses of all the FBGs used in this work. These spectra were measured with an optical network analyser (ONA).

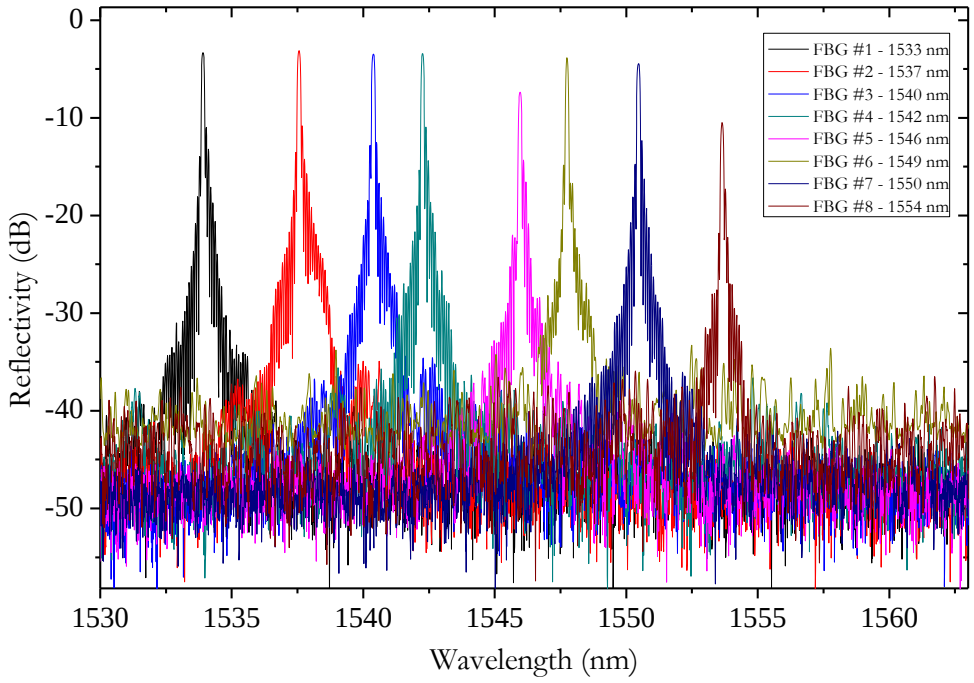

Figure 4.16 - FBGs reflectivities measured with an optical resolution of 0.01 nm

The initial objective was to analyse the limits of the network applying the setup presented in Figure 4.15 a) and using only the first row of FBGs (5, 6, 7 and 8). The attenuation imposed by the VOA1 was increased in order to measure the limits of attenuation that still allows lasing to occur.

In Figure 4.17 is displayed the OSNR for the FBG reflected signals, as function of the fibre span. The OSNR, within all the presented experimental data, was measured with the OSA, considering a noise bandwidth of 0.01nm.

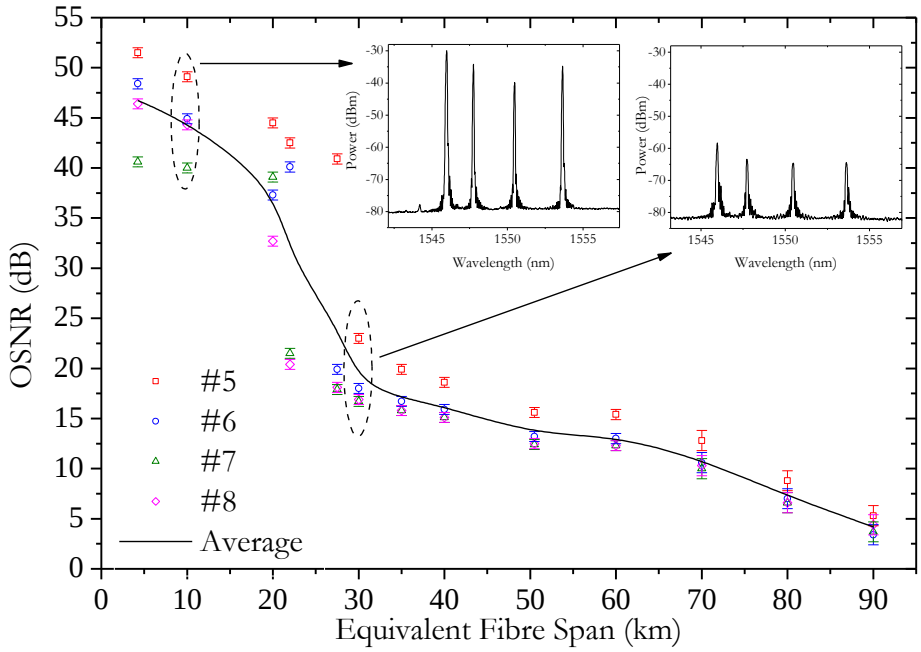

Figure 4.17 - OSNR of the monitoring signals as function of the equivalent distance between OLT and the remote node. Line represents the average OSNR value. The insets show the spectra of the reflected signals for two different fibre spans (10 and 30 km).

These results show two distinct operational regimes. The first one, for low attenuation (up to the equivalent of 20 km), the reflected signals present a high OSNR, which is due to the lasing effect in the cavity. Once the network length reaches a threshold value (20-30 km), the reflected signal optical power is too low to induce the lasing. However, the reflected signals still have an acceptable OSNR, around 20 dB. As the fibre length increases, the OSNR of the reflected signals decrease in a predictable manner.

Between 20 and 30 km is observed a transitory regime. While the signals from the FBGs with high reflectivity are able to induce lasing, the others, with lower reflectivity, do not, creating high differences between the OSNR of the reflected signals.

The insets of Figure 4.17 show the optical spectra obtained for two different network lengths: for 10 km where lasing is clearly visible at all the signals and for 30 km, where none of the reflected signals generate the lasing.

The extension of this scenario, with the inclusion of more FBGs, distributed along the monitored network was also analysed with the setup shown in Figure 4.15 a). In Figure 4.18 are shown the obtained results for the reflected signal OSNR for all 8 FBGs, as function of the distance to the OLT. In Figure 4.18 a) the attenuation at VOA2 through VOA5 was fixed at an equivalent span of 5 km, while VOA1 was varied in order to emulate different distances between the OLT and the remote node. In Figure 4.18 b) are shown the results where the VOA1 is kept constant (equivalent to 30 km of span) while the attenuation imposed by VOA2 to VOA5 was increased.

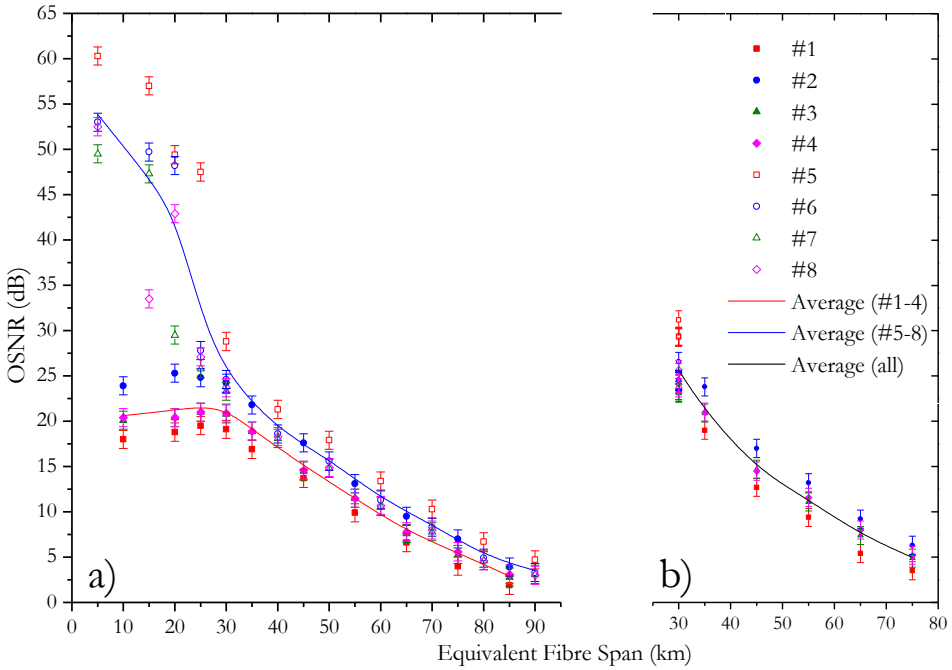

Figure 4.18 - OSNR of the monitoring signals as function of the equivalent distance between the FBG monitors and the OLT: a) considering an equivalent fixed distance (5 km) between the RN and the ONU; b) where the equivalent distance between the OLT and the RN was fixed (30 km). The lines represent the represent the OSNR average values.

The results shown in Figure 4.18 a) are identical to the ones derived Figure 4.17, regarding that for shorter fibre spans the reflected signals from monitors closer to the OLT are able to induce lasing, and, therefore, present higher OSNR values. The reflected signals from the FBG monitors placed at longer distances have a reduced OSNR, due to the lower lasing effect resulting from the gain competition with the monitor placed closer to the OLT. The OSNR from these signals is approximately constant with the increase of fibre span until lasing ceases, which occurs, in this situation, approximately at 30 km. For high network lengths, the OSNR for all signals decreases with the distance, which is also verified in Figure 4.18 b).

The implementation of a scheme with an amplification medium creating this way a lasing cavity becomes irrelevant when the network has long spans (more than 20 km, for the tested conditions). Therefore, we proposed a simplified method to monitor the network that is illustrated in in Figure

4.15 b). This monitoring architecture was considered in a passive optical network with a total length of 60 km, and an FBG monitoring unit located every 30 km.

The reflection spectrum obtained in this situation is displayed in Figure 4.19, where is also included, for comparison purposes, the spectrum obtained with the amplification configuration for an identical propagation distance.

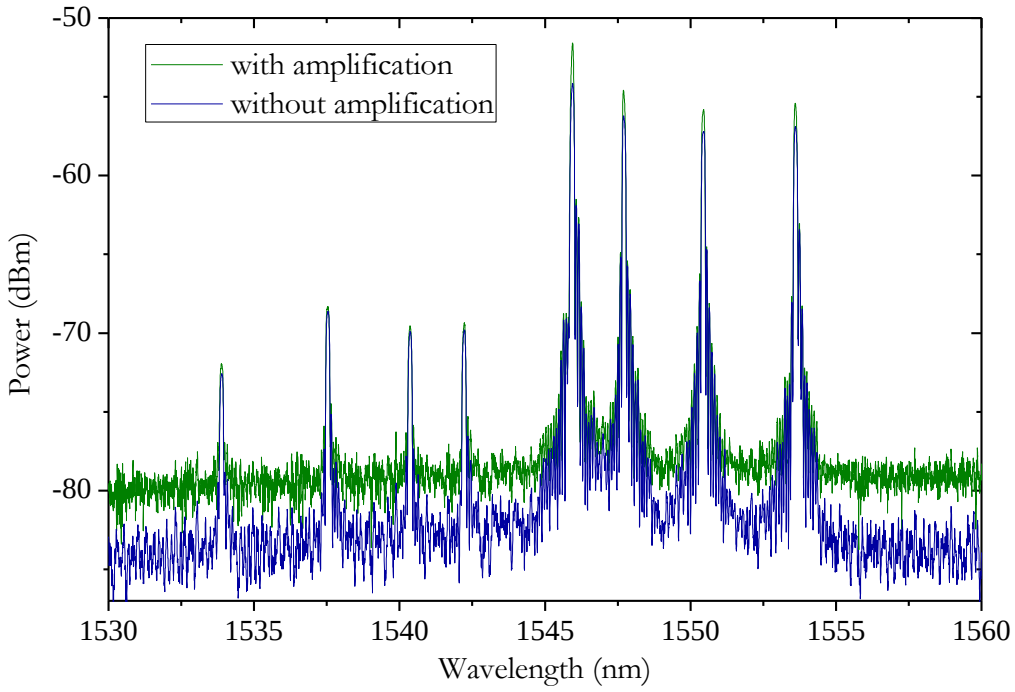

Figure 4.19 - Optical spectra obtained for different scenarios: simplified (blue line) and with amplification (green line).

As expected, the intensity of the reflected signals is not sufficient to promote lasing when the total cavity attenuation is high (green line), which occurs when the monitoring units are far from the monitoring unit (more than 30 km). Using the simplified scheme (blue line), the reflected signals are still visible in the spectrum providing a similar result.

With the simplified scheme, different scenarios with failures along the network were also tested. In Figure 4.20 are displayed the spectra obtained in the eventuality of a fibre fault in the network.

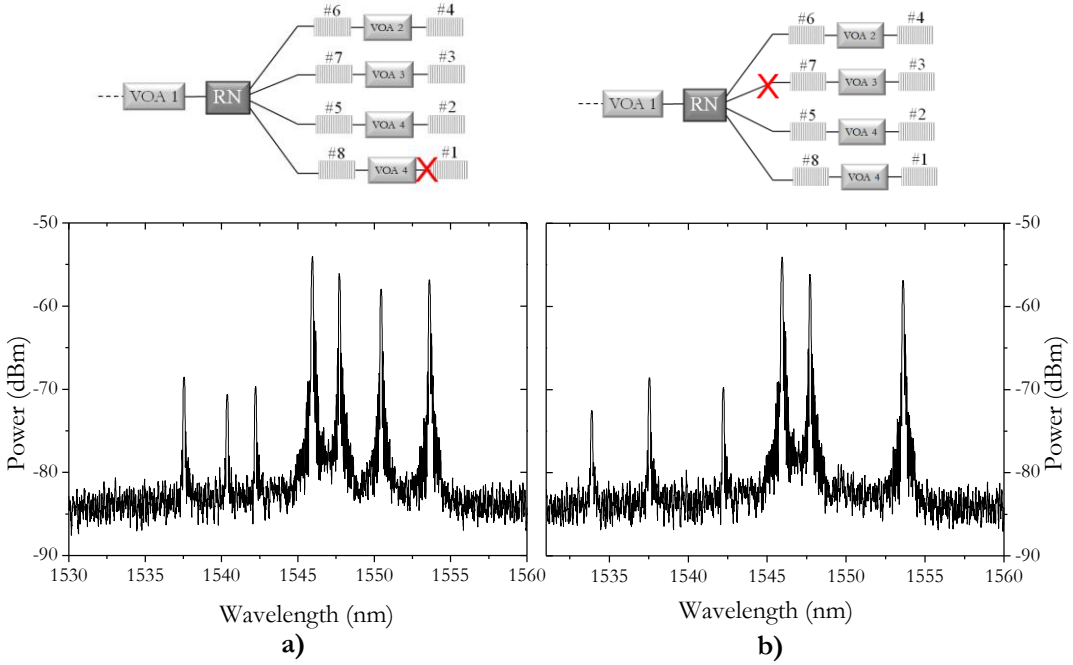

Figure 4.20 - Spectra obtained for the scenarios with fibre faults in the network: a) fault between FBG 8 and FBG 1; b) fault before FBG 7

With a fault in the network, the reflected spectrum does not have the contribution of all the FBGs. In the first case, it's clear from Figure 4.20 a) that FBG 1 is missing, meaning that there is a fault located somewhere between FBG 8 and FBG 1, as it can be seen from the scheme above. In the second situation (Figure 4.20 b)), both FBG 7 and 3 are missing, meaning that there is a fault located somewhere before the signal reaches FBG 7, like is shown by the respective upper figure.

The expansion of this method on larger networks and the attained resolution of the fault localization only depend on the number of used FBGs.

4.4 Summary and Conclusions

In this chapter a study on the application of FBGs as monitoring points along an access network has been presented. By placing FBGs in strategic places in the network and using, at monitor end, an amplifying medium, such as a SOA, it is possible to induce a lasing state to the reflected components from each of the FBGs. However, it is demonstrated that once the FBGs are placed far from the monitor unit (further than 20 km, for the mentioned conditions) the lasing effect ceases and the FBGs are identified as mere Bragg reflections. In these situations the scenario with the amplifying medium becomes unnecessary, so a simplified one is proposed.

The applicability of the simplified setup is successfully tested, in a conceptual passive optical network with an emulated total reach of 60 km. However, from Figure 4.18 a) the reflected signals from the FBGs are detected for distances as long as 90 km (if an OSNR threshold detection limit of 5 dB is considered).

References

[1] K. Yuksel, V. Moeyaert, M. Wuilpart, and P. Megret, "Optical layer monitoring in passive optical networks (PONs): A review," *Icton 2008: Proceedings of 2008 10th Anniversary International Conference on Transparent Optical Networks,* vol. 1, pp. 92-98, 2008.

[2] J. Hehmann and T. Pfeiffer, "New monitoring concepts for optical access networks," *Bell Labs Technical Journal,* vol. 13, pp. 183-198, Spr 2008.

[3] NTT. (2007, May 22nd, 2013). Searching for Optical Failure Locations. *Special Feature on Technical Solutions to Real-world Problems 5(8).* Available: https://www.ntt-review.jp/archive/ntttechnical.php?contents=ntr200708sf4.html

[4] J. Park, J. Baik, and C. Lee, "Fault-detection technique in a WDM-PON," *Optics Express,* vol. 15, pp. 1461-1466, 2007.

[5] N. Honda, D. Iida, H. Izumita, and Y. Azuma, "In-Service Line Monitoring System in PONs Using 1650-nm Brillouin OTDR and Fibers With Individually Assigned BFSs," *Journal of Lightwave Technology,* vol. 27, pp. 4575-4582, 2009.

[6] M. A. Esmail and H. Fathallah, "Physical Layer Monitoring Techniques for TDM-Passive Optical Networks: A Survey," *IEEE Communications Surveys & Tutorials,* vol. 15, pp. 943-958, 2013.

[7] K. Yuksel, M. Wuilpart, V. Moeyaert, and P. Megret, "Novel Monitoring Technique for Passive Optical Networks Based on Optical Frequency Domain Reflectometry and Fiber Bragg Gratings," *Journal of Optical Communications and Networking,* vol. 2, pp. 463-468, Jul 1 2010.

[8] K. Enbutsu, N. Araki, N. Honda, and Y. Azuma, "Individual fiber line testing technique for PON using wavelength assigned FBG termination and TLS-OTDR enhanced with reflected trace analysis method," in *Joint conference of the Opto-Electronics and Communications Conference and the Australian Conference on Optical Fibre Technology*, 2008, pp. 1-2.

[9] M. S. Ab-Rahman, N.F. Naim, M. Tanra and H. Ramza, "Optical system monitoring based on reflection spectrum of fiber Bragg grating," *Journal of Computer Science,* vol. 8, pp. 1001-1007, 2012.

[10] C.-H. Yeh and S. Chi, "Fiber-fault monitoring technique for passive optical networks based on fiber Bragg gratings and semiconductor optical amplifier," *Optics Communications,* vol. 257, pp. 306-310, 2006.

Chapter 5: Conclusion

5.1 Final Conclusions

Throughout the realization of this work, the development of techniques, covering three different parameters inherent to the quality of the signal or the network itself, was successfully accomplished. Although the introduction of different and novel methods seemed challenging and difficult, it was possible to innovate and experimentally test different methods.

Regarding the monitoring of the signal quality itself, two techniques were successfully developed: one dedicated to the measurement of the signal OSNR and another dedicated to the measurement of the group velocity dispersion.

To monitor the signal OSNR, the application of HiBi FBGs enabled the utilization of its polarization properties to distinguish the signal from the noise. Results show the successful application of the methods on single channel systems. Two variations based on the same principle were experimentally tested. In the first method, where the reflected signal by the HiBi FBG is analysed, the OSNR of a signal modulated at 10 Gb/s was measured over a range of [14,31] dB with a maximum error of 2.2 dB. The second and alternative approach also takes into account the transmission side of the HiBi FBG, and from this method the OSNR of a signal modulated at 10 Gb/s was monitored over a range of [5, 20] dB with a maximum error of 0.8 dB.

The application of this method on multi-channel scenarios is more challenging as it requires a high rejection filter so that the neighbouring channels do not interfere in the analysis of the monitored channel. The main objective was the development of a cost-effective solution based on optical processes, which was possible due to the relatively low-cost associated to the HiBi FBGs.

To monitor the group-velocity dispersion, the chosen approach is based on a known theoretical principle: the dependence of the clock component peak power on the dispersion. We've tested a simple setup that allows the estimation of both the magnitude and the sign of GVD and, its application on amplitude modulated signals as well as phase modulated signals, was successfully demonstrated. Results show that this technique is able to measure the GVD of a 10 Gb/s OOK signal over a range of [-600, 600] ps/nm where a maximum error of 100 ps/nm was achieved. The method was also applied on a 40 Gb/s OOK signal, where the GVD was measured over a range of [-60, 60] ps/nm. Near the point of zero dispersion, the measurement is challenging, but for $|GVD|>15$ ps/nm the maximum error verified drastically decreased to 3 ps/nm. The application of the method on a phase modulated signal confirms that it is also possible to measure the GVD of a QPSK (20 Gb/s) system

using the same technique, due to the fact that the modulator also imposes a slight variation on the amplitude. In this case the GVD was measured over a range of [-600, 600] ps/nm with a maximum error of 120 ps/nm.

This method is not totally based on optical processes, as the estimation of the GVD is determined via measurements on the electric domain. However it is a relatively cost effective method to estimate the GVD, especially on the coherent communications field, as it doesn't require the presence of coherent detection.

The experimental implementation of both of these methods (OSNR and GVD monitoring on amplitude modulated signals) was also supported by simulations that provide a very close to reality scenario of the studied techniques as is shown by the obtained results.

The physical state of an optical access network was also covered. The work regarding this topic, which is presented in this thesis, is a proof-of-concept experiment to be applied in a PON and consists of using several FBGs as identification points along the network. By injecting a broadband optical signal and measuring the reflections generated by the FBGs, the existence of a failure can be detected. The exact location of the failure is not extractable through this method. However, the faulty PON branch is identified and, depending on the number of monitoring FBGs present in that branch, the fault location can be narrowed down. The applicability of the presented method is successfully tested, in a conceptual passive optical network with an emulated total reach of 60 km, under the tested conditions. This method, being based on the application of FBGs, provides a cost-effective solution to perform this kind of monitoring.

5.2 Suggestions for future work

One of the most important factors to take into consideration in future approaches for optical performance monitoring is the development of techniques suitable for multi-channel systems, as they are the predominant technology in the core communications field. Monitoring based on tuneable filters that scan the spectrum isn't viable, as it was already explained on the second chapter. The need to monitor channels individually is evident. The method proposed in this thesis works well once the channel to be monitored is selected. However in a multi-channel, the rejection of the neighbour channels proved to be challenging. The solution presented in Figure 2.21 b) (the application of a double FBG in order to eliminate the neighbour channel) works very well, but becomes unpractical for systems with more optical channels. So, with the objective of analysing the optical channels individually, an alternative is needed. Another important aspect to consider is the fact that the transmission of optical coherent signals will definitely be the future of optical communications. For

long-haul networks there are some commercial solutions already available and research is also betting strong on the development of coherent access networks. Consequently, the implementation of monitoring techniques for this kind of transmission systems becomes more important.

Regarding the monitoring of the physical integrity of an access network, the implementation of FBGs along the network pathway seems very promising, due to the relative low-cost of those components. In chapter 4, a primordial experiment is carried out where several FBGs are placed in different regions of a hypothetical network. However, the Bragg wavelengths of the used FBGs coincide with the wavelengths used for data transmission of PON standards. So, the next step would be the use of Bragg wavelengths outside of the already occupied spectral range where the attenuation imposed by the fibre will be slightly different. We also suggest the implementation of this monitoring technique with the simultaneous propagation of downstream and upstream data in order to further validate its performance.